

UC Berkeley

UC Berkeley Electronic Theses and Dissertations

Title

Measurement techniques for atmospheric nitrogen oxides and observational constraints on alkyl nitrate chemistry

Permalink

<https://escholarship.org/uc/item/9hc717q9>

Author

Sparks, Tamara

Publication Date

2018

Peer reviewed|Thesis/dissertation

Measurement techniques for atmospheric nitrogen oxides and observational constraints on
alkyl nitrate chemistry

By

Tamara L Sparks

A dissertation submitted in partial satisfaction of the

requirements for the degree of

Doctor of Philosophy

in

Chemistry

in the

Graduate Division

of the

University of California, Berkeley

Committee in charge:

Professor Ronald Cohen, Chair
Professor Kristie Boering
Professor Allen Goldstein

Summer 2018

Measurement techniques for atmospheric nitrogen oxides and observational constraints on
alkyl nitrate chemistry

Copyright 2018

by

Tamara L Sparks

Abstract

Measurement techniques for atmospheric nitrogen oxides and observational constraints on alkyl nitrate chemistry

by

Tamara L Sparks

Doctor of Philosophy in Chemistry

University of California, Berkeley

Professor Ronald Cohen, Chair

NO_x ($\text{NO} + \text{NO}_2$) molecules act as a control over atmospheric oxidation rates. The chemical lifetime of NO_x is controlled by daytime OH-initiated photochemical reactions and nighttime NO_3 -initiated reactions. One class of products of this chemistry, alkyl nitrates (denoted by the general formula RONO_2), is formed by both daytime and nighttime processes, but the balance between these processes is not well understood. In order to investigate mechanisms of RONO_2 production and thus shed light on this balance, measurements of reactive nitrogen and other relevant species were taken during three field campaigns, two in Colorado during summer 2014, the Front Range Air Pollution and Photochemistry Experiment (FRAPPE) and Deriving Information on Surface Conditions from COLUMN and VERTically Resolved Observations Relevant to Air Quality (Discover-AQ), and one in the northeast US in winter 2015, Wintertime INvestigation of Transport, Emissions, and Reactivity (WINTER). Evidence is presented showing that the nighttime pathway for RONO_2 formation, often considered a negligible source compared to daytime production, results in concentrations that are up to half of observed daytime concentrations. High RONO_2 concentrations observed in the morning at constant ozone that cannot be explained by loss processes, mixing, or other sources point to rapid nighttime production via NO_3 chemistry. This result is surprising because, while nighttime NO_3 chemistry has often been shown to be a significant source of organic aerosol, especially in rural regions dominated by biogenic emissions, it has not been shown to be a significant source of alkyl nitrates in an urban area. In addition, measurement comparisons are presented in order to evaluate the accuracy of the observations used in this analysis and to evaluate the winter and nighttime performance of instruments that have been previously well characterized for summer and daytime operation. For the WINTER campaign, comparisons between measurements of the same species using different operating principles showed agreement to better than 20%. The measurements from WINTER show a comprehensive observation-based view of the partitioning of nitrogen oxides under winter and nighttime conditions not previously demonstrated. For FRAPPE and Discover-AQ, a method is presented for comparing measurements between instruments flown on two different aircraft with different flight paths. This comparison shows agreement to within expected accuracies for all 13 species compared except for the total RONO_2 measurement (ΣRONO_2), a measurement of the sum of all species

with the RONO_2 general formula. A comparison of ΣRONO_2 with measurements of individual RONO_2 species scaled to approximate ΣRONO_2 reveals a systematic error in the Discover-AQ ΣRONO_2 measurements; reasons for this error are discussed.

Table of Contents

Acknowledgements	iii
------------------------	-----

Chapter 1

1.1 The study of NO _x and its sinks	1
1.2 Nighttime chemistry is a significant RONO ₂ source in the Colorado Northern Front Range Metropolitan Area.....	2
1.3 Comparison of nitrogen oxide measurements during WINTER	3
1.4 Comparison of measurements by separate thermal-dissociation laser-induced fluorescence instruments in the Northern Front Range Metropolitan Area of Colorado.....	4
References	5

Chapter 2

2.1 Introduction	8
2.1.1 Daytime alkyl nitrate formation pathway.....	8
2.1.2 Nighttime alkyl nitrate formation pathway.....	9
2.1.3 Alkyl nitrates in Colorado.....	9
2.2 Observations	10
2.3 Results	11
2.3.1 Hypotheses for lack of morning correlation between ozone and alkyl nitrates	11
2.3.2 Daytime RONO ₂ production.....	16
2.4 Conclusion.....	19
2.A Appendix: Aromatic branching ratios	21
References	22

Chapter 3

3.1 Introduction	26
3.2 Instrumentation	27
3.2.1 TD-LIF	28
3.2.2 Chemiluminescence.....	29
3.2.3 CRDS.....	30
3.2.4 I-ToF-CIMS	31
3.2.5 Particle-phase nitrate	31
3.3 Comparison	32
3.3.1 NO ₂	32
3.3.2 NO	34
3.3.3 NO _y and NO _z	35
3.3.4 N ₂ O ₅	39
3.3.5 ClNO ₂	40
3.3.6 HNO ₃	43
3.4 Conclusion.....	44
References	45

Chapter 4

4.1 Introduction	49
4.2 Observations	49
4.2.1 Campaign summaries	49
4.2.2 Instrumentation	50
4.3 Measurement discrepancy between campaigns	52
4.3.1 Validation of FRAPPE measurements	57
4.3.2 Validation of Discover-AQ measurements	59
4.3.3 Possible explanations for discrepancy	60
4.3.4 Comparison of other species for validation	62
4.4 Conclusion	64
References	64

Acknowledgements

I would like to thank Ron Cohen for his mentorship and guidance throughout my graduate career. None of the work in this dissertation would have been possible without him. I would also like to thank my other committee members, Kristie Boering and Allen Goldstein, for their helpful comments that improved my analysis and clarified my writing in this dissertation.

None of the data I used would have been collected without a multitude of participants. I would like to thank those who helped collect data for the TD-LIF team: Carly Ebben, Ben Nault, Paul Romer, and Paul Wooldridge. Thanks to all the scientists who were a part of the Discover-AQ Colorado, FRAPPE, and WINTER projects, as well as the crews for the P-3B and C-130 that got us up in the air. Thanks to the NSF, NASA, and Colorado Department of Public Health and Environment for funding. I would especially like to thank the NSF for my graduate research fellowship funding (grant number DGE 1106400).

It was a pleasure to spend my day-to-day surrounded with the wonderful people who have been a part of the Cohen lab during my time there. I appreciate all the helpful guidance and interesting discussions. You all made for an excellent working environment and kept me sane. I will miss eating delicious desserts together.

I couldn't have made it through these five years without the love and support of my family and friends. I met so many wonderful friends here and am so thankful for all the fun times we had. Thanks especially to Ali Fischer and Alexis Shusterman for all of the froyo breaks, movie nights, and always listening to me and encouraging me when I needed it. The love and support of my family has been a steady throughout my life and has brought me to where I am today. Thank you to my parents, Margaret and Randy Sparks, and my sister and brother-in-law, Michelle and Keith Forsyth, for always being a refuge and source of encouragement. And last but not least, thanks to Matthew Koc for all of the love you give and for sticking with me through it all.

Chapter 1

Introduction

1.1 The study of NO_x and its sinks

NO_x (NO_x ≡ NO + NO₂) is an important atmospheric oxidant that controls the production of ozone (O₃) and contributes to secondary organic aerosol (SOA) formation. Ozone is a pollutant when present in the troposphere as it is a respiratory irritant and decreases crop yields (Avnery et al., 2011; Bell et al., 2004). SOA affects global climate and cloud production and is also associated with increased mortality (Forester et al., 2007; Pope III, 2007). NO_x is emitted by combustion processes, and so in urban areas emissions are primarily anthropogenic and come from transportation, power plants, and industrial processes. Concentrations of NO_x along with volatile organic compounds (VOCs) determine ozone and SOA production rates (Atkinson, 2000).

The lifetime of NO_x is controlled by loss through its various sinks, which happens by different processes in the daytime and nighttime. During the daytime, NO_x is lost through photochemical, OH-initiated reactions that primarily produce peroxy nitrates (RO₂NO₂), alkyl and multifunctional nitrates (RONO₂), and nitric acid (HNO₃) (Perring et al., 2013). At night, when photochemistry is inactive, loss of NO_x is dominated by reaction with ozone to form NO₃. NO₃ can react with NO₂ to form N₂O₅, which can go on to form HNO₃ and ClNO₂, or it can react with alkenes to form alkyl nitrates (Brown & Stutz, 2012). A full picture of the daytime and nighttime NO_x loss processes is necessary to understand the lifetime of NO_x and to be able to accurately model and therefore predict its chemistry. One of the less well understood sinks of NO_x is conversion to alkyl nitrates, which are formed in the daytime by OH-initiated oxidation of VOCs or at nighttime by NO₃-initiated oxidation of alkenes.

Studies on NO₃ reaction with alkenes have mostly looked at alkenes that are biogenic VOCs (BVOCs) as the reactant, especially isoprene, and organic aerosol as the product. These studies have shown that this NO₃-initiated reaction contributes significantly to aerosol formation (Fisher et al., 2016; Ng et al., 2017; Pye et al., 2015). As BVOCs are prevalent in rural areas, many studies have taken place in rural areas and focused on how NO_x outflow from anthropogenic sources intermingling with biogenic emissions impacts SOA production. A recent study by Edwards et al. (2017) examined nighttime oxidation of BVOCs in the southeast US and found that the ratio of BVOC loss to reaction with NO₃ vs. that for reaction with O₃ depends on NO_x concentrations. At NO_x/BVOC ratios above 0.5, BVOC oxidation is primarily by NO₃, while below this threshold oxidation is primarily by O₃. This suggests that in air influenced by urban NO_x emissions, oxidation by NO₃ becomes a more important pathway for oxidation of alkenes than reaction with O₃. Additionally, in their observations 90% of NO₃ loss was due to rapid reaction with BVOCs, showing that NO₃-initiated oxidation of alkenes was also the dominant pathway for NO₃ loss. These results show an example where reaction between NO₃ and BVOCs is the dominant loss process for both reactants and that this dominance over other reactions

would only grow at higher NO_x concentrations. For example, Wang et al. (2018) found high production rates of organic nitrates, which are formed by NO₃ oxidation of alkenes, at NO_x/BVOC ratios around 10 in the outflow of Beijing.

Despite the evidence that this reaction pathway would be prominent in urban areas with high NO_x and alkene concentrations, this process is less well studied in urban environments. Most studies have taken place in rural and forested areas where the large majority of alkenes available for reaction are BVOCs (Boyd et al., 2015; Fry et al., 2009; Griffin et al., 1999; Ng et al., 2008, 2017; Pye et al., 2015), while fewer have considered the effect of anthropogenic alkene emissions in urban regions.

Often, the products of interest in studies of the reaction of NO₃ with BVOCs are particle-phase alkyl nitrates, but these reactions also produce a significant amount of gas-phase alkyl nitrates (Fisher et al., 2016; Fry et al., 2009; Hallquist et al., 1999; Lee et al., 2016; Rollins et al., 2012). Fry et al. (2009) found that in the NO₃-initiated oxidation of β-pinene, less than half of the total alkyl nitrates were in the aerosol phase. Fisher et al. (2016) found only 10 – 20% of total alkyl nitrates were in the particle phase. Reaction of NO₃ with BVOCs is a significant source of SOA, but it is also a significant source of gas-phase nitrates.

While nighttime NO₃-initiated oxidation of VOCs has been shown to be an important source of gas-phase nitrates, studies of daytime organic nitrate observations have often assumed the nighttime source to be negligible. Several studies have used the ratio of ozone and total alkyl nitrate (ΣRONO_2) concentrations as a proxy for the ratio of their production rates in order to determine the branching ratio of the RO₂ + NO reaction (Cleary et al., 2005; Day et al., 2003; Perring et al., 2010, 2013; Rosen et al., 2004). This reaction either forms an NO₂ that goes on to produce ozone (along with an RO) or an RONO₂. However, such an analysis relies on the assumption that there is negligible nighttime production of RONO₂. Additionally, many of these studies find disagreement between the branching ratio they derive from observations and that derived from calculations based on precursors, an indication that the assumptions used in this analysis may not hold.

Given the evidence suggesting that nighttime NO₃-initiated oxidation of alkenes to form RONO₂ could be significant in urban areas with high concentrations of NO_x, that this reaction has primarily been studied in rural areas dominated by biogenic emissions, and that urban studies on RONO₂ have often considered this production pathway to be negligible, in this dissertation I examine the importance of the nighttime RONO₂ production pathway and evaluate instrument performance of measurements of NO_x and its loss products used for this analysis.

1.2 Nighttime chemistry is a significant RONO₂ source in the Colorado Northern Front Range Metropolitan Area

In Chapter 2, I present an analysis of the production of RONO₂ in the Colorado Northern Front Range Metropolitan Area (NFRMA) during the Front Range Air Pollution and Photochemistry Experiment (FRAPPE). Measurements were made from the NSF/NCAR C-130 aircraft platform

over the Denver metropolitan area as well as rural areas with agricultural and oil and natural gas activity to the northeast. Observations used are limited to the planetary boundary layer. An observation of ΣRONO_2 concentrations up to 3.59 ppbv before 11:00AM local time at constant ozone near background levels is unusual. In the daytime, RONO_2 and ozone are produced by the same chemical process, so one would expect that the high concentrations of ΣRONO_2 observed would coincide with elevated ozone concentrations. I explore possible explanations for this unusual finding, including loss and mixing processes as well as other sources of RONO_2 . The most plausible explanation is that nighttime RONO_2 production from the reaction of NO_3 with alkenes, which does not produce ozone, is significant and greater than has been previously assumed in other urban regions. NO_3 production rates at night are sufficient for there to be plentiful NO_3 as a reactant, so the limiting factor in the reaction of NO_3 with alkenes is the alkenes. Evidence for alkene concentrations sufficient to support 1.3 ppbv of RONO_2 at night are presented.

While I was able to infer nighttime production using daytime measurements, the question of how much RONO_2 are produced at night compared to the daytime would be further elucidated by experiments where measurements are taken continuously throughout the day and night at a fixed location or locations in this region. While a variety of air quality monitoring sites continuously measure ozone and NO_2 (CDPHE, 2016), the addition of ΣRONO_2 and VOC measurements would provide a wealth of data for addressing this question. It would also provide measurements during the transition between the daytime and nighttime regimes, allowing observation of RONO_2 as the boundary layer expands and photochemistry initiates.

The question remains whether this influence of nighttime production is widespread or unique to the Colorado NFRMA and other similar regions. Nighttime production has often been considered to be negligible in previous analyses that use the relationship between RONO_2 and O_3 to determine daytime production rates and branching ratios for RONO_2 , even though the rates and branching ratios inferred from observation often disagree with calculations based on precursors (Perring et al., 2013). Further analysis or additional studies in those regions could determine whether nighttime production was the source of this disagreement in other locations. This method for studying the daytime mechanism will need to be reevaluated if the assumptions used prove to be untrue.

Many studies of NO_3 -initiated oxidation of VOCs have taken place in rural areas dominated by biogenic alkene VOCs. Urban plumes contain anthropogenic alkene emissions that are also oxidized by NO_3 , and further study should evaluate how much these emissions contribute to urban alkyl nitrate and SOA formation.

1.3 Comparison of Nitrogen Oxide Measurements During WINTER

In Chapter 3, I present a comparison of observations from instruments measuring nitrogen oxide species during the Wintertime INvestigation of Transport, Emissions, and Reactivity (WINTER) experiment in the northeast US during winter 2015. The instrument techniques compared include chemiluminescence (CL), thermal dissociation laser-induced fluorescence

(TD-LIF), cavity ring-down spectroscopy (CRDS), iodide-adduct time-of-flight chemical ionization mass spectrometry (I-ToF-CIMS), and aerosol mass spectrometry (AMS). Species investigated include NO_2 , NO , NO_y , NO_z , N_2O_5 , ClNO_2 , HNO_3 , and particulate nitrate. Measurements from the different instruments generally agreed to instrument uncertainty and often much better, with overall agreement within 20%. Budget closure for NO_z , a measure of total reactive nitrogen minus NO_x , is demonstrated. I find nonlinearity in NO_2 and NO_y correlations at concentrations above ~ 40 ppbv. We present evidence that the temperature used for ClNO_2 thermal dissociation was too low and that the TD-LIF, CL, and CRDS instruments observe little particle-phase nitrate in their NO_y measurements.

This represents a comprehensive comparison of measurements of nitrogen oxides by a variety of techniques that has not been done with wintertime and nighttime observations. Due to the lack of photochemistry at night and the colder temperatures of winter, the partitioning of nitrogen oxides differs under these conditions compared to the daytime summer conditions that many experiments studying nitrogen oxides take place during. This work demonstrates overall successful instrument performance under these different conditions and demonstrates that we were able to measure all of the nitrogen oxide species that have substantial concentrations under these conditions.

Some issues with instrument performance were revealed in this analysis and should be addressed to improve performance in future experiments, including nonlinearity of measurement comparisons at high concentrations, too low temperature settings for thermal dissociation, and inconsistency between flights in the agreement for N_2O_5 and other species.

Despite these issues, these results show that the current state of nitrogen-measuring instrumentation is well-suited to study nighttime and wintertime conditions, and I recommend more of these studies be done to shed light on atmospheric chemical processes in dark and cold conditions.

1.4 Comparison of measurements by separate thermal dissociation laser-induced fluorescence instruments in the Northern Front Range Metropolitan Area of Colorado

In Chapter 4, I compare the performance of two thermal dissociation laser-induced fluorescence (TD-LIF) instruments present in Colorado during July – August 2014. One instrument was on board the NSF/NCAR C-130 aircraft as part of the FRAPPE campaign, and the other was on the NASA P-3B aircraft for the Deriving Information on Surface Conditions from Column and VERTically Resolved Observations Relevant to Air Quality (Discover-AQ) study. I develop a new method for comparing performance between instruments that were not co-located and demonstrate the appropriateness of this method for comparison using a variety of species measured on both aircraft platforms. While comparison is good for most of these species, I present evidence of a disagreement between the ΣRONO_2 measurements from the two TD-LIFs that is due to a systematic error in the Discover-AQ instrument's measurements. The error is isolated to ΣRONO_2 and does not affect the other 3 measurements from the

instruments (NO_2 , $\Sigma\text{RO}_2\text{NO}_2$, and HNO_3). I explore possible sources for this error and present recommendations for usage of the data.

The method I develop in this analysis can be used in future studies from aircraft platforms to verify data quality when co-located measurements of a species by a different instrument or technique are unavailable.

References

- Atkinson, R. (2000). Atmospheric chemistry of VOCs and NO_x . *Atmos. Environ.*, *34*(12–14), 2063–2101. [https://doi.org/10.1016/S1352-2310\(99\)00460-4](https://doi.org/10.1016/S1352-2310(99)00460-4)
- Avnery, S., Mauzerall, D. L., Liu, J., & Horowitz, L. W. (2011). Global crop yield reductions due to surface ozone exposure: 1. Year 2000 crop production losses and economic damage. *Atmospheric Environment*, *45*(13), 2284–2296. <https://doi.org/10.1016/j.atmosenv.2010.11.045>
- Bell, M. L., Mcdermott, A., Zeger, S. L., Samet, J. M., & Dominici, F. (2004). Ozone and Short-term Mortality in 95 US Urban Communities, 1987–2000. *Journal of the American Medical Association*, *292*(19), 2372–2378.
- Boyd, C. M., Sanchez, J., Xu, L., Eugene, A. J., Nah, T., Tuet, W. Y., et al. (2015). Secondary organic aerosol formation from the β -pinene+ NO_3 system: effect of humidity and peroxy radical fate. *Atmospheric Chemistry and Physics*, *15*(13), 7497–7522. <https://doi.org/10.5194/acp-15-7497-2015>
- Brown, S. S., & Stutz, J. (2012). Nighttime radical observations and chemistry. *Chemical Society Reviews*, *41*(19), 6405–47. <https://doi.org/10.1039/c2cs35181a>
- CDPHE. (2016). *Moderate Area Ozone SIP for the Denver Metro and North Front Range Nonattainment Area*.
- Cleary, P. a., Murphy, J. G., Wooldridge, P. J., Day, D. A., Millet, D. B., McKay, M., et al. (2005). Observations of total alkyl nitrates within the Sacramento Urban Plume. *Atmospheric Chemistry and Physics Discussions*, *5*(4), 4801–4843. <https://doi.org/10.5194/acpd-5-4801-2005>
- Day, D. A., Dillon, M. B., Wooldridge, P. J., Thornton, J. A., Rosen, R. S., Wood, E. C., & Cohen, R. C. (2003). On alkyl nitrates, O_3 , and the “missing NO_y .” *Journal of Geophysical Research*, *108*(D16), 4501. <https://doi.org/10.1029/2003JD003685>
- Edwards, P. M., Aikin, K. C., Dube, W. P., Fry, J. L., Gilman, J. B., De Gouw, J. A., et al. (2017). Transition from high- to low- NO_x control of night-time oxidation in the southeastern US. *Nature Geoscience*, *10*(7), 490–495. <https://doi.org/10.1038/ngeo2976>
- Fisher, J. A., Jacob, D. J., Travis, K. R., Kim, P. S., Marais, E. A., Miller, C. C., et al. (2016). Organic nitrate chemistry and its implications for nitrogen budgets in an isoprene- and monoterpene-rich atmosphere: Constraints from aircraft (SEAC⁴RS) and ground-based (SOAS) observations in the Southeast US. *Atmospheric Chemistry and Physics*, *16*(9), 5969–5991. <https://doi.org/10.5194/acp-16-5969-2016>
- Forester, P., Artaxo, P., Berntsen, T., Betts, R., Fahey, D. W., Haywood, J., et al. (2007). Changes in Atmospheric Constituents and in Radiative Forcing. In S. Solomon, D. Qin, M. Manning, Z. Chen, M. Marquis, K. B. Averyt, et al. (Eds.), *Climate Change 2007: The Physical Science*

- Bases. Contribution of Working Group I to the Fourth Assessment Report of the Intergovernmental Panel on Climate Change* (pp. 131–217). Cambridge, United Kingdom and New York, NY, USA: Cambridge University Press.
<https://doi.org/10.1103/PhysRevB.77.220407>
- Fry, J. L., Kiendler-Scharr, A., Rollins, A. W., Wooldridge, P. J., Brown, S. S., Fuchs, H., et al. (2009). Organic nitrate and secondary organic aerosol yield from NO₃ oxidation of β-pinene evaluated using a gas-phase kinetics / aerosol partitioning model. *Atmospheric Chemistry and Physics*, 9, 1431–1449.
- Griffin, R. J., Cocker, D. R., Flagan, R. C., & Seinfeld, J. H. (1999). Organic aerosol formation from the oxidation of biogenic hydrocarbons. *Journal of Geophysical Research*, 104, 3555–3567.
- Hallquist, M., Wängberg, I., Ljungström, E., Barnes, I., & Becker, K. H. (1999). Aerosol and product yields from NO₃ radical-initiated oxidation of selected monoterpenes. *Environmental Science and Technology*, 33(4), 553–559.
<https://doi.org/10.1021/es980292s>
- Lee, B. H., Mohr, C., Lopez-Hilfiker, F. D., Lutz, A., Hallquist, M., Lee, L., et al. (2016). Highly functionalized organic nitrates in the southeast United States: Contribution to secondary organic aerosol and reactive nitrogen budgets. *Proceedings of the National Academy of Sciences*, 113(6), 1516–1521. <https://doi.org/10.1073/pnas.1508108113>
- Ng, N. L., Kwan, A. J., Surratt, J. D., Chan, A. W. H., Chhabra, P. S., Sorooshian, A., et al. (2008). Secondary organic aerosol (SOA) formation from reaction of isoprene with nitrate radicals (NO₃). *Atmospheric Chemistry and Physics*, 8(14), 4117–4140. <https://doi.org/10.5194/acp-8-4117-2008>
- Ng, N. L., Brown, S. S., Archibald, A. T., Atlas, E., Cohen, R. C., Crowley, J. N., et al. (2017). Nitrate radicals and biogenic volatile organic compounds: oxidation, mechanisms, and organic aerosol. *Atmospheric Chemistry and Physics*, 17(3), 2103–2162.
<https://doi.org/10.5194/acp-17-2103-2017>
- Perring, A. E., Bertram, T. H., Farmer, D. K., Wooldridge, P. J., Dibb, J., Blake, N. J., et al. (2010). The production and persistence of ΣRONO₂ in the Mexico City plume. *Atmospheric Chemistry and Physics*, 10(15), 7215–7229. <https://doi.org/10.5194/acp-10-7215-2010>
- Perring, A. E., Pusede, S. E., & Cohen, R. C. (2013). An observational perspective on the atmospheric impacts of alkyl and multifunctional nitrates on ozone and secondary organic aerosol. *Chemical Reviews*, 113(8), 5848–70. <https://doi.org/10.1021/cr300520x>
- Pope III, C. A. (2007). Mortality effects of longer term exposures to fine particulate air pollution: Review of recent epidemiological evidence. *Inhalation Toxicology*, 19(sup1), 33–38.
<https://doi.org/10.1080/08958370701492961>
- Pye, H. O. T., Luecken, D. J., Xu, L., Boyd, C. M., Ng, N. L., Baker, K. R., et al. (2015). Modeling the Current and Future Roles of Particulate Organic Nitrates in the Southeastern United States. *Environmental Science & Technology*, 49(24), 14195–14203.
<https://doi.org/10.1021/acs.est.5b03738>
- Rollins, A. W., Browne, E. C., Pusede, S. E., Wooldridge, P. J., Gentner, D. R., Goldstein, A. H., et al. (2012). Evidence for NO_x Control over Nighttime SOA Formation. *Science*, 267(September), 1210–1212.
- Rosen, R. S., Wood, E. C., Wooldridge, P. J., Thornton, J. A., Day, D. A., Kuster, W., et al. (2004). Observations of total alkyl nitrates during Texas Air Quality Study 2000: Implications for O₃

and alkyl nitrate photochemistry. *Journal of Geophysical Research*, 109(D7), D07303.
<https://doi.org/10.1029/2003JD004227>

Wang, H., Lu, K., Guo, S., Wu, Z., Shang, D., Tan, Z., et al. (2018). Efficient N₂O₅ Uptake and NO₃ Oxidation in the Outflow of Urban Beijing. *Atmospheric Chemistry and Physics Discussions*, (3), 1–27. <https://doi.org/10.5194/acp-2018-88>

Chapter 2

Nighttime chemistry is a significant RONO₂ source in the Colorado Northern Front Range Metropolitan Area

2.1 Introduction

Alkyl nitrates are a group of compounds sharing the chemical formula RONO₂ whose production is a sink for the important atmospheric oxidant NO_x (NO + NO₂). NO_x contributes to the formation of ozone (O₃), a harmful pollutant that is a respiratory irritant and damages crop yields. In order to understand the efficacy of NO_x at forming ozone in a region, it is important to understand its lifetime against loss processes, including the production of RONO₂. Previous studies have shown that RONO₂ can form a significant portion of the total of NO_x loss products (Day et al., 2003), but they are the least well understood among them. As NO_x pollution decreases in urban regions, alkyl nitrates will become a more significant influence on NO_x chemistry (Perring et al., 2013).

The formation of alkyl nitrates follows two different chemical oxidation pathways, one initiated by OH during the daytime, and the other initiated by NO₃ at nighttime (Perring et al., 2013). Ozone is formed during the OH-initiated sequence that forms alkyl nitrates, but no ozone is formed during the NO₃-initiated reactions, which are a net O_x sink (O_x = O₃ + NO₂). Because of this, nighttime and daytime processes both influence alkyl nitrate concentrations, but daytime production rates of alkyl nitrates are correlated with ozone and nighttime production may be anticorrelated.

2.1.1 Daytime alkyl nitrate formation pathway

During the daytime, RONO₂ are produced from the oxidation of volatile organic compounds (VOCs, RH) and subsequent reaction with NO as in reactions R1-R2a. (If the VOC is an alkane, the OH will abstract a hydrogen followed by addition of an O₂, as shown in reaction R1. Otherwise the OH will react by addition, again followed by addition of an O₂ but without formation of H₂O.)



However, the major path for reaction R2 is not to produce RONO₂ but an RO and NO₂ (reaction R2b), which generally go on to form 2 ozone molecules (R3-R5).





The ratio of ozone production to RONO_2 production is related to the branching ratio (α) between the minor and major pathways of reaction R2, defined as $\alpha = k_{2a} / (k_{2a} + k_{2b})$. If α is small, more ozone will be formed from the oxidized VOCs, whereas a larger α would more frequently divert RO_2 to a nitrate termination product, suppressing ozone production. Values of α are generally smallest for small molecules, such as short-chain alkanes, and larger for longer and less saturated molecules. Therefore, ozone production is suppressed more in the presence of larger VOCs than with smaller ones.

2.1.2 Nighttime alkyl nitrate formation pathway

Alkyl nitrates are formed by a different chemical pathway at night. Without sunlight to produce OH, a different oxidant drives these reactions. At all times of day, NO_2 can react with O_3 to form NO_3 as in reaction 6. During the day, NO_3 is rapidly photolyzed, but at night it is long-lived enough to react with alkenes to form alkyl nitrates.



The product in R7 is then stabilized by addition of O_2 followed by another radical such as HO_2 , RO_2 , or another NO_3 (Perring et al., 2013). Since this nighttime process is an addition reaction and often occurs with larger molecules such as monoterpenes, nighttime-produced alkyl nitrates are heavier and more readily partition into aerosol (Fry et al., 2009). NO_3 -initiated H-abstraction is possible at night but is too slow to be considered significant (Perring et al., 2013). While NO_3 can react with species other than alkenes, previous examples have shown that 90% of NO_3 loss is to reaction with alkenes (Edwards et al., 2017).

2.1.3 Alkyl nitrates in Colorado

Here we present a study of the sources of alkyl nitrates in the Colorado Northern Front Range Metropolitan Area (NFRMA). This region comprises the urban area around Denver as well as more rural areas with booming oil and natural gas activity to the northeast. It has been well established that the air in the Colorado NFRMA is influenced by the oil and natural gas industry, which in particular causes elevated levels of alkanes (Abeleira et al., 2017, 2018; Bahreini et al., 2018; Cheadle et al., 2017; Gilman et al., 2013; McDuffie et al., 2016; Pétron et al., 2012, 2014; Swarthout et al., 2013). Swarthout et al. (2013) found that non-methane VOCs from oil and natural gas activity in the region comprised ~24% of OH reactivity. Using summer observations with a box model, McDuffie et al. (2016) found that 50% of VOC OH reactivity was attributable to alkanes from oil and natural gas activity. Abeleira et al. (2017) found 40 – 60% of VOC OH reactivity was due to oil and natural gas. Since alkyl nitrates are formed from VOCs, much of the focus on alkyl nitrates in the region has been on those derived from oil and natural gas.

In an effort to study alkyl nitrates derived from oil and natural gas activity, Abeleira et al. (2018) measured select $C_1 - C_5$ $RONO_2$ in the Colorado NFRMA and found good agreement between measurements and model for the production and loss of these species. These simpler alkyl nitrates are derived from alkanes that have been shown to be largely emitted from oil and natural gas activity (Gilman et al., 2013). However, these $RONO_2$ do not represent the entirety of alkyl nitrates in the region. While Abeleira et al. (2017) found that 40 – 60% of VOC OH reactivity was attributable to oil and natural gas activity, this only constitutes around half of the reactivity with the rest attributable to biogenic VOCs, which were on average 21% of VOC OH reactivity, and other anthropogenic activity. Abeleira et al. (2018) found that the $C_1 - C_5$ alkyl nitrate species measured are dominated by daily photochemistry with little carry over from previous days, but none of the species measured would be formed by the nighttime process or from larger or more functionalized VOCs by the daytime process.

Individual alkyl nitrates are typically measured by collecting samples for detection by gas chromatography, in which case the number of speciated $RONO_2$ measured is limited as each must be calibrated for and detected individually (Abeleira et al., 2018; Flocke et al., 1991; Perring et al., 2013; Swanson et al., 2003). Measurements of total alkyl nitrates by thermal dissociation laser-induced fluorescence are not speciated but give a total measurement that can give an overall picture of alkyl nitrate chemistry (Day et al., 2002). Here we use total alkyl nitrate ($\Sigma RONO_2$) measurements to examine the sources of alkyl nitrates. We show an example in the Colorado NFRMA where nighttime NO_3 -initiated chemistry is more significant than expected. We explore the consequences of this conclusion for interpreting $\Sigma RONO_2$ observations.

2.2 Observations

The Front Range Air Pollution and Photochemistry Experiment (FRAPPE) took place in the NFRMA region in Colorado during July – August 2014. Measurements were taken on the NSF/NCAR C-130 aircraft platform based out of Rocky Mountain Metropolitan Airport in Jefferson County. Fifteen flights were flown primarily between 10:00AM and 8:00PM local MDT time. We use data in this analysis within the bounds of 39.5N to 40.65N latitude and 254.75 E to 255.5 E longitude. We only use data at or below 2.5 km ASL which is approximately 1 km AGL, thus restricting the analysis to air in the planetary boundary layer.

Measurements of NO_2 and $\Sigma RONO_2$ were by thermal dissociation laser-induced fluorescence (TD-LIF) (Day et al., 2002). CO , CH_4 , and VOC measurements were by a trace organic gas analyzer (TOGA) and whole air sampler (WAS) (Apel et al., 2003, 2010; Colman et al., 2001). OH , HO_2 , and RO_2 were measured by a HO_x chemical ionization mass spectrometer (CIMS) (Hornbrook et al., 2011; Mauldin et al., 2001). Total and inorganic nitrate aerosol were measured by aerosol mass spectrometry (AMS) and particle-into-liquid sampling (PILS), respectively (Jayne et al., 2000; Orsini et al., 2003). Additional measurements of NO_x , O_3 , and temperature are taken from the CAMP and Boulder Atmospheric Observatory (BAO) ground sites. The CAMP site is in downtown Denver and is located near some of the highest urban emissions. NO_x and O_3 are measured by the EPA Federal Reference Method using

chemiluminescence (Dunlea et al., 2007). The BAO site is 20 miles north of Denver at the transition from urban to rural. At the BAO site, NO_x and O_3 are measured by cavity ring-down spectroscopy (McDuffie et al., 2016).

2.3 Results

The average daytime ΣRONO_2 concentration within the boundary layer is 964 pptv with concentrations up to 3.76 ppbv. Concentrations are highest during the middle of the day, from 11:00AM – 1:00PM local time with an average concentration of 1191 pptv. Geographically, the highest concentrations are observed around Denver with a small hotspot near Greeley (Figure 2.1). Particle organic nitrate, taken as the difference between total nitrate aerosol and inorganic nitrate aerosol, comprises on average 23% of ΣRONO_2 , although it varies widely. Concentrations of organic nitrate aerosol were observed as high as 1.8 ppbv.

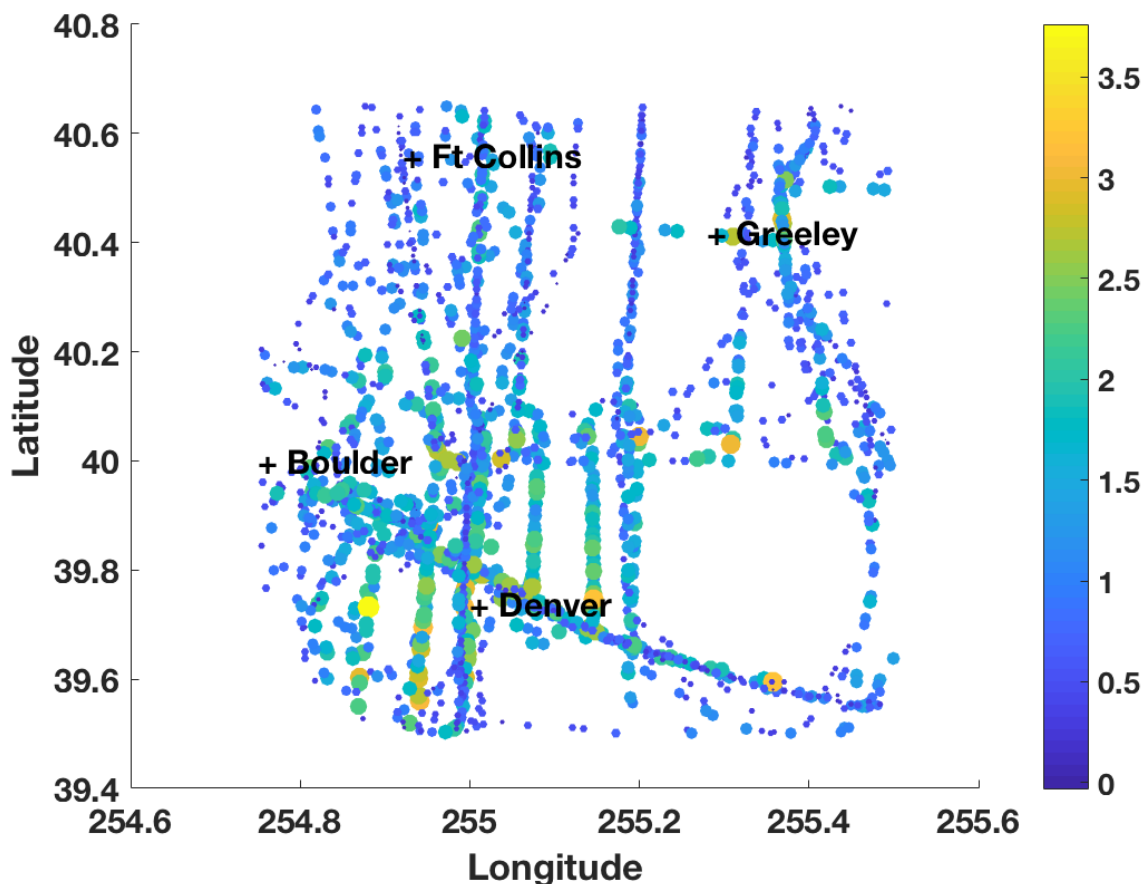


Figure 2.1. Geographical distribution of ΣRONO_2 from FRAPPE flight tracks, colored and sized by ΣRONO_2 (ppbv).

2.3.1 Hypotheses for lack of morning correlation between ozone and alkyl nitrates

Figure 2.2 shows the lack of correlation of O_x and ΣRONO_2 during the 10:00AM hour. From 10:00AM – 11:00AM, the relationship is essentially flat, showing locations with high RONO_2 that

are not associated with high ozone. All photochemical ΣRONO_2 production mechanisms also produce ozone. Using a branching ratio α of 3%, we would expect approximately 67 ppbv of ozone production for every 1 ppbv of RONO_2 . Figure 2.2 shows measurements greater than 1 ppbv of ΣRONO_2 with ozone barely above background levels.

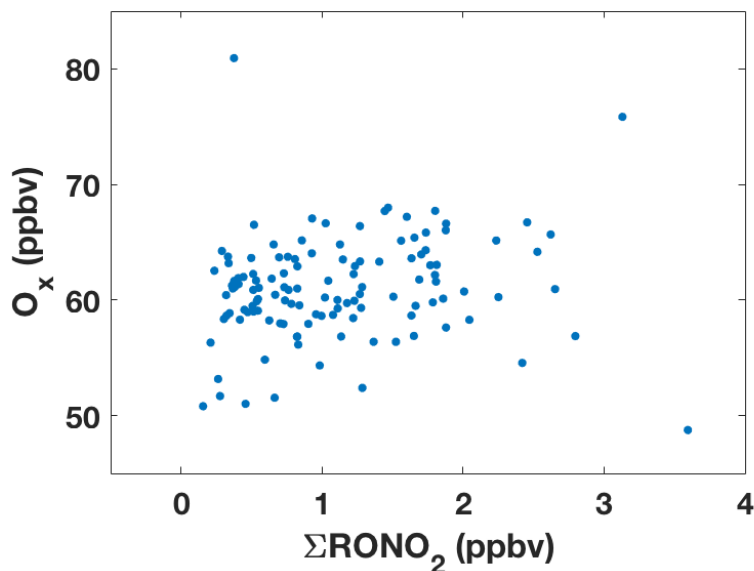


Figure 2.2. O_x vs. ΣRONO_2 for FRAPPE from 10:00AM – 11:00AM local MDT time.

There are a few possible explanations for this lack of correlation, which include (1) different timescales for loss of O_x and RONO_2 , (2) mixing of different air masses, and (3) a large non-photochemical source of ΣRONO_2 , such as direct emissions or nighttime production. We explore these possibilities below.

2.3.1.1 Different timescales for loss

Daytime chemical loss of ozone includes reaction with OH, HO_2 , NO_2 , and photolysis followed by reaction with water. These chemical losses give an average O_3 loss rate of 2%/hr. Chemical loss of alkyl nitrates can happen via reaction with OH, photolysis, or hydrolysis to form nitric acid. The lifetime of alkane-derived alkyl nitrates against loss to OH and photolysis has been shown to be on the order of days to weeks at this latitude in the summer, so these losses are unlikely to be significant for the bulk of alkyl nitrates in the region that are alkane-derived (Clemmitshaw et al., 1997).

Chemical loss is faster for larger and functionalized alkyl nitrates, so biogenic-derived alkyl nitrates would contribute disproportionately to total loss. Isoprene-derived nitrates were shown to have a lifetime on the order of 2 hours in an isoprene-dominated Alabama forest (Romer et al., 2016). As discussed below, biogenic VOCs contribute to on average about a quarter of alkyl nitrate production, although it varies by location, and the bulk of these come from isoprene. The percentage of total ΣRONO_2 that is isoprene-derived varies from 0 to 50%,

so the ΣRONO_2 chemical loss could vary from 0 to 25%/hr. Alkyl nitrate chemical loss would only be substantial in areas with a lot of biogenic influence, which is not the case in locations with heavy urban emissions. Based on just daytime loss, a loss rate for ozone of 2%/hr and for alkyl nitrates of 25%/hr cannot account for the lack of correlation in Figure 2.2 as the greater loss rate for alkyl nitrates would cause lower alkyl nitrate concentrations than expected compared to ozone rather than the higher concentrations that were observed.

Nighttime loss is more likely the source for a difference in loss rates. At night, the OH and photolysis loss mechanisms for alkyl nitrates turn off. Since ozone can no longer be formed by NO_2 photolysis at night, reaction with NO to form NO_2 that in the daytime results in no net loss of ozone is now a large loss. Kaser et al. (2017) observed an ozone loss of around 20 ppbv on average overnight at a site in the region during FRAPPE. Ozone and alkyl nitrates should still be correlated during the day regardless of their starting concentrations at sunrise, but if the loss of ozone varies across the region, with greater loss in urban areas with high NO, the correlation would be distorted since measurements from a variety of locations are included in the correlation.

Deposition is another potential source of loss for ozone and alkyl nitrates. A previous study estimated deposition rates for HNO_3 during FRAPPE and found substantial deposition at a rate of 0.07 hr^{-1} with a deposition velocity of 2 cm s^{-1} (Ebben et al., 2017). Ozone and alkyl nitrates are not as sticky as HNO_3 , so their deposition velocities should be slower. Using the deposition velocity of 0.5 cm s^{-1} from Cleary et al. (2005), similar to the 0.47 cm s^{-1} from Lenschow et al. (1981), for both ozone and alkyl nitrates and a 1 km boundary layer, we calculate a lifetime for loss to deposition of 55 hrs, indicating that loss to deposition should be insignificant on the timescale of this analysis. Additionally, if ozone and alkyl nitrates have a similar timescale for deposition, this loss cannot explain their lack of correlation in the morning.

Overall, chemical loss and deposition are minimal and unlikely to have a large effect on the correlation of ozone and alkyl nitrates with the exceptions of greater alkyl nitrate loss in biogenic-influenced areas and that regional variation in overnight ozone loss could create different morning concentration starting points that could distort the correlation.

2.3.1.2 Mixing of different air masses

The effect of mixing and boundary layer expansion is another possible explanation for the lack of morning correlation between ozone and alkyl nitrates. Pfister et al. (2017) demonstrated that this region is generally very well mixed due to recirculation from upslope and downslope patterns and highly variable local winds within that pattern. At night, they found that air full of urban emissions from Denver generally migrated northeast near oil and natural gas activity, and then in the morning the plume returned bringing a mixture of emissions back towards the city.

One effect of mixing that could affect the correlation of ozone and alkyl nitrates is the growing boundary layer in the morning. Kaser et al. (2017) examined the effect of the expanding boundary layer on ozone concentrations during the same experiment. The effect of

entrainment depends on the difference in concentration above and below the boundary layer. In the morning, the boundary layer is depleted of ozone due to overnight titration by NO, with the residual layer less so due to its isolation from the surface. As the boundary layer expands, the higher ozone concentrations at higher altitudes increase ozone concentrations beyond the increase from production. Later in the day, when production has increased concentrations in the boundary layer enough to overcome the difference, entrainment would switch to decreasing ozone concentrations. This pattern can change depending on background concentrations.

Kaser et al. (2017) found a couple days where particularly clean air came into the region such that in the morning, boundary layer expansion decreased ozone concentrations due to the clean air aloft. The effect of the growing boundary layer on ozone concentrations and therefore on the correlation of ozone and alkyl nitrates depends on the cleanliness of air aloft. One day with clean air aloft, July 21, had measurements in the 10:00AM hour that showed the pattern in Figure 2.2 where ozone only varied between 60 – 68 ppbv while alkyl nitrates varied from 0.8 – 2.2 ppbv. It is conceivable that the boundary layer expansion into cleaner air made ozone concentrations grow slower than expected compared to alkyl nitrates. However, the lack of correlation is also observed on days that higher ozone aloft, so pattern in Figure 2.2 can't be entirely due to mixing with ozone-depleted air aloft.

The effect of boundary layer growth on alkyl nitrates also depends on the air aloft. If the residual layer contains the ingredients for nighttime formation, concentrations of alkyl nitrates could be high such that the concentration in the boundary layer increases as it expands. Alternatively, if air aloft is flushed out and the boundary layer expands into cleaner air, the concentration would decrease. The direction of the effect of the growing boundary layer would be the same for both ozone and alkyl nitrates, as their concentrations would both be higher in stagnant air and lower in clean air, but the effect on their correlation may not be proportional.

Overall, when it comes to loss by chemistry, deposition, or mixing, we don't find enough evidence to explain the lack of correlation in Figure 2.2. Chemical ozone loss is likely insignificant. While alkyl nitrate loss is less well constrained and most likely greater than ozone loss, it cannot be the reason for the unrealistic observed relationship as significant alkyl nitrate loss would mean lower alkyl nitrates per ozone than expected, while the opposite is observed.

Evidence that loss and mixing partially explain the observations includes a scenario where different areas experience different nighttime depletion of ozone, such that in areas with urban emissions, ozone starts out lower than in more rural areas. In this scenario, ozone produced concurrently with alkyl nitrates in urban areas could result in the same concentration as rural areas where less ozone is produced along with fewer alkyl nitrates but ozone concentrations were higher to begin with. The scale of this possible scenario cannot explain the scale of alkyl nitrates observed. If an additional 20 ppbv of ozone were produced in an urban area compared to a rural one, at a 3% branching ratio only 300 pptv of extra alkyl nitrates would be formed. This cannot explain observations where alkyl nitrates have a difference of 2 ppbv at the same ozone concentration, and also assumes that the region is not well-mixed, which is not the case

(Pfister et al., 2017). Entrainment of air as the boundary layer expands can distort the correlation in ozone and alkyl nitrate concentrations, but again cannot alone account for such a large difference in alkyl nitrates without an additional source. We therefore conclude that a large non-photochemical source of ΣRONO_2 is responsible for the range of ΣRONO_2 observations at constant ozone.

2.3.1.3 Direct emissions

Little evidence has been shown for direct emissions of RONO_2 that would be relevant for this study. Chuck et al. (2002) showed evidence of C_1 and C_2 alkyl nitrates from the ocean, which would not be an important source in a land-locked state. The other situation where direct emissions have been observed is from biomass burning in Australia by Simpson et al. (2002). In this case, $\text{C}_1 - \text{C}_4$ alkyl nitrates were observed, but the air in Colorado during these studies was largely unaffected by any fire emissions (Bahreini et al., 2018). Additionally, the variable ΣRONO_2 at constant O_3 in the morning is observed on many days while influence of biomass burning would likely vary across the campaign. It is unlikely a source of multiple ppbv of direct emissions would have been previously undetected, so we eliminate this possibility.

2.3.1.4 Nighttime RONO_2 production

A source of RONO_2 that is consistent with the observations in Figure 2.2 is nighttime production by reaction of NO_3 with alkenes. We estimate the nighttime formation of RONO_2 by looking at the availability of the reactants NO_3 and alkenes. While NO_3 is short-lived once it is produced, the amount of NO_x lost to ozone over the night is an integrated total of NO_3 available for reaction with alkenes. We estimate production of NO_3 using concentrations of reactants at the start of the night using equation 2.1:

$$\text{NO}_3 \text{ production} = \text{NO}_{x,\text{initial}} - \text{NO}_{x,\text{initial}} * e^{-t(\text{O}_3 * k_{\text{NO}+\text{O}_3})} \quad (2.1)$$

For a 10-hour night and 60 ppbv ozone approximately two-thirds of NO_x would be converted to NO_3 overnight. We use NO_2 and O_3 observations after 5:00PM local time to estimate potential for NO_3 production. NO_3 integrated production is calculated as 1.59 ppbv on average, with values up to 9.39 ppbv. The areas of highest potential for NO_3 are between Boulder and Denver, the same region that saw higher ΣRONO_2 values. At the surface, at the CAMP site in downtown Denver, 12 ppbv NO_3 would be produced on average. At the BAO site, the average production of NO_3 is 1.6 ppbv.

Since the integrated NO_3 production, especially at CAMP, is sufficient for producing the observed ΣRONO_2 , we next consider whether the alkenes are sufficient. Measurements on the C-130 of anthropogenic alkenes included ethene, propene, and butene (see Table 2.1). These are likely 70-85% of total anthropogenic alkenes (Gentner et al., 2013; Perring et al., 2010; Rosen et al., 2004). Adding the measured biogenic alkenes listed in Table 2.1, the average alkene measurement is 513 pptv with a maximum of 2.22 ppbv. Geographically, the highest alkene concentrations occur around downtown Denver where the highest RONO_2 are also

observed. RONO₂ yields in the reaction of NO₃ with alkenes are in the range 10-80% (Perring et al., 2013). Using the yield for propene of 58% (Barnes et al., 1990), the observed alkenes give an ΣRONO₂ production range of about 300 – 1.3 ppbv overnight, which could account for up to half of the concentrations observed in the 10:00AM hour.

On average 67% of alkene concentrations are from the three anthropogenic alkenes measured, with 33% from biogenic. At night, biogenic emissions are lower, so the alkenes available would be reduced at night in the boundary layer compared to daytime. However, the estimate of alkyl nitrates produced from anthropogenic alkenes is low, as anthropogenic alkenes are present that were not among the three measured. Additionally, the lower boundary layer height at night will result in greater concentrations for any nighttime alkene emissions than for equivalent emissions during the daytime, increasing reaction rates. Biogenic and anthropogenic alkene emissions isolated in the residual layer will also contribute to overnight production.

While nighttime concentrations of alkenes are poorly constrained, estimates based on daytime concentrations show that the reaction of NO₃ and alkenes can explain much of the observed variation of ΣRONO₂ at a constant ozone at 10:00AM, up to around 50%. Higher concentrations may be a result of buildup of ΣRONO₂ during stagnation events.

2.3.2 Daytime RONO₂ production

Daytime production of ΣRONO₂ was calculated as:

$$P(\Sigma RONO_2) = \sum_i \alpha_i [VOC_i] k_{VOC_i+OH} [OH] f_{NO} \quad (2.2)$$

Individual VOC measurements and their corresponding rate constants and α branching ratios used are shown in Table 2.1. OH concentrations were measured, and f_{NO} is the fraction of RO₂ radicals that react with NO.

The average instantaneous ΣRONO₂ daytime production rate in the boundary layer is 60 pptv/hr with a maximum of 578 pptv/hr. Alkanes are the greatest daytime source of RONO₂, contributing to 66% of RONO₂ production as shown in Figure 2.3. Of those alkanes, n/i-butane and n/i-pentane are the largest contributors. This is consistent with previous studies in the area that show that alkanes account for a large portion of VOC reactivity in the region (McDuffie et al., 2016). The next largest contributor at 24% is biogenic species, of which most contribution is from isoprene. Previous studies have shown a variable prevalence of isoprene in the Colorado Front Range that is correlated with changing drought conditions (Abeleira et al., 2017).

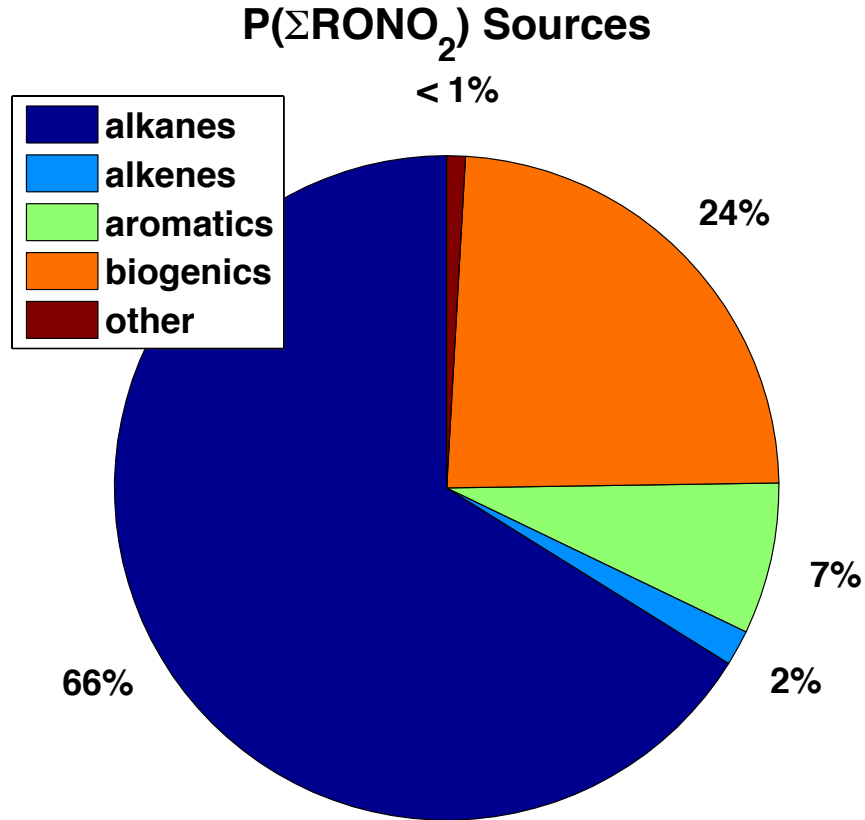


Figure 2.3. Composition of VOCs that RONO₂ are derived from in the daytime during FRAPPE from equation 2.2.

Since ambient air contains VOCs with a variety of α 's, it is a common approach to determine an effective average (α_{eff}) for the mixture. An effective α can be calculated from individual α_i values weighted by the corresponding VOC concentrations as in equation 2.3:

$$\alpha_{eff} = \frac{\sum_i \alpha_i [VOC_i] k_{VOC_i+OH}}{\sum_i [VOC_i] k_{VOC_i+OH}} \quad (2.3)$$

The calculated average α_{eff} for the region is 0.014, or 1.4%. This value is low compared to α_{eff} 's found in other major cities, including Houston (4.5%) and Mexico City (2.6%) (Perring et al., 2010, 2013; Rosen et al., 2004). Since RONO₂ production is dominated by C₄ – C₅ alkanes with α 's on the order of 0.07-0.1, this low effective α is due to an abundance of low α species such as CO and formaldehyde that contribute to VOC reactivity and ozone production but not to nitrate formation.

Ozone is produced concurrently with RONO₂ in the OH-initiated process. The photochemical production of these species is correlated as shown in equation 2.4:

$$\frac{P_{O_3}}{P_{RONO_2}} \approx \frac{2(1-\alpha_{eff})}{\alpha_{eff}} \approx \frac{2}{\alpha_{eff}} \quad (2.4)$$

The approximation that the change in concentrations ($\Delta O_3/\Delta RONO_2$) follow the production rates, which has been widely used in other analyses (Cleary et al., 2005; Day et al., 2003; Perring et al., 2010, 2013; Rosen et al., 2004), assumes that production by daytime mechanisms is fast and larger than other production or loss mechanisms. That this approximation does not hold for this dataset is shown in Figure 2.2, where large $\Sigma RONO_2$ concentrations without an increase in ozone were attributed to the influence of nighttime production. Later in the day, correlation with ozone is observed, but the scale of that correlation is still inconsistent with the widely-used approximation.

Figure 2.4 shows O_x and $\Sigma RONO_2$ concentrations from 2:00PM – 3:00PM local time. An inference of the branching ratio, α , from the slope of the correlation results in an implausibly high value of 8% compared to the 1.4% calculated from the VOC mix (red line). The difference suggests the correlation is a result of chemistry as well as mixing that occurs during the day with $RONO_2$ that was previously present from earlier daytime production, nighttime production, or carryover from previous days (although Abeleira et al. (2018) found little carryover from previous days in the region for smaller $C_1 - C_5$ alkyl nitrates). It was determined this discrepancy is not due to loss of the species as discussed above, as $\Sigma RONO_2$ is expected to have a faster loss rate than O_x , and if loss rates were significant, this would result in an erroneously high slope rather than an erroneously low one, as observed.

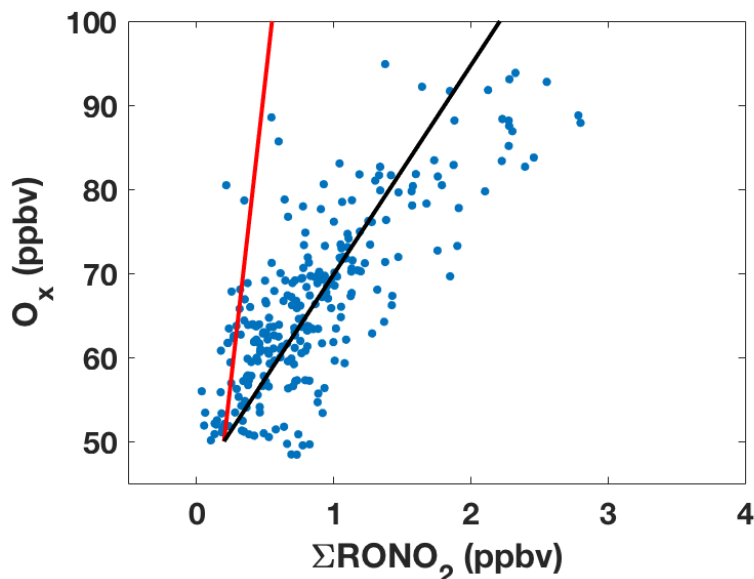


Figure 2.4. O_x vs. $\Sigma RONO_2$ for FRAPPE between local MDT time 2:00PM – 3:00PM. The black line corresponds with an α of 8%. The red line indicates what the slope would look like using the calculated α of 1.4%.

These measurements represent a variety of days and locations, so measurements at 2:00PM in Figure 2.4 don't necessarily have a corresponding measurement at 10:00AM in Figure 2.2. In other words, concentrations of 3 ppbv observed at 2:00PM aren't necessarily from the same location as concentrations of 3 ppbv observed at 10:00AM, so it is not necessarily the case that

no RONO₂ were produced in that time. Measurements represent a campaign average and may have sampling biases where areas with higher or lower emissions may be measured more than others or at different times of day. The question of how concentrations evolve over the day and throughout the night would be better answered by stationary measurements of a full diel cycle. While several ground sites measure continuous ozone and NO_x, measurements of alkyl nitrates and a large variety of VOCs have been limited.

2.4 Conclusion

Evidence for contribution from the nighttime Σ RONO₂ production pathway includes sufficient production rates of NO₃ at night, particularly near the surface and closer to downtown Denver, and sufficient alkenes available for reaction. Other hypotheses to explain the lack of correlation between ozone and alkyl nitrates in the morning were shown to be insignificant or too small in scale to be a sufficient explanation. The relationship between RONO₂ and O₃ production has been used in many previous studies to determine the effect RONO₂ production has on the lifetime of NO_x and therefore on reducing O₃ production, but the lack of morning correlation between the species and evidence for significance of nighttime production in this location render this analysis inappropriate. It is the difference between the calculated branching ratio of 1.4% and the observed afternoon ratio of 8%, which is the difference between producing 143 ozone molecules per every alkyl nitrate and producing 25 ozone per alkyl nitrate, respectively. Previous studies using the assumption that relative daytime production rates of RONO₂ and O₃ are related to their concentrations have also found an effective α that is much greater than what was calculated from precursors (Perring et al., 2010). In some of these cases, the discrepancy may also be due to nighttime production and conclusions may need to be revisited.

Table 2.1. VOCs used for RONO₂ production calculation with α 's and rates for reaction with OH.

VOC	α	k_{OH}
Alkanes		
ethane	0.019 ^a	1.12e-11 x exp(-250/T) ^b
methane	0.0005 ^a	2.45e-12 x exp(-1775/T) ^j
propane	0.036 ^a	8.7e-12 x exp(-615/T) ^j
i-butane	0.096 ^a	1.16e-17 x T ² x exp(225/T) ^b
n-butane	0.077 ^a	9.8e-12 x exp(-425/T) ^b
i-pentane	0.07 ^a	1.23e-11 x exp(-362/T)
n-pentane	0.105 ^a	2.44e-17 x T ² x exp(183/T) ^b
2-methylpentane	0.097 ^a	1.96e-11 x exp(-383/T) ^l
3-methylpentane	0.109 ^a	1.77e-11 x exp(-330/T) ^l
n-hexane	0.141 ^a	1.53e-17 x T ² x exp(414/T) ^b
n-heptane	0.178 ^a	1.59e-17 x T ² x exp(478/T) ^b

2-2-dimethylbutane	0.152 ^a	$3.22e-11 \times \exp(-781/T)^b$
2-3-dimethylbutane	0.152 ^h	$1.24e-17 \times T^2 \times \exp(494/T)^b$
cyclopentane	0.045 ^a	$4.97e-12^a$
methylcyclopentane	0.14 ^a	$5.60e-12^a$
cyclohexane	0.16 ^a	$2.88e-17 \times T^2 \times \exp(309/T)^b$
methylcyclohexane	0.17 ^a	$9.64e-12^m$
2-4-dimethylpentane	0.1 ⁱ	$5.26e-12^o$
2-2-4-trimethylpentane	0.14 ^a	$3.34e-12^m$
n-octane	0.226 ^a	$2.76e-17 \times T^2 \times \exp(378/T)^b$
Alkenes		
ethene	0.0086 ^a	See source ^j
propene	0.015 ^a	$4.85e-12 \times \exp(504/T)^k$
i-butene and 1-butene	0.034 ^a	Ave. of $6.55e-12 \times \exp(467/T)$, $9.4e-12 \times \exp(505/T)^{b,k}$
Aromatics*		
benzene	0.03 ^e	$2.3e-12 \times \exp(-190/T)^b$
toluene	0.03 ^e	$1.8e-12 \times \exp(340/T)^b$
ethylbenzene	0.03 ^e	$7e-12^b$
m-xylene and p-xylene	0.03 ^e	Ave. of $2.31e-11$, $1.43e-11^b$
o-xylene	0.03 ^e	$1.36e-11^b$
1-2-3-trimethylbenzene	0.03 ^e	$3.27e-11^b$
1-2-4-trimethylbenzene	0.03 ^e	$3.25e-11^b$
1-3-5-trimethylbenzene	0.03 ^e	$5.67e-11^b$
2-ethyltoluene	0.03 ^e	$1.19e-11^b$
3-ethyltoluene	0.03 ^e	$1.86e-11^b$
4-ethyltoluene	0.03 ^e	$1.18e-11^b$
Biogenics		
isoprene	0.09 ^d	$25.4e-12 \times \exp(410/T)^k$
methacrolein	0.15 ^a	$8.0e-12 \times \exp(380/T)^b$
methyl vinyl ketone	0.11 ^a	$1.88e-11^b$
2-methyl-3-buten-2-ol	0.05 ^b	$8.1e-12 \times \exp(610/T)^b$
α -pinene	0.26 ^f	$12.1e-12 \times \exp(444/T)^k$
camphene	0.24 ^g	$5.33e-11^m$
β -pinene	0.24 ^a	$23.8e-12 \times \exp(357/T)^l$

limonene and carene	0.23 ^a	Ave. of $4.28e-11 \times \exp(401/T)$, $8.7e-11^{b,n}$
Other		
CO	0 ^a	$1.5e-13(1+0.6(M/2.69e19)(T/273))^j$
CH ₃ OOH	0.0006 ^b	$3.8e-12 \times \exp(200/T)^j$
HCOOH	0 ^b	$4.0e-13^j$
CH ₃ COOH	0.001 ^b	$8e-13^b$
formaldehyde	0 ^a	$5.5e-12 \times \exp(125/T)^j$
acetaldehyde	0 ^a	$4.7e-12 \times \exp(345/T)^b$
butanal	0.013 ^b	$6.0e-12 \times \exp(410/T)^b$
methanol	0 ^c	$2.9e-12 \times \exp(-345/T)^j$
ethanol	0 ^c	$3.0e-12 \times \exp(20/T)^b$
propanal	0 ^b	$4.9e-12 \times \exp(405/T)^j$
acrolein	0.0033 ^b	$2.00e-11^b$
acetone	0 ^c	$8.8e-12 \times \exp(-1320/T) + 1.7e-14 \times \exp(423/T)^b$
methyl ethyl ketone	0.015 ^b	$1.5e-12 \times \exp(-90/T)^b$
ethyne	0 ^b	See source ^b

Sources for α 's and rates: ^aPerring et al. (2013), ^bMaster Chemical Mechansim (MCM) v3.3, ^cPerring et al. (2010), ^dXiong et al. (2015), ^eElrod, (2011)*, ^fRindelaub et al. (2015), ^gassumed to be the same as β -pinene, ^hassumed to be the same as 2-2-dimethylbutane, ⁱassumed to be the same as 2-2-dimethylpentane from Perring et al. (2013), ^jSander et al. (2011), ^kAtkinson et al. (1992), ^lWilson et al. (2006), ^mAtkinson & Arey (2003), ⁿAtkinson (1986), ^oAtkinson et al. (1984). * See Appendix 3.A for explanation of adaptation of α for aromatics.

2.A Appendix: Aromatic branching ratios

One significant change in the literature α 's we use from those used in previous studies is our treatment of aromatic compounds. Up until recently, no aromatic α measurements had been made. Instead, estimates were used from the Master Chemical Mechanism (MCM), which gave values in the vicinity of 0.1 using the assumption that aromatics form nitrates using the same mechanism as non-aromatics. However, Elrod (2011) studied four aromatic species and found all of their α 's were around 0.03. His results suggested that these lower values are due to a ring-opening mechanism that is inherently different from how non-aromatics form nitrates. While previous studies have used a mixture of MCM aromatic estimates and Elrod's measured aromatic α 's, we used an α of 0.03 for all aromatics. While it is unlikely that all aromatics have this exact α , we see this as the better estimate based on the logic from Elrod's work that MCM estimates use an incorrect mechanism. The difference between these treatments of aromatic α 's is significant, as in this dataset it is the difference between aromatics accounting for 7% of RONO₂ production using 0.03 for all aromatics, as in Figure 2.3, and 20% using a mixture. It is

likely that other studies where aromatics were a significant player overestimated RONO₂ production and the calculated α_{eff} .

References

- Abeleira, A., Pollack, I. B., Sive, B., Zhou, Y., Fischer, E. V., & Farmer, D. K. (2017). Source Characterization of Volatile Organic Compounds in the Colorado Northern Front Range Metropolitan Area during Spring and Summer 2015. *Journal of Geophysical Research: Atmospheres*, *122*(6), 3595–3613. <https://doi.org/10.1002/2016JD026227>
- Abeleira, A., Sive, B., Swarthout, R. F., Fischer, E. V., Zhou, Y., & Farmer, D. K. (2018). Seasonality, sources and sinks of C₁ – C₅ alkyl nitrates in the Colorado Front Range. *Elementa: Science of the Anthropocene*, *6*(45).
- Apel, E. C., Hills, A. J., Lueb, R., Zindel, S., Eisele, S., & Riemer, D. D. (2003). A fast-GC/MS system to measure C₂ to C₄ carbonyls and methanol aboard aircraft. *Journal of Geophysical Research*, *108*(D20), 8794. <https://doi.org/10.1029/2002JD003199>
- Apel, E. C., Emmons, L. K., Karl, T., Flocke, F., Hills, a. J., Madronich, S., et al. (2010). Chemical evolution of volatile organic compounds in the outflow of the Mexico City Metropolitan area. *Atmospheric Chemistry and Physics*, *10*(5), 2353–2375. <https://doi.org/10.5194/acp-10-2353-2010>
- Atkinson, R. (1986). Kinetics and Mechanisms of the Gas-Phase Reactions of the Hydroxyl Radical with Organic Compounds under Atmospheric Conditions. *Chemical Reviews*, *86*(1), 69–201. <https://doi.org/10.1021/cr00071a004>
- Atkinson, R., & Arey, J. (2003). Atmospheric Degradation of Volatile Organic Compounds. *Chemical Reviews*, *103*(12), 4605–4638. <https://doi.org/10.1021/cr0206420>
- Atkinson, R., Aschmann, S. M., Carter, W. P. L., Winer, A. M., & Pitts, J. N. (1984). Formation of alkyl nitrates from the reaction of branched and cyclic alkyl peroxy radicals with NO. *International Journal of Chemical Kinetics*, *16*(9), 1085–1101. <https://doi.org/10.1002/kin.550160904>
- Atkinson, R., Baulch, D. L., Cox, R. a., R. F. Hampson, J., Kerr, J. a., Rossi, M. J., & Troe, J. (1992). Evaluated Kinetic and Photochemical Data for Atmospheric Chemistry: Supplement IV. IUPAC Subcommittee on Gas Kinetic Data Evaluation for Atmospheric Chemistry. *J. Phys. Chem. Ref. Data*, *21*, 1125. [https://doi.org/10.1016/1352-2310\(96\)87633-3](https://doi.org/10.1016/1352-2310(96)87633-3)
- Bahreini, R., Ahmadov, R., Mckeen, S. A., Vu, K. T., Dingle, J. H., Apel, E. C., et al. (2018). Sources and Characteristics of Summertime Organic Aerosol in the Colorado Front Range: Perspective from Measurements and WRF-Chem Modeling. *Atmospheric Chemistry and Physics*, *18*, 8293–8312. <https://doi.org/10.5194/acp-2018-57>
- Barnes, I., Bastian, V., Becker, K. H., & Tong, Z. (1990). Kinetics and products of the reactions of NO₃ with monoalkenes, dialkenes, and monoterpenes. *Journal of Physical Chemistry*, *94*(6), 2413–2419. <https://doi.org/10.1021/j100369a041> [doi]
- Cheadle, L. C., Oltmans, S. J., Pétron, G., Schnell, R. C., Mattson, E. J., Herndon, S. C., et al. (2017). Surface ozone in the Colorado Northern Front Range and the influence of oil and gas development during FRAPPE/DISCOVER-AQ in summer 2014. *Elementa: Science of the Anthropocene*, *5*(61). <https://doi.org/http://doi.org/10.1525/elementa.254>
- Chuck, A. L., Turner, S. M., & Liss, P. S. (2002). Direct Evidence for a Marine Source of C₁ and C₂

- Alkyl Nitrates. *Science*, 297, 1151–1154.
- Cleary, P. a., Murphy, J. G., Wooldridge, P. J., Day, D. A., Millet, D. B., McKay, M., et al. (2005). Observations of total alkyl nitrates within the Sacramento Urban Plume. *Atmospheric Chemistry and Physics Discussions*, 5(4), 4801–4843. <https://doi.org/10.5194/acpd-5-4801-2005>
- Clemitchaw, K. C., Williams, J., Rattigan, O. V, Shallcross, D. E., Law, K. S., & Cox, R. a. (1997). Gas-phase ultraviolet absorption cross-sections and atmospheric lifetimes of several C₂-C₅ alkyl nitrates. *Journal of Photochemistry and Photobiology A: Chemistry*, 102, 117–126. [https://doi.org/10.1016/S1010-6030\(96\)04458-9](https://doi.org/10.1016/S1010-6030(96)04458-9)
- Colman, J. J., Swanson, A. L., Meinardi, S., Sive, B. C., Blake, D. R., & Rowland, F. S. (2001). Description of the analysis of a wide range of volatile organic compounds in whole air samples collected during PEM-Tropics A and B. *Analytical Chemistry*, 73(15), 3723–3731. <https://doi.org/10.1021/ac010027g>
- Day, D. A., Wooldridge, P. J., Dillon, M. B., Thornton, J. A., & Cohen, R. C. (2002). A thermal dissociation laser-induced fluorescence instrument for in situ detection of NO₂, peroxy nitrates, alkyl nitrates, and HNO₃. *Journal of Geophysical Research*, 107(D6), 4046. <https://doi.org/10.1029/2001JD000779>
- Day, D. A., Dillon, M. B., Wooldridge, P. J., Thornton, J. A., Rosen, R. S., Wood, E. C., & Cohen, R. C. (2003). On alkyl nitrates, O₃, and the “missing NO_y.” *Journal of Geophysical Research*, 108(D16), 4501. <https://doi.org/10.1029/2003JD003685>
- Dunlea, E. J., Herndon, S. C., Nelson, D. D., Volkamer, R. M., San Martini, F., Sheehy, P. M., et al. (2007). Evaluation of nitrogen dioxide chemiluminescence monitors in a polluted urban environment. *Atmospheric Chemistry and Physics*, 7(10), 2691–2704. <https://doi.org/10.5194/acp-7-2691-2007>
- Ebben, C. J., Sparks, T. L., Wooldridge, P. J., Campos, T. L., Cantrell, C. A., Mauldin, R. L., et al. (2017). Evolution of NO_x in the Denver Urban Plume during the Front Range Air Pollution and Photochemistry Experiment. *Atmospheric Chemistry and Physics Discussions*, 1–13. <https://doi.org/10.5194/acp-2017-671>
- Edwards, P. M., Aikin, K. C., Dube, W. P., Fry, J. L., Gilman, J. B., De Gouw, J. A., et al. (2017). Transition from high- to low-NO_x control of night-time oxidation in the southeastern US. *Nature Geoscience*, 10(7), 490–495. <https://doi.org/10.1038/ngeo2976>
- Elrod, M. J. (2011). Kinetics Study of the Aromatic Bicyclic Peroxy Radical+ NO Reaction: Overall Rate Constant and Nitrate Product Yield Measurements. *The Journal of Physical Chemistry A*, 115(28), 8125–30. <https://doi.org/10.1021/jp204308f>
- Flocke, F., Volz-Thomas, A., & Kley, D. (1991). Measurements of alkyl nitrates in rural and polluted air masses. *Atmospheric Environment*, 25A(9), 1951–1960. [https://doi.org/10.1016/0960-1686\(91\)90276-D](https://doi.org/10.1016/0960-1686(91)90276-D)
- Fry, J. L., Kiendler-Scharr, A., Rollins, A. W., Wooldridge, P. J., Brown, S. S., Fuchs, H., et al. (2009). Organic nitrate and secondary organic aerosol yield from NO₃ oxidation of β-pinene evaluated using a gas-phase kinetics / aerosol partitioning model. *Atmospheric Chemistry and Physics*, 9, 1431–1449.
- Gentner, D. R., Worton, D. R., Isaacman, G., Davis, L. C., Dallmann, T. R., Wood, E. C., et al. (2013). Chemical composition of gas-phase organic carbon emissions from motor vehicles and implications for ozone production. *Environmental Science and Technology*, 47, 11837–

11848.

- Gilman, J. B., Lerner, B. M., Kuster, W. C., & De Gouw, J. A. (2013). Source signature of volatile organic compounds from oil and natural gas operations in northeastern Colorado. *Environmental Science and Technology*, 47(3), 1297–1305. <https://doi.org/10.1021/es304119a>
- Hornbrook, R. S., Crawford, J. H., Edwards, G. D., Goyea, O., Mauldin, R. L., Olson, J. S., & Cantrell, C. A. (2011). Measurements of tropospheric HO₂ and RO₂ by oxygen dilution modulation and chemical ionization mass spectrometry. *Atmospheric Measurement Techniques*, 4(4), 735–756. <https://doi.org/10.5194/amt-4-735-2011>
- Jayne, J. T., Leard, D. C., Zhang, X., Davidovits, P., Smith, K. A., Kolb, C. E., & Worsnop, D. R. (2000). Development of an aerosol mass spectrometer for size and composition analysis of submicron particles. *Aerosol Science and Technology*, 33(1), 49–70. <https://doi.org/10.1080/027868200410840>
- Kaser, L., Patton, E. G., Pfister, G. G., Weinheimer, A. J., Montzka, D. D., Flocke, F., et al. (2017). The effect of entrainment through atmospheric boundary layer growth on observed and modeled surface ozone in the Colorado front range. *Journal of Geophysical Research: Atmospheres*, 122, 6075–6093. <https://doi.org/10.1002/2016JD026245>
- Lenschow, D. H., Pearson Jr., R., & Stankov, B. B. (1981). Estimating the Ozone Budget in the Boundary Layer by Use of Aircraft Measurements of Ozone Eddy Flux and Mean Concentration. *J. Geophys. Res.*, 86(C8), 7291–7297. <https://doi.org/10.1029/JC086iC08p07291>
- Mauldin, R. L., Eisele, F. L., Cantrell, C. A., Kosciuch, E., Ridley, B. A., Lefer, B., et al. (2001). Measurements of OH aboard the NASA P-3 during PEM-Tropics B. *Journal of Geophysical Research*, 106(D23), 32657–32666.
- McDuffie, E. E., Edwards, P. M., Gilman, J. B., Lerner, B. M., Dubé, W. P., Trainer, M., et al. (2016). Influence of oil and gas emissions on summertime ozone in the Colorado Northern Front Range. *Journal of Geophysical Research : Atmospheres*, 121. <https://doi.org/doi:10.1002/2016JD025265>.
- Orsini, D. A., Ma, Y., Sullivan, A., Sierau, B., Baumann, K., & Weber, R. J. (2003). Refinements to the particle-into-liquid sampler (PILS) for ground and airborne measurements of water soluble aerosol composition. *Atmospheric Environment*, 37, 1243–1259. [https://doi.org/10.1016/S1352-2310\(02\)01015-4](https://doi.org/10.1016/S1352-2310(02)01015-4)
- Perring, A. E., Bertram, T. H., Farmer, D. K., Wooldridge, P. J., Dibb, J., Blake, N. J., et al. (2010). The production and persistence of ΣRONO₂ in the Mexico City plume. *Atmospheric Chemistry and Physics*, 10(15), 7215–7229. <https://doi.org/10.5194/acp-10-7215-2010>
- Perring, A. E., Pusede, S. E., & Cohen, R. C. (2013). An observational perspective on the atmospheric impacts of alkyl and multifunctional nitrates on ozone and secondary organic aerosol. *Chemical Reviews*, 113(8), 5848–70. <https://doi.org/10.1021/cr300520x>
- Pétron, G., Frost, G. J., Miller, B. R., Hirsch, A. I., Montzka, S. A., Karion, A., et al. (2012). Hydrocarbon emissions characterization in the Colorado Front Range: A pilot study. *Journal of Geophysical Research*, 117, D04304. <https://doi.org/10.1029/2011JD016360>
- Pétron, G., Karion, A., Sweeney, C., Miller, B. R., Montzka, S. A., Frost, G. J., et al. (2014). A new look at methane and nonmethane hydrocarbon emissions from oil and natural gas operations in the Colorado Denver-Julesburg Basin. *Journal of Geophysical Research:*

- Atmospheres*, 119, 6836–6852. <https://doi.org/10.1002/2013JD021272>
- Pfister, G. G., Reddy, P. J., Barth, M. C., Flocke, F. F., Fried, A., Herndon, S. C., et al. (2017). Using Observations and Source-Specific Model Tracers to Characterize Pollutant Transport During FRAPPÉ and DISCOVER-AQ. *Journal of Geophysical Research: Atmospheres*, 122(19), 10510–10538. <https://doi.org/10.1002/2017JD027257>
- Rindelaub, J. D., McAvey, K. M., & Shepson, P. B. (2015). The photochemical production of organic nitrates from α -pinene and loss via acid-dependent particle phase hydrolysis. *Atmospheric Environment*, 100, 193–201. <https://doi.org/10.1016/j.atmosenv.2014.11.010>
- Romer, P. S., Duffey, K. C., Wooldridge, P. J., Allen, H. M., Ayres, B. R., Brown, S. S., et al. (2016). The Lifetime of Nitrogen Oxides in an Isoprene Dominated Forest. *Atmospheric Chemistry and Physics*, (16), 7623–7637. <https://doi.org/10.5194/acp-16-7623-2016>
- Rosen, R. S., Wood, E. C., Wooldridge, P. J., Thornton, J. A., Day, D. A., Kuster, W., et al. (2004). Observations of total alkyl nitrates during Texas Air Quality Study 2000: Implications for O₃ and alkyl nitrate photochemistry. *Journal of Geophysical Research*, 109(D7), D07303. <https://doi.org/10.1029/2003JD004227>
- Sander, S. P., Abbatt, J., Barker, J. R., Burkholder, J. B., Friedl, R. R., Golden, D. M., et al. (2011). *Chemical Kinetics and Photochemical Data for Use in Atmospheric Studies, Evaluation No. 17. JPL Publication 10-6*. Pasadena. <https://doi.org/10.1002/kin.550171010>
- Simpson, I. J., Meinardi, S., Blake, D. R., Blake, N. J., Rowland, F. S., Atlas, E., & Flocke, F. (2002). A biomass burning source of C₁–C₄ alkyl nitrates. *Geophysical Research Letters*, 29(24), 2168. <https://doi.org/10.1029/2002GL016290>
- Swanson, A. L., Blake, N. J., Atlas, E., Flocke, F., Blake, D. R., & Rowland, F. S. (2003). Seasonal variations of C₂–C₄ nonmethane hydrocarbons and C₁–C₄ alkyl nitrates at the Summit research station in Greenland. *Journal of Geophysical Research*, 108(D2), 4065. <https://doi.org/10.1029/2001JD001445>
- Swarthout, R. F., Russo, R. S., Zhou, Y., Hart, A. H., & Sive, B. C. (2013). Volatile organic compound distributions during the NACHTT campaign at the Boulder Atmospheric Observatory: Influence of urban and natural gas sources. *Journal of Geophysical Research Atmospheres*, 118(18), 10614–10637. <https://doi.org/10.1002/jgrd.50722>
- Wilson, E. W., Hamilton, W. a., Kennington, H. R., Evans, B., Scott, N. W., & Demore, W. B. (2006). Measurement and estimation of rate constants for the reactions of hydroxyl radical with several alkanes and cycloalkanes. *Journal of Physical Chemistry A*, 110, 3593–3604. <https://doi.org/10.1021/jp055841c>
- Xiong, F., McAvey, K. M., Pratt, K. A., Groff, C. J., Hostetler, M. A., Lipton, M. A., et al. (2015). Observation of isoprene hydroxynitrates in the southeastern United States and implications for the fate of NO_x. *Atmospheric Chemistry and Physics*, 15(19), 11257–11272. <https://doi.org/10.5194/acp-15-11257-2015>

Chapter 3

Comparison of nitrogen oxide measurements during WINTER

3.1 Introduction

Nitrogen oxides, including NO_x ($\text{NO}_x \equiv \text{NO} + \text{NO}_2$) and higher oxides (RO_2NO_2 , RONO_2 , HNO_3 , N_2O_5 , ClNO_2 , and other molecules) both influence and are affected by atmospheric oxidation rates. The concentrations of NO and NO_2 have direct effects on production of ozone, a pollutant when near the surface, and on ambient concentrations of OH and peroxy radicals (e.g. RO_2), molecules which in turn affect the lifetime of NO and NO_2 (Thornton et al., 2002). The higher oxides of nitrogen can contribute to aerosol mass through the formation of soluble nitrate, serve as terminal sinks or reservoirs of NO_x that are transported downwind of initial emission sources, and are diagnostics of our understanding of emissions and chemistry affecting NO and NO_2 .

As a consequence of their central role in atmospheric chemistry, many independent approaches to observing NO_x , the higher oxides (collectively known as NO_z), total reactive nitrogen ($\text{NO}_y = \text{NO}_x + \text{NO}_z$), and the aerosol-phase nitrogen oxides have been developed. Examples include chemiluminescent detection of NO (CL) (Ridley & Grahek, 1990), laser-induced fluorescence (LIF) detection of NO_2 (Day et al., 2002; George & O'Brien, 1991), cavity ring-down spectroscopy (CRDS) applied to detection of NO_2 and NO_3 (Brown, 2003; Wagner et al., 2011), luminol detection of NO_2 (Drummond et al., 1991; Wendel et al., 1983), chemical ionization mass spectrometry (CIMS) applied to detection of HNO_3 , organic nitrates, and organic peroxy nitrates (Beaver et al., 2012; Crouse et al., 2006; B. H. Lee et al., 2014), and ion chromatography for detection of nitrate and nitrite (Dibb et al., 1996; Orsini et al., 2003).

In addition to the primary detection of species indicated above many of these techniques have been coupled to strategies for converting all or selected fractions of NO_z to lower oxides (e.g. NO_3 , NO_2 , or NO) that can be more easily measured directly. Examples include photolytic conversion of NO_2 to NO (Walega et al., 1991), catalytic conversion of NO_y to NO (Walega et al., 1991), and thermal conversion of classes of NO_z to NO_3 , NO_2 , or NO (Day et al., 2002; Wagner et al., 2011).

Nitrogen oxides are challenging to measure because some of the molecules of interest can react on, adsorb or desorb from the walls of sampling lines or be partially thermally dissociated as air moves from outside into the temperature-controlled environment where the instrument is located. Aerosol sampling efficiency through inlets optimized for different instruments (especially those optimized for gas-phase sampling) may not be the same and thus detection of aerosol NO_y species can affect interpretation of observations and comparison of different instruments. The detected aerosol fraction could also change with the ambient size distribution and humidity, as well as the specific aircraft and inlet location (even for the same instrument and physical inlet).

A number of previous papers have compared methods for detection of nitrogen oxides. LIF and CL detection of NO₂ was found to agree within 5% during the 1999 Southern Oxidant Study (SOS) (Thornton et al., 2003). A CRDS comparison with CL in 2009 found NO₂ and NO agreed within 1% and 3%, respectively (Fuchs et al., 2009).

A laboratory comparison of n-propyl nitrate measurements by LIF with thermal dissociation (TD-LIF) and CL using a molybdenum oxide catalytic converter found agreement within 1% (Day et al., 2002). In ambient conditions during a study at Blodgett forest, the same instruments agreed within 7% for NO_y without NO measurements (Day et al., 2002). CRDS with thermal dissociation (TD-CRDS) agreed within 1% with a CL instrument during the 2013 Southern Oxidant and Aerosol Study (SOAS) and within 14% of a sum of NO_y components at the 2013 Uintah Basin Winter Ozone Study (UBWOS) (Wild et al., 2014). Some of the latter difference is likely due to the lack of organic nitrate measurements available. In the forested region of the Biosphere Effects on Aerosol and Photochemistry Experiment (BEARPEX) 2009 study, two-thirds of the TD-LIF organic nitrate measurement was accounted for by I-ToF-CIMS measurements of individual biogenic nitrates, indicating good agreement given the difficulty of individually accounting for all nitrates (Beaver et al., 2012).

Although these comparisons show that many different approaches to nitrogen oxide detection can deliver measurements that are accurate and cross-calibrated to within about 15%, there remain concerns in the community that different approaches are inconsistent with each other and that many of the newer I-ToF-CIMS and CRDS approaches have not been extensively compared to better established methods. During the Wintertime INvestigation of Transport, Emissions, and Reactivity (WINTER) field experiment in the northeast US during February and March 2015, seven different instruments measured one or more constituents of NO_y from aboard the National Center for Atmospheric Research (NCAR)-National Science Foundation (NSF) C-130 aircraft. The lower temperatures of winter and the extensive nighttime flying provided the opportunity to observe nitrogen oxide species over a wider range of conditions than in prior experiments. In this paper we present instrument intercomparisons of NO, NO₂, NO_y, NO_z, N₂O₅, ClNO₂, and HNO₃. In general, instruments agree to within their stated uncertainties. In most cases the agreement is better than the stated uncertainties, an indication that the uncertainties are estimated conservatively.

3.2 Instrumentation

The WINTER campaign (www.eol.ucar.edu/field_projects/winter) took place in February and March 2015. Based out of the NASA Langley Research Center in Virginia, 13 research flights with the NSF/NCAR C-130 aircraft were flown, collecting data over the eastern US with roughly equal attention given to daytime and nighttime conditions. After the WINTER campaign, a laboratory experiment in July 2015 was conducted to explore the TD-LIF and I-ToF-CIMS measurements of ClNO₂. In these experiments, ClNO₂ was produced by reaction of gas-phase N₂O₅ over a NaCl salt bed (Kercher et al., 2009). The instruments used in this study are each described briefly below and summarized in Table 3.1.

Table 3.1. Summary of species measured and their uncertainties and detection limits.

Instrument	Species	Uncertainty	Detection limit
TD-LIF ^a	NO ₂	5%	20 pptv
	ΣRO ₂ NO ₂ , N ₂ O ₅	10%	30 pptv
	ΣRONO ₂ , ClNO ₂	25%	49 pptv
	HNO ₃ , NO ₃	25%	65 pptv
	NO _y (minus NO)	10%	48 pptv
CL ^b	NO	30 pptv ± 10%	—
	NO _y	100 pptv ± 50%	—
CRDS ^c	NO	4% ± 700 pptv*	40 pptv*
	NO ₂	3% ± 300 pptv*	90 pptv*
	NO _y	12% ± 600 pptv*	65 pptv*
	N ₂ O ₅	12% ± 7.1 pptv*	4.5 pptv*
I-ToF-CIMS ^d	N ₂ O ₅	20%	2 pptv
	ClNO ₂	20%	2 pptv
	HNO ₃	20%	30 pptv
AMS ^e	Particle NO ₃	35%	24 pptv

Note. Values taken from data files reported for WINTER, available at data.eol.ucar.edu, except for the AMS for which values were taken from Schroder et al. (2018).

*varies between flights. Representative values from RF8 shown.

^a(Day et al., 2002)

^b(Walega et al., 1991)

^c(Wagner et al., 2011; Wild et al., 2014)

^d(B. H. Lee et al., 2014, 2018)

^e(Schroder et al., 2018)

3.2.1 TD-LIF

NO₂ was measured by a laser-induced fluorescence (LIF) instrument from the University of California, Berkeley. The compound classes ΣRO₂NO₂ and N₂O₅, ΣRONO₂ and ClNO₂, and HNO₃ and NO₃ were measured by thermal dissociation and LIF detection (TD-LIF) of the NO₂ product (Day et al., 2002). Each channel measures the sum of molecules in the gas and aerosol phase (see for example Rollins et al. (2013)). During WINTER, ambient air was brought in at 4.1 slpm through a 28 cm long PFA Teflon tube heated to 45°C to maximize transmission of HNO₃ and RONO₂. Air was sampled perpendicular to the flow direction. A 532 nm Nd:YAG laser with 20 ns pulses at 15 kHz excites NO₂ and fluorescence >700 nm is focused onto a photomultiplier tube (PMT—Hamamatsu model no. H7421-50) and recorded as single photons. Time gating is used to discriminate against scattered laser light (George & O'Brien, 1991). An NO₂ standard (4.39 ppmv, 5% uncertainty, PRAXAIR) diluted in zero air to deliver mixing ratios in the range 0 – 20 ppbv was used to calibrate the instrument. A correction for fluorescence quenching by water (which is approximately 5 times faster than quenching by nitrogen or oxygen) developed in the laboratory is applied to the data. In addition, a correction for nonlinearity arising from multiple

photons arriving in the same time gate was developed and tested for concentrations up to 500 ppbv.

Four channels were used during WINTER, one that detects ambient NO_2 and three that utilize separate fused silica tubes heated to 190°C , 350°C , and 540°C to dissociate classes of NO_2 compounds. These temperature set points were determined from previous studies on the range of dissociation temperatures in combination with laboratory studies with this specific setup to determine appropriate set points (Wooldridge et al., 2010). At 190°C , all peroxy nitrates ($\Sigma\text{RO}_2\text{NO}_2$) will be dissociated (Wooldridge et al., 2010). Also at 190°C , N_2O_5 has been shown to be dissociated to NO_2 and NO_3 , resulting in one molecule of NO_2 detected per molecule of N_2O_5 (Fuchs et al., 2012; Wood et al., 2003). By 350°C , all alkyl and multifunctional nitrates (ΣRONO_2) including particulate organic nitrate and ClNO_2 dissociate (Wooldridge et al., 2010). At 540°C , HNO_3 , particulate volatile inorganic nitrate, and NO_3 have dissociated (Day et al., 2002; Womack et al., 2017; Wooldridge et al., 2010). The largest source of NO_3 is N_2O_5 dissociation. The total signal at 540°C is a measurement of total NO_y , excluding NO and HONO . Mixing ratios for each class of compounds are determined by subtracting the mixing ratio of the next lowest temperature channel. Throughout this paper, the 190°C , 350°C , and 540°C channels refer to the difference between that temperature channel and the next lowest temperature channel. For example, the 190°C channel refers to the signal in the line heated to 190°C minus the signal in the unheated line, such that it includes signal from $\Sigma\text{RO}_2\text{NO}_2$ and N_2O_5 but not from NO_2 . The 350°C and 540°C channels measure particle-phase nitrates, with particle-phase organic nitrate observed in the 350°C channel and inorganic nitrate in the 540°C channel, but the inlet has not been characterized to determine the number and size distribution of transmitted particles.

The uncertainty for NO_2 is $\sim 5\%$ and includes both the uncertainty in the NO_2 standard and uncertainty in the delivery of diluted samples of that cylinder. In addition, uncertainties in the higher oxides include the uncertainty of subtraction of the signal from lower temperature channels. We estimate these are 10%, 25%, and 25% for the 190°C , 350°C , and 540°C channels, respectively, and 10% for the total NO_y without NO measurement. Data is available for all WINTER flights for the NO_2 and 190°C channels, and all flights except research flights (RFs) 5 – 6 for the 350°C channel, RFs 2 – 3 and 5 – 7 for the 540°C channel, and RF 3 for NO_y without NO .

3.2.2 Chemiluminescence

NO and NO_y were measured using a chemiluminescence (CL) instrument from the National Center for Atmospheric Research (NCAR) (Ridley & Grahek, 1990). The chemiluminescent reaction of NO with excess O_3 in a reaction vessel designed to operate at 8 – 10 torr with 1000 sccm flow produces light that is captured by a dry ice-cooled PMT to measure NO . An NO standard diluted in zero air (Walega et al., 1991) is used to calibrate the instrument. NO_y is detected in a separate channel by catalytic conversion to NO . The gold catalyst is operated at 300°C and CO is added to the flow. The catalyst is cleansed pre-flight by heating the gold surface to $500 - 550^\circ\text{C}$ for 30 – 50 minutes (Bollinger et al., 1983; Fahey et al., 1986; Walega et

al., 1991). A Teflon, heated (30°C) inlet with a flow rate of 1 slpm is rear-facing to reduce particle intake. Uncertainties for NO and NO_y are 30 pptv ± 10% and 100 pptv ± 50%, respectively. NO and NO_y data are available for all flights except RFs 7, 10, and 11.

3.2.3 CRDS

NO, NO₂, N₂O₅, and NO_y were measured using a National Oceanic and Atmospheric Administration (NOAA), custom-built cavity ring-down spectrometer (CRDS). In cavity ring-down spectroscopy, a laser beam is coupled to a high-finesse cavity. When the laser is turned off, the time constant of light decay (τ) is compared with and without an absorber present to determine the absorber's concentration. The CRDS deployed during WINTER measured NO, NO₂, and NO_y in separate channels by direct absorption of NO₂ at 405 nm. In the first channel, NO is quantitatively converted to NO₂ in excess O₃ prior to detection (Fuchs et al., 2009). Ambient NO₂ concentrations measured on the second channel are subtracted to derive ambient concentrations of NO. During WINTER, NO and NO₂ were sampled through a 0.198 cm inner diameter Teflon sampling line held at a constant volumetric flow rate of 2.7 liters per minute. NO_y was measured as NO₂ on a separate channel after thermal dissociation in a nichrome-wrapped, 650°C quartz heater at the inlet, as described by Wild et al. (2014). After thermal reduction, excess O₃ is added to quantitatively convert NO to NO₂. Semivolatile particles that enter the heated inlet are vaporized and oxidized nitrogen molecules are converted to NO₂, but the inlet has not been characterized to determine a particle size cutoff (Wild et al., 2014; Womack et al., 2017). All measurement channels were zeroed every 3-5 minutes during WINTER by the overflow addition of zero air at the front of each inlet. Offline calibrations of NO₂ were conducted in each channel using standard additions of NO₂, generated by the chemical oxidation of NO by known concentrations of O₃.

Instrument accuracy, error, and lower detection limits were compound-dependent and reported separately for each flight. CRDS NO and NO₂ data from RFs 1 – 4 were corrected due to discovery of an inlet and zeroing error that was fixed prior to RF 5. These data were corrected by scaling the CRDS NO and NO₂ observations to the ratio of CRDS/CL NO_y measurements for RFs 1-4. Accuracies on these flights were 9% and 8% for NO and NO₂, respectively, with errors ranging from 3.5 ppbv – 3.8 ppbv and 3.2 ppbv – 4 ppbv. For all remaining flights, the accuracy for NO and NO₂ are 4% and 3% with respective error ranges of 0.4 ppbv– 2 ppbv and 0.1 ppbv – 0.5 ppbv. Lower detection limits ranged from 25 pptv – 112 pptv and 35 pptv – 140 pptv. The NO_y measurement was reported with a 12% accuracy for all flights, an error range of 0.3 ppbv – 1.4 ppbv, and a limit of detection range from 45 pptv – 380 pptv. Measurement accuracies in each channel are subject to uncertainties in the NO₂ calibration procedure (~3%). An additional uncertainty of 1% in the NO measurement is associated with uncertainty in sample dilution from the O₃ addition. The NO_y accuracy has been previously determined by Wild et al. (2014) based on in-field comparisons to other NO_y instruments and is consistent with estimated uncertainties in the thermal conversion efficiencies of common NO_y components.

Ambient N_2O_5 concentrations were measured on an additional channel of the same CRDS instrument. Prior to entering the channel, N_2O_5 is thermally dissociated at 130°C and then measured as NO_3 via direct absorption at 662 nm (Wagner et al., 2011). Measurement zeros were performed every ~ 3 -7 minutes during WINTER by the addition of excess NO to chemically convert NO_3 to NO_2 . The CRDS measurement of N_2O_5 was calibrated offline as described in Fuchs et al. (2008) and Wagner et al. (2011) by the addition of a constant N_2O_5 amount to determine the inlet transmission and thermal conversion efficiencies of N_2O_5 in the measurement channel. During WINTER, the accuracy was 12% with an error range of 3.3 pptv – 15.8 pptv and limit of detection range of 1.3 pptv – 4.9 pptv. The measurement accuracy is subject to uncertainty in the temperature dependence of the NO_3 absorption cross section (σ_{NO_3} , used to calculate ambient concentrations from measured τ) ($\sim 5\%$) and variation between individual calibrations ($\sim 6.5\%$).

CRDS NO , NO_2 , NO_y , and N_2O_5 data are available for all WINTER flights except for N_2O_5 on RF 11, which was the result of an instrument zeroing error.

3.2.4 I-ToF-CIMS

An iodide-adduct time-of-flight chemical ionization mass spectrometer (I-ToF-CIMS) from the University of Washington measured N_2O_5 , ClNO_2 , and HNO_3 (B. H. Lee et al., 2014, 2018). Intake is at 22 slpm through a polytetrafluoroethylene (PTFE), 72 cm inlet after which compounds are ionized with iodide and then detected according to their mass to charge ratios. The instrument background was determined by periodic displacement of ambient air with ultra high purity nitrogen. The limits of detection for N_2O_5 , ClNO_2 , and HNO_3 were 2 pptv, 2 pptv, and 30 pptv, respectively, with an uncertainty of 20% for each.

3.2.5 Particle-phase Nitrate

Nitrate from submicron particles (PM_{10}) was measured by the high-resolution time of flight aerosol mass spectrometer (HR-TOF-AMS, or AMS) from the University of Colorado, Boulder (Canagaratna et al., 2007; DeCarlo et al., 2006; Hu et al., 2017; Knote et al., 2011). Details on the AMS configuration in WINTER can be found in Schroder et al. (2018). Briefly, particles were sampled through an NCAR HIMIL inlet (Stith et al., 2009) at 10 slpm into a pressure controlled inlet and then focused with an aerodynamic lens. Non-refractory particle species are vaporized upon impact with a 600°C porous tungsten vaporizer under high-vacuum, and vapors are ionized by electron ionization. Ions (for particle nitrate: NO^+ , NO_2^+ , and HNO_3^+) are then detected by time-of-flight mass spectrometry ($\Delta m/m \sim 2500$ at m/z 46). Instrument response was calibrated after nearly every flight with monodisperse ammonium nitrate particles, with collection efficiency estimated from Middlebrook et al. (2012). The accuracy and typical detection limit for 1-second data were 35% and 24 pptv, respectively (Schroder et al., 2018).

Additional particle nitrate measurements were made by a particle-into-liquid sampler with ion chromatography (PILS-IC) from Georgia Tech that measures submicron inorganic nitrate (Orsini et al., 2003) and a particle filter with post-flight ion chromatography detection that measures

inorganic nitrate up to 4 μm from the University of New Hampshire (Dibb et al., 1996, 2000). Guo et al. (2016) and Schroder et al. (2018) show agreement within 43% for these three techniques for particulate nitrate, with disagreements largely attributable to differences in size ranges and type (inorganic vs. organic) of nitrate detected by each instrument.

3.3 Comparisons

The timescales for 1-second data were aligned prior to comparison by synchronizing features in the time series relative to the CRDS NO , NO_2 , or N_2O_5 measurements. These shifts were typically less than 2 seconds. Analysis was done with the 1-second dataset for NO_2 , NO , and NO_y comparisons and a 1-minute average for all other species. Data is taken from the merged dataset (Revision 3, available at data.eol.ucar.edu) except for the I-ToF-CIMS and AMS 1-minute timescale datasets that were updated after assembly of the merge. All best fit lines are 2-sided fits assuming equal weights for each variable.

3.3.1 NO_2

The comparison between CRDS and TD-LIF measurements of NO_2 for flights RFs 5 – 13 are shown in Figure 3.1. The measurements agree with a slope of 1.02 (Figure 3.1a). Allowing the intercept to vary from zero did not improve the R^2 or reduce the residuals of the fit. This is well within the expected 6% based on the two instruments' estimated uncertainties added in quadrature. At the highest concentrations there is a slight deviation from linearity with the TD-LIF measuring slightly lower than CRDS. Agreement is poorer at low concentrations below around 1 ppbv (Figure 3.1b).

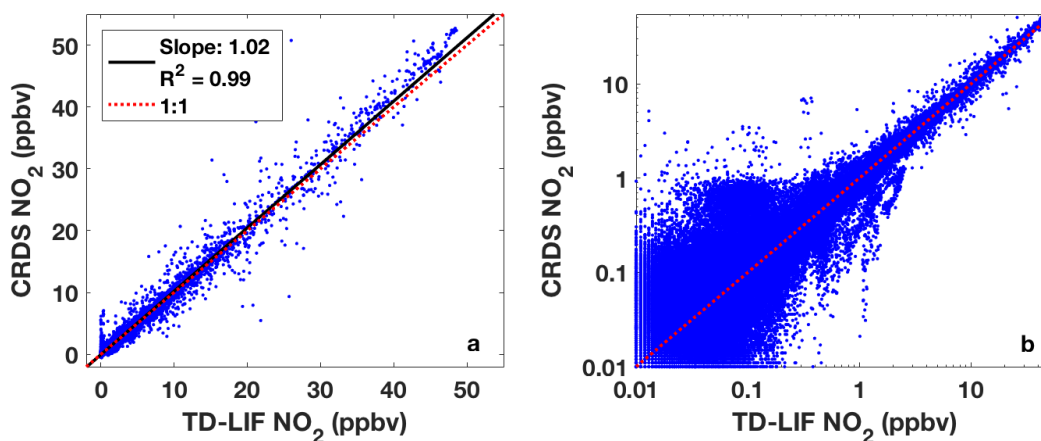


Figure 3.1. Comparison between CRDS and TD-LIF NO_2 for RFs 5 – 13 (a) on a linear scale and (b) on a log scale.

Agreement on individual flights is often (but not always) better than overall comparison, so the comparison for RF5 is shown as an example flight with excellent agreement in Figure 3.2. The flight has less scatter (Figure 3.2a) and agrees well down to lower concentrations around a few hundred pptv (Figure 3.2b) compared to the overall comparison. The slopes for each individual flight excluding RFs 1 – 4 ranged from 0.97 – 1.04, as shown in Table 3.2, which shows better

consistency than other species measured. On RFs 1 – 4 there was an inlet issue causing higher uncertainty in CRDS and contributing to differences within a flight of as much as 9% between the two measurements.

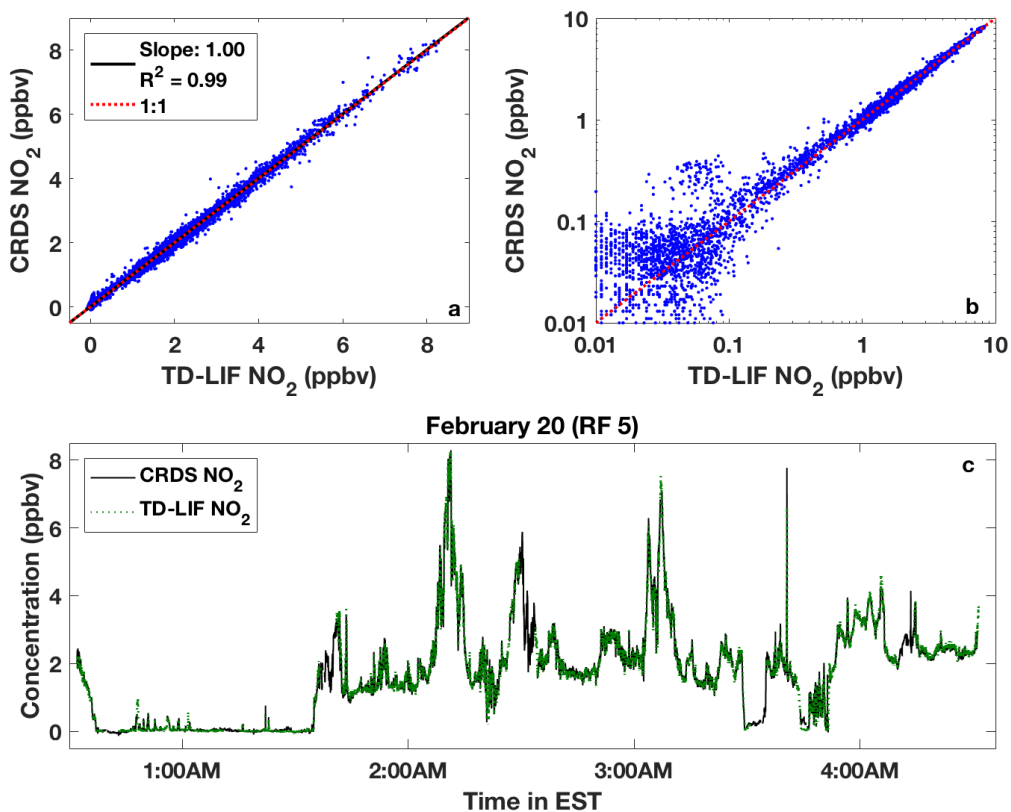


Figure 3.2. Comparison between CRDS and TD-LIF NO₂ for RF 5 on February 23 (a) on a linear scale, (b) on a log scale, and (c) as a timeseries.

Table 3.2. Slopes and correlation coefficient for individual flights.

Research Flight #	CRDS vs. TD-LIF NO ₂		CRDS vs. CL NO		CRDS vs. CL NO _y		CRDS vs. CIMS N ₂ O ₅	
	Slope	R ²	Slope	R ²	Slope	R ²	Slope	R ²
1	1.079	0.994	1.16	0.937	0.94	0.996	0.85	0.995
2	0.99	0.994	1.22	0.995	1.12	0.990	0.78	0.980
3	1.09	0.982	1.37	0.989	1.01	0.989	0.69	0.979
4	1.07	0.988	1.21	0.956	1.02	0.981	0.80	0.921
5	1.00	0.995	1.00	0.161	0.96	0.983	0.98	0.925
6	1.03	0.997	1.14	0.990	0.98	0.993	0.93	0.985
7	1.03	0.985	—	—	—	—	0.85	0.970
8	1.00	0.997	1.15	0.982	1.08	0.994	0.76	0.989
9	1.04	0.988	1.16	0.955	0.93	0.979	1.14	0.947
10	0.99	0.975	—	—	—	—	0.82	0.992
11	1.01	0.941	—	—	—	—	—	—
12	1.00	0.993	1.14	0.990	0.99	0.993	0.70	0.345
13	0.97	0.594	1.27	0.192	1.00	0.901	0.00	0.001

3.3.2 NO

The comparison of CRDS and CL for NO excluding RFs 1 – 4 has slope of 1.18, as shown in Figure 3.3a. Allowing the intercept to vary from zero did not improve the fit. This 18% difference is larger than the combined uncertainty of 11%. The high slope persists when looking only at NO below 5 ppbv, so the slope is not being skewed by high concentrations that fall above the 1:1 line. The correlation coefficient is still high at 0.96, indicating a consistent comparison. As shown below, the same two instruments agree better for their measurements of NO_y, so the disagreement is specific to NO even though the instruments are calibrated using the same standard for both NO_y and NO. The NO comparison is linear at the highest concentrations observed but correlation is poor at concentrations below 500 pptv (Figure 3.3b).

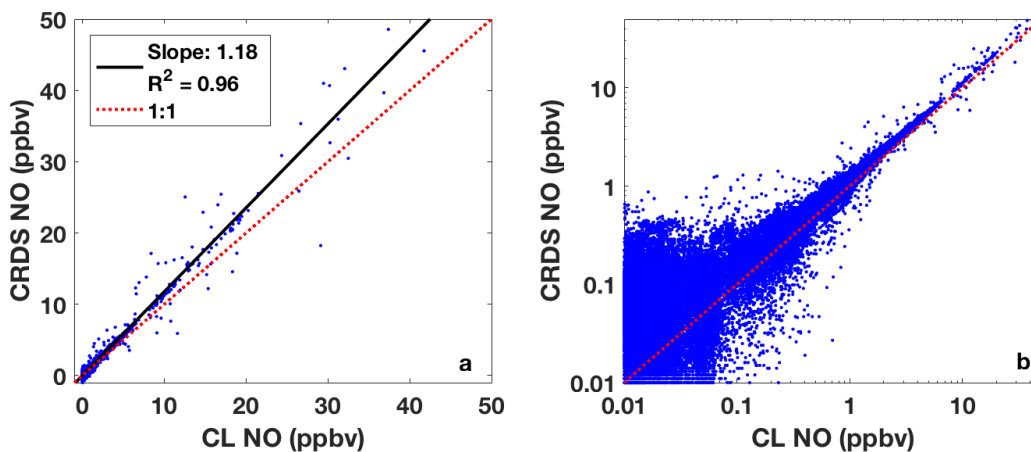


Figure 3.3. Comparison between CRDS and CL NO for RFs 5 – 13 (a) on a linear scale and (b) on a log scale.

The NO comparison for RF 12 shown in Figure 3.4 shows less scatter than the overall comparison. The slopes shown in Table 3.2 for each individual flight excluding RFs 1 – 4 are fairly consistent with the exception of RFs 5 and 13 which were not well correlated as the majority of NO observations on those flights were below 500 pptv.

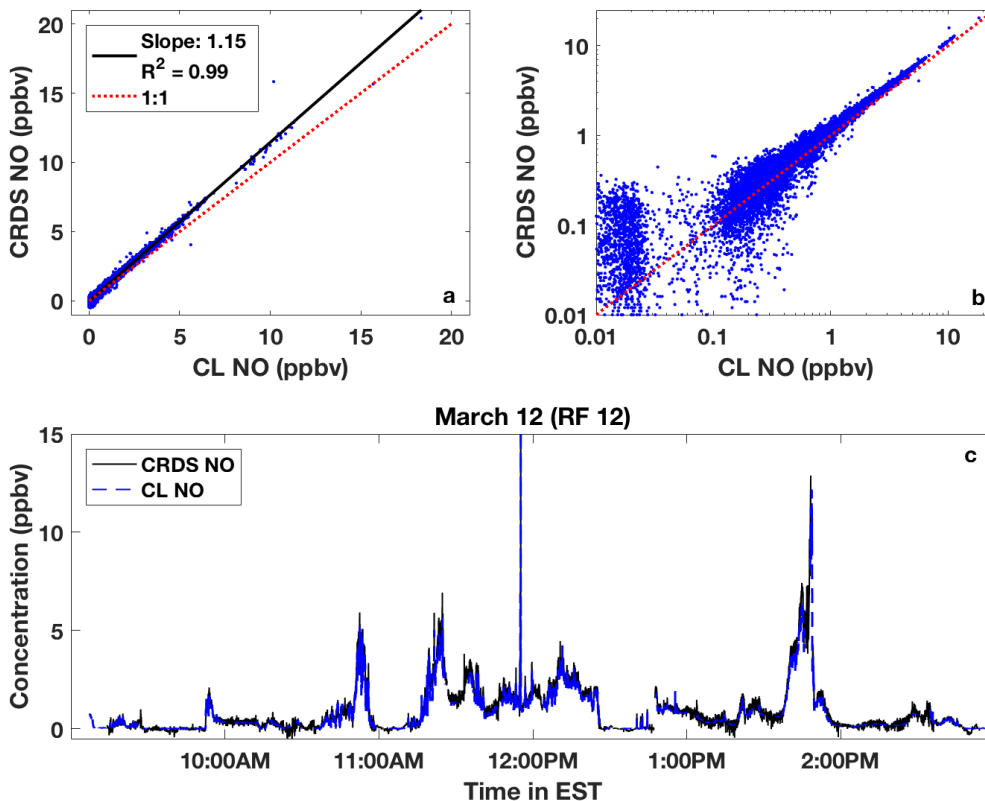


Figure 3.4. Comparison between CRDS and CL NO for RF 12 on March 12 (a) on a linear scale, (b) on a log scale, and (c) as a timeseries.

3.3.3 NO_y and NO_z

There are three NO_y measurements to compare: the CRDS NO_y , the CL NO_y measurement, and the TD-LIF measurement NO_y minus NO. The CRDS vs. CL observations have a slope of 1.01 and the fit is not improved by allowing the intercept to vary (Figure 3.5). This is well within the combined instrument uncertainty. Similar to the NO_2 and NO comparisons, the NO_y correlation is better at higher concentrations, in this case above 1 ppbv.

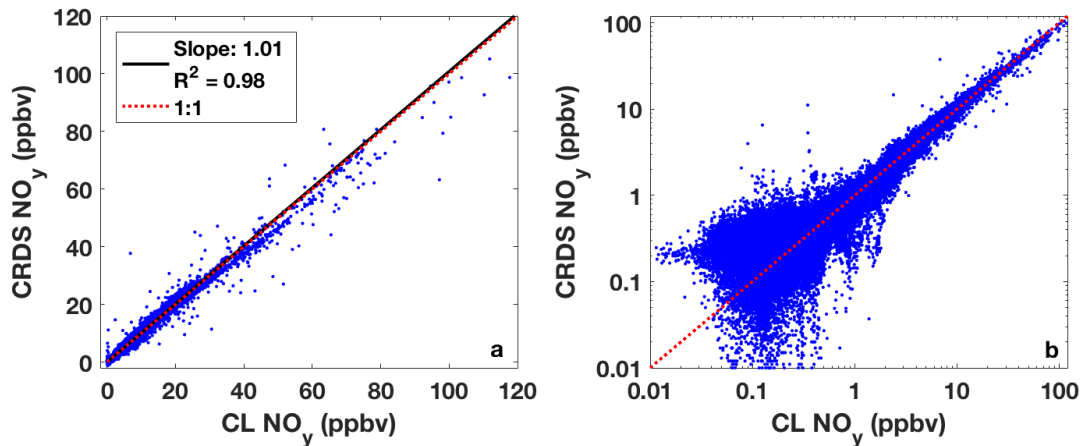


Figure 3.5. Comparison between CRDS and CL NO_y (a) on a linear scale and (b) on a log scale.

The example NO_y comparison from RF 6 shown in Figure 3.6 demonstrates a correlation with little scatter close to a 1:1 correlation. The agreement at lower concentrations is better than the overall agreement, in this case with CRDS measurements that stay at a consistent value above 100 pptv while CL measurements get down to 10 pptv. The opposite pattern of consistent CL concentrations while CRDS measures lower values is observed in other flights, so there is not a consistent pattern to the disagreement.

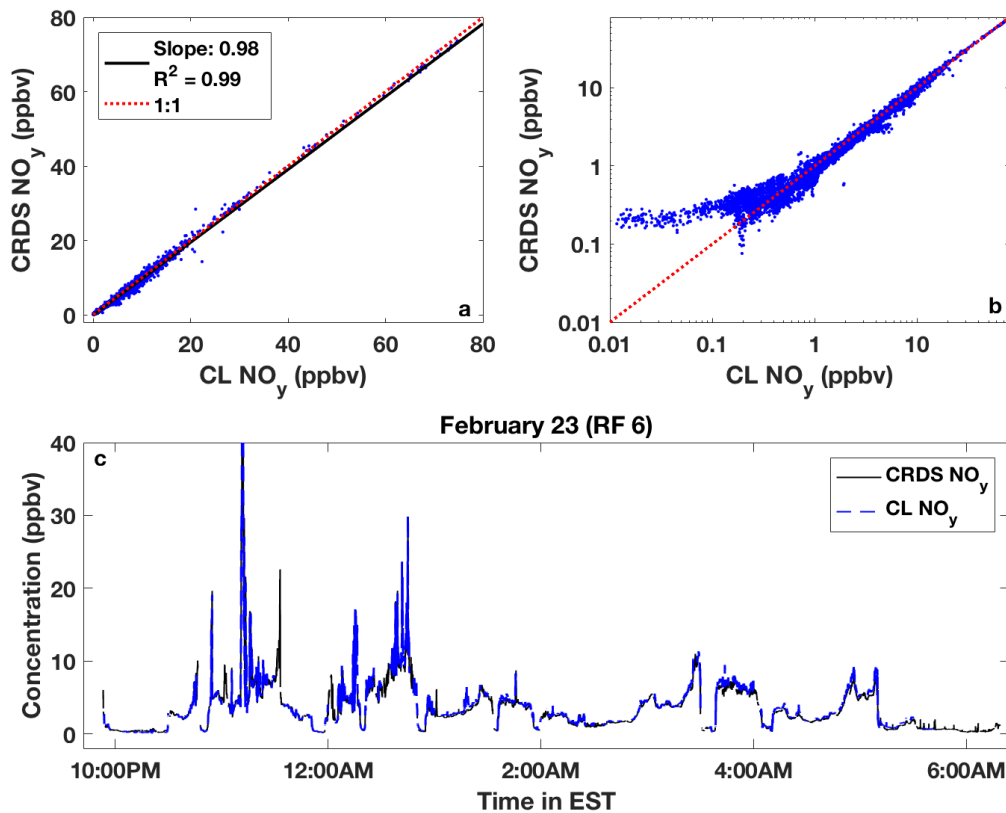


Figure 3.6. Comparison between CRDS and CL NO_y for RF 6 on February 23 (a) on a linear scale, (b) on a log scale, and (c) as a timeseries.

The slopes from flight-to-flight (Table 3.2) vary from 0.93 – 1.12, all with correlation coefficients of at least 0.90. While the instrument’s measurements agree within their uncertainty for all flights, there is inter-flight variability in their measurements relative to each other.

Since the TD-LIF does not measure NO, comparisons of NO_y minus NO are shown between all three instruments in Figure 3.7. For CL and CRDS, each respective instrument’s NO measurement is subtracted from its NO_y to make a proper comparison. The CRDS vs. TD-LIF comparison has a slope of 0.93 (Figure 3.7a). A slope of 0.91 for the CL vs. TD-LIF comparison was determined using data below 20 ppb due to nonlinearity at higher concentration (Figure 3.7b). The comparison between CRDS and CL of NO_y minus NO is shown in Figure 3.7c as an equivalent comparison. Nonlinearity at high concentrations is present in all of these comparisons, suggesting nonlinearity in the instruments. The greater slope in the CRDS vs. CL NO correlation compared to that for NO_y exaggerates the nonlinearity, but given that nonlinearity is present in all panels of Figure 3.7, there is a source of nonlinearity outside of the NO disagreement.

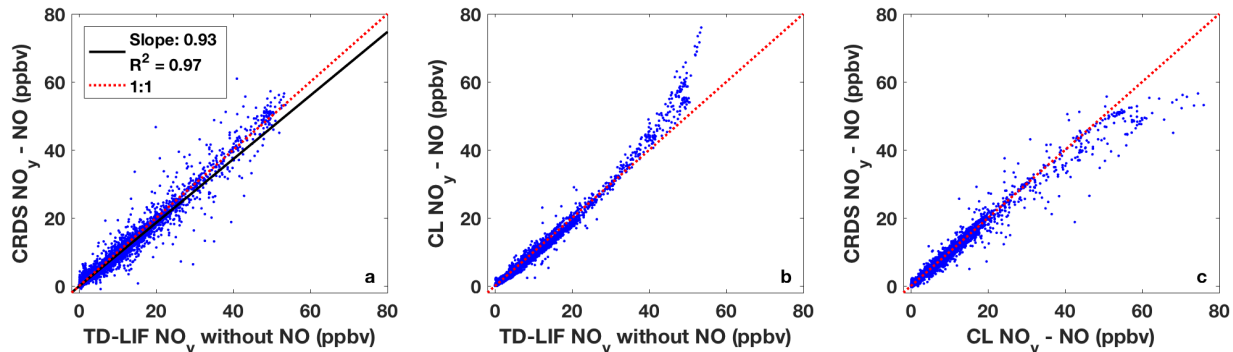


Figure 3.7. NO_y minus NO comparisons between (a) CRDS and TD-LIF, (b) CL and TD-LIF, and (c) CRDS and CL. Comparisons including CRDS exclude RFs 1 – 4 as discussed above. The red line indicates a 1:1 comparison.

NO_y is often dominated by NO₂ and NO, such that an NO_y comparison is largely a comparison of those species. This can make it difficult to compare the sum of NO_y components with NO_y measurements. Instead we compare NO_y minus NO₂ and NO, defined as NO_z, to determine if there is nitrogen budget closure with the WINTER measurements. Figures 3.8 and 3.9 show timeseries from RFs 6 and 8 of the main components of NO_z— 2 x CRDS N₂O₅, I²ToF-CIMS ClNO₂, I²ToF-CIMS HNO₃, and AMS particle-phase nitrate— along with NO₂ measurements from the CRDS, CL, and TD-LIF instruments. (CRDS NO_z was calculated as CRDS NO_y minus CRDS NO and NO₂, CL NO_z was calculated as CL NO_y minus CL NO and CRDS NO₂, and TD-LIF NO_z is the sum of all channels except the unheated NO₂ channel.) Alkyl and peroxy nitrates are additional components of NO_z that would be part of the total NO_z measurements, but we do not have independent measurements of them to include in the sum of components. It is likely that the NO_z-measuring instruments do not measure 100% of the particle-phase nitrate as their inlets are not optimized for particle transmission.

RF 6 took place on February 22 – 23 off the eastern seaboard throughout the night. Overall the sum of components tracks well with NO_z (Figure 3.8). The TD-LIF NO_z is noticeably higher than the CRDS and CL NO_z measurements that track more closely to the sum of components. On average the sum of NO_z components comprises 105% of CRDS NO_z , 89% of CL NO_z , and 77% of TD-LIF NO_z . This flight demonstrates an example where HNO_3 is the dominant NO_z component throughout most of the night. At times, N_2O_5 concentrations are a substantial portion, sometimes but not always coinciding with a rise in ClNO_2 . Particle-phase nitrate is a small component of NO_z . If the sum of components is less than total NO_z , the rest may be comprised of alkyl nitrates, peroxy nitrates or other NO_z components, but in this example, these other components appear to contribute little to the total NO_z . Despite variation in total NO_z measurements, good NO_z budget closure is demonstrated.

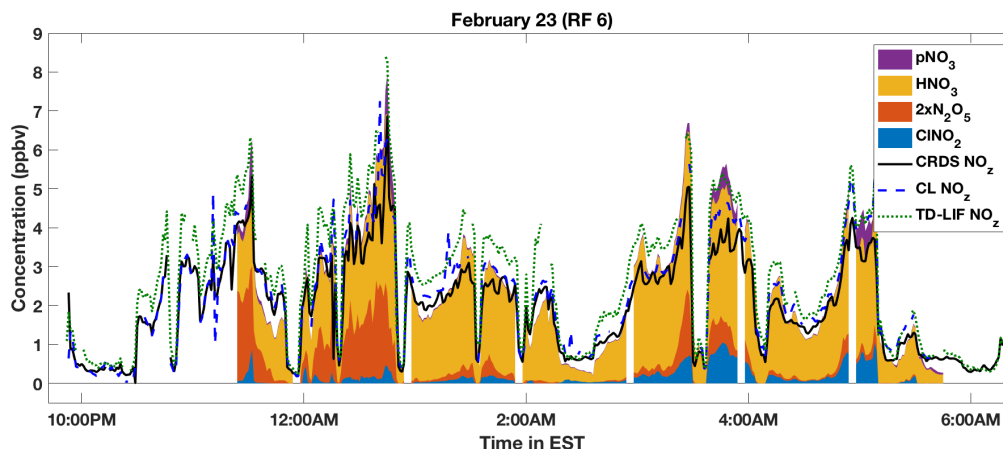


Figure 3.8. A timeseries in EST time from RF 6 on February 22 – 23 of stacked, speciated NO_z components (ToF-CIMS ClNO_2 , 2 x CRDS N_2O_5 , ToF-CIMS HNO_3 , and AMS particle-phase nitrate), along with timeseries of total NO_z measurements from the CRDS, CL, and TD-LIF instruments.

RF 8 took place on March 1 off the eastern seaboard straddling sunrise by a few hours on either side. Agreement between the sum of components with NO_z is slightly better than for RF 6, with the sum comprising 98%, 102%, and 81% of NO_z for the CRDS, CL, and TD-LIF instruments, respectively (Figure 3.9). TD-LIF NO_z is still higher than CRDS and CL which track more closely to each other. In the early morning before sunrise, N_2O_5 is the dominant component of NO_z , but shortly after sunrise around 6:30AM, N_2O_5 nearly disappears and HNO_3 becomes dominant. ClNO_2 lingers after sunrise. Particle-phase nitrate is a larger component of NO_z during this flight, especially after sunrise. All three NO_z measurements are lower than the sum of components during some of the peaks with high particle-phase nitrate (see between 7:00AM – 9:00AM), indicating that the instruments may not be seeing all or much of particle-phase nitrate. Other components of NO_z appear to comprise little of the total for the majority of this flight, except for the last stretch after 10:00AM where organic nitrates may be the missing component.

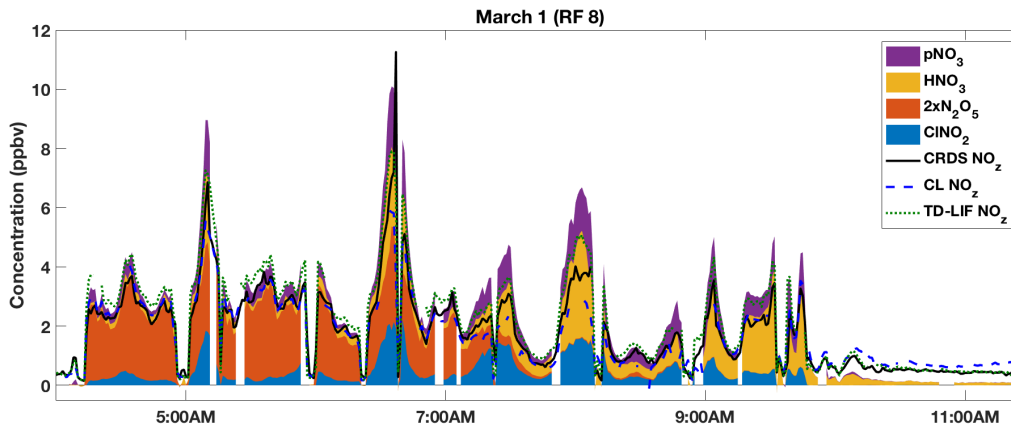


Figure 3.9. A timeseries in EST time from RF 8 on March 1 of stacked, speciated NO_2 components I-ToF-CIMS ClNO_2 , 2 x CRDS N_2O_5 , I-ToF-CIMS HNO_3 , and AMS particle-phase nitrate, along with timeseries of total NO_2 measurements from the CRDS, CL, and TD-LIF instruments.

3.3.4 N_2O_5

Observations of N_2O_5 by CRDS and I-ToF-CIMS from all WINTER flights are compared in Figure 3.10a. Across the entire campaign, the slope between CRDS and I-ToF-CIMS is 0.81. This difference is within the combined instrument uncertainty of 23% but may indicate an offset in calibration. Although the correlation coefficient is above 0.9 for most flights, slopes vary widely from 0.69 to 1.14 (Table 3.2). The example shown in Figure 3.10b from RF 3 demonstrates strong correlation within a flight at a different slope than that for all observations. While overall agreement is within the combined instrument uncertainty, the comparison between these measurements could be improved with better consistency between flights of the slope.

N_2O_5 is detected in the TD-LIF 190°C channel along with $\Sigma\text{RO}_2\text{NO}_2$, and at night, a large portion of the signal in this channel is attributable to N_2O_5 . Figures 3.10c and 3.10d show the comparison of each N_2O_5 measurement with the TD-LIF 190°C channel. Since the TD-LIF measurement includes N_2O_5 and $\Sigma\text{RO}_2\text{NO}_2$, we expect TD-LIF to be equal to or greater than the other measurements. This expectation is consistent with the observations shown in Figures 3.10c and 3.10d. The collections of points well below the 1:1 line indicate measurements with notable $\Sigma\text{RO}_2\text{NO}_2$ concentrations. While the I-ToF-CIMS reports some data larger than TD-LIF measurements (Figure 3.10d), scaling the I-ToF-CIMS measurements by 0.82 to agree with CRDS N_2O_5 (Figure 3.10a) brings the data into agreement with the TD-LIF assumptions provided above.

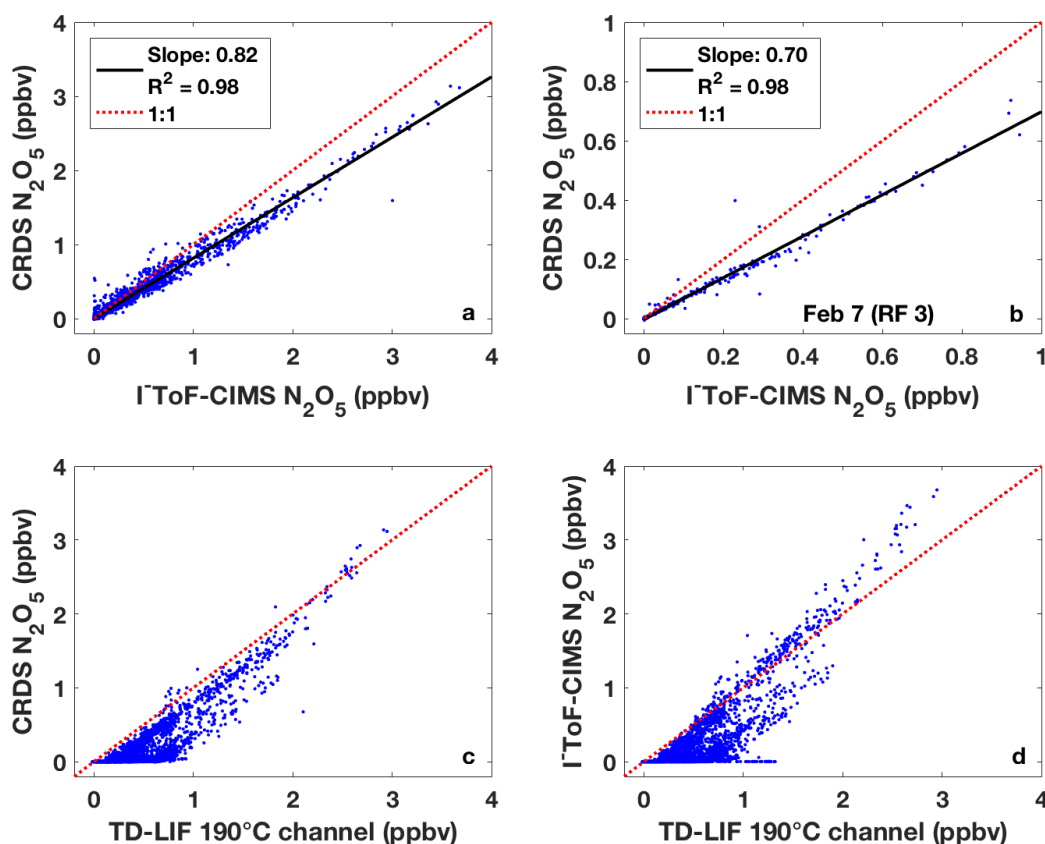


Figure 3.10. Comparisons for N_2O_5 for (a) all flights between CRDS and I-ToF-CIMS and (b) RF 3 on February 7 between CRDS and I-ToF-CIMS. Comparison between (c) CRDS or (d) I-ToF-CIMS N_2O_5 with the TD-LIF 190°C channel, which observes N_2O_5 and ΣRONO_2 . All red lines indicate a 1:1 comparison.

3.3.5 ClNO_2

ClNO_2 is expected to be detected by the TD-LIF in the 350°C channel along with ΣRONO_2 . Through a series of simulations, Wooldridge et al. (2010) found that ClNO_2 would dissociate over a range of 300°C – 425°C, which most closely overlaps with the TD-LIF ΣRONO_2 temperature range of 300°C – 400°C. Since the dissociation range for HNO_3 was 475°C – 625°C, with no overlap with the range for ClNO_2 or ΣRONO_2 , this suggests that there is a temperature set point at which all ClNO_2 will have dissociated while all HNO_3 remains intact. This would completely separate the ClNO_2 and HNO_3 signals with ClNO_2 detected in the same channel as ΣRONO_2 . The actual temperature ranges for dissociation depend on the particular oven setup in each experiment, including residence time in the heated section, so experiments are done after any instrument reconfiguration to determine the temperature set points that in between ranges of dissociation. Temperature set points for WINTER were chosen based on experiments with *n*-propyl nitrate and HNO_3 directly prior to the campaign to determine the best temperature set point to avoid species overlap.

After the WINTER campaign, additional experiments were conducted in July 2015 with the TD-LIF and I-ToF-CIMS instruments sampling the ClNO₂ calibration source (Kercher et al., 2009) in the laboratory. Both instruments sampled air coming from the same oven as the temperature was gradually raised from room temperature to 600°C. The instrument responses to the heater temperature are opposite, since I-ToF-CIMS measures ClNO₂ directly and the TD-LIF measures it as NO₂ after thermal dissociation, measuring the total at the highest temperatures. These opposite trends of each instrument are observed (Figure 3.11). However, the TD-LIF signal flattens before the I-ToF-CIMS signal does. Then there is a secondary rise in the TD-LIF signal at 500°C due to HNO₃ impurity in the source. The red line at 350°C indicates the temperature set point used during WINTER. This was verified to still be appropriate for *n*-propyl nitrate.

For the TD-LIF, ClNO₂ appears to dissociate over the range 250°C – 350°C, suggesting that all ClNO₂ would be observed in the 350°C channel. The dissociation temperature range observed by the I-ToF-CIMS is around 250°C – 400°C, suggesting that not all ClNO₂ is dissociated at 350°C. Gas-phase recombination of ClNO₂ was determined to be too slow to explain the difference. A possible explanation for the difference could be surface reactions in the tubing, as the tubing from the oven to each instrument was of different lengths. This tentatively suggests that all the ClNO₂ would be observed in the 350°C channel, but the temperature set point is on the edge and a small portion of ClNO₂ may be observed in the 540°C channel.

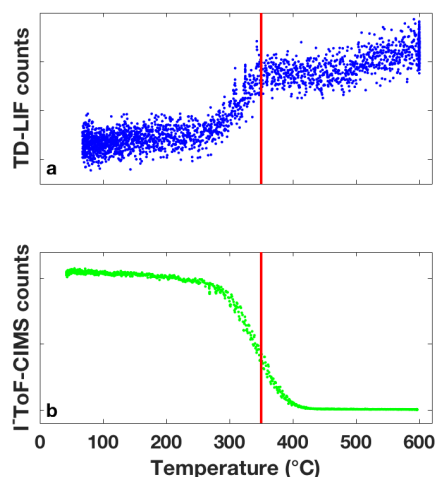


Figure 3.11. Response of the (a) TD-LIF and (b) I-ToF-CIMS to a ClNO₂ source with increasing temperature. The red line indicates the temperature set point for the 350°C channel oven during WINTER.

Observations during WINTER show periods of time where the I-ToF-CIMS ClNO₂ measurement is higher than the TD-LIF 350°C channel measurement that is supposed to encompass ClNO₂ along with any RONO₂. Figure 3.12a shows a timeseries where this is the case from RF 8, which had some of the highest ClNO₂ concentrations observed. If anything, the TD-LIF measurement should be higher than that of ClNO₂ due to detection of ΣRONO₂. Reasons for this unexpected result include that some ClNO₂ signal is observed in the 540°C channel due to too low of a

temperature set point, some ClNO_2 is converted in such a way that it does not form NO_2 , which the TD-LIF detects, or one of the measurements is problematic.

To determine if ClNO_2 is observed in the 540°C channel, we compare the sum of the 350°C and 540°C channels with the sum of their components to determine if the gap persists or is closed. Figure 3.12b shows this comparison for the same RF 8 timeseries where the sum of components being compared to the 350°C and 540°C channels is of ClNO_2 and HNO_3 from I-ToF-CIMS, N_2O_5 from CRDS, and pNO_3 from AMS. Much of the gap persists, with the sum of components still being higher than the TD-LIF channels. This would suggest that the ClNO_2 signal is not found in the 540°C channel but is lost.

The amount of particle-phase nitrate observed by the TD-LIF is uncertain. Evidence from the NO_2 comparison suggests little particle-phase nitrate is observed by the TD-LIF, but previous deployments of a TD-LIF have successfully measured particle-phase nitrate. Previous TD-LIF measurements of gas + particle nitrate from an aircraft platform compared well with a PILS measurement on particle-phase nitrate during the winter when it was cold enough that much of the HNO_3 was in the particle phase (Pusede et al., 2016). Particle-phase nitrate has also been measured separately from gas-phase by TD-LIF instruments, demonstrating that particles were transmitted to the instrument (L. Lee et al., 2015; Rollins et al., 2010). However, those experiments were under different conditions and used different inlets and platforms than that for WINTER, so transmission of particles may be different. Additionally, only volatile particle-phase nitrate is detected by the TD-LIF, which does not include the NaNO_3 that may be prevalent in sea spray, so if the particle-phase nitrate is in a different form it may not be detected as readily as in other studies. To investigate this, a timeseries where particle-phase nitrate is not included in the sum of components in the 350°C and 540°C channels is shown in Figure 3.12c. In this case the gap disappears showing excellent budget closure for the 350°C and 540°C channels. This result would indicate that ClNO_2 signal is not lost but that what is not observed in the 350°C channel is seen in the 540°C channel.

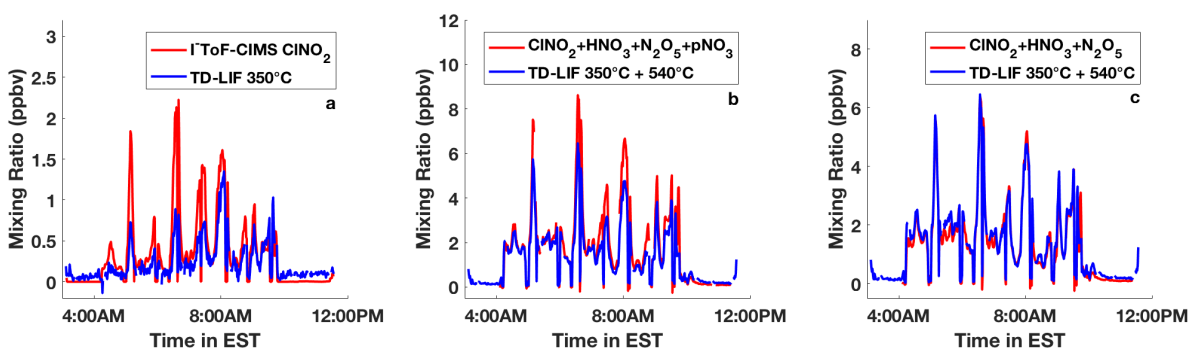


Figure 3.12. Timeseries for RF 8 with (a) I-ToF-CIMS ClNO_2 (red) and TD-LIF 350°C channel (blue), (b) I-ToF-CIMS $\text{ClNO}_2 + \text{HNO}_3 + \text{CRDS } \text{N}_2\text{O}_5 + \text{AMS } \text{pNO}_3$ (red) and TD-LIF $350^\circ\text{C} + 540^\circ\text{C}$ channels (blue), and (c) I-ToF-CIMS $\text{ClNO}_2 + \text{HNO}_3 + \text{CRDS } \text{N}_2\text{O}_5$ (red) and TD-LIF $350^\circ\text{C} + 540^\circ\text{C}$ channels (blue).

The uncertainty in the amount of particle-phase nitrate observed by the TD-LIF makes it difficult to conclude how the TD-LIF observes ClNO₂. However, evidence supporting that all ClNO₂ is detected between the two channels is that for the NO₂ comparison, the TD-LIF was consistently higher than the other NO₂ measurements. If ClNO₂ signal is lost in the TD-LIF, at least a similar amount would also have to be lost in the measurements by the other instruments as well. The mechanism for this loss is unclear, potentially surface reactions, and since the CL and CRDS instruments detect any species dissociating to form NO₂ or NO, the mechanism for ClNO₂ loss could not form either of these products.

If all ClNO₂ signal is detected between the two channels, it would indicate that very little particle-phase nitrate is observed due to the budget closure in Figure 3.12c. This is consistent with the NO₂ timeseries observations in Figure 3.9 where the NO₂ totals are often lower than the sum of components that includes particle-phase nitrate.

The example of RF 8 was chosen because it exhibits high ClNO₂ and particle-phase nitrate concentrations with seemingly little influence from RO₂NO₂ or RONO₂, but this is only one example and the evidence from other flights regarding ClNO₂ is less clear. It is also still possible that the ClNO₂ or 350°C channel measurements are problematic in such a way that causes this discrepancy.

Given the evidence, the most plausible conclusion is that the temperature set point of the 350°C oven was too low to ensure that all ClNO₂ was dissociated and observed in that channel, and that some ClNO₂ is seen in the 540°C channel. This also would mean that little particle-phase nitrate is detected by the TD-LIF, and by extension, given that the TD-LIF NO₂ is for the most part greater than the other measurements, little particle-phase nitrate is detected by the CL or CRDS NO₂ measurements, which is discussed further below.

The proportion of ClNO₂ signal that is not seen in the 350°C channel is variable. For measurements throughout the campaign where ClNO₂ is at least 100 pptv, the median 350°C signal as a percentage of total ClNO₂ is 67%, but this varies widely with a standard deviation of 55%. Due to this ClNO₂ measurement discrepancy, data was not reported for the 350°C and 540°C channels individually at night when ClNO₂ was present.

3.3.6 HNO₃

The 540°C channel of the TD-LIF sees HNO₃ and the volatile inorganic particle-phase nitrate that is sampled through the inlet, along with the second thermal dissociation of N₂O₅ (Womack et al., 2017) and possibly some proportion of ClNO₂. The question of how much particle-phase nitrate is detected in the 540°C channel is confounded by the uncertainty of how much ClNO₂ is observed in the channel. In order to answer this question while avoiding the effect of ClNO₂ and to compare with the I-ToF-CIMS HNO₃ measurement, we present a comparison using data between 10:00AM and 4:00PM.

Figure 3.13a shows the daytime comparison of the TD-LIF 540°C channel with I⁻ToF-CIMS HNO₃ with a slope of 0.82. The same comparison but with AMS particle-phase nitrate (pNO₃) is in Figure 3.13b and has a slope of 1.22. The comparison without particle-phase nitrate is more consistent with TD-LIF NO_y and NO₂ comparisons (Figures 3.7 – 3.9) where the TD-LIF was measuring higher than CL and CRDS. This would also be consistent with previous evidence from this chapter suggesting little particle-phase nitrate is detected by the TD-LIF. Comparisons using the filter or PILS-IC particle-phase nitrate instead of AMS yield a similar result.

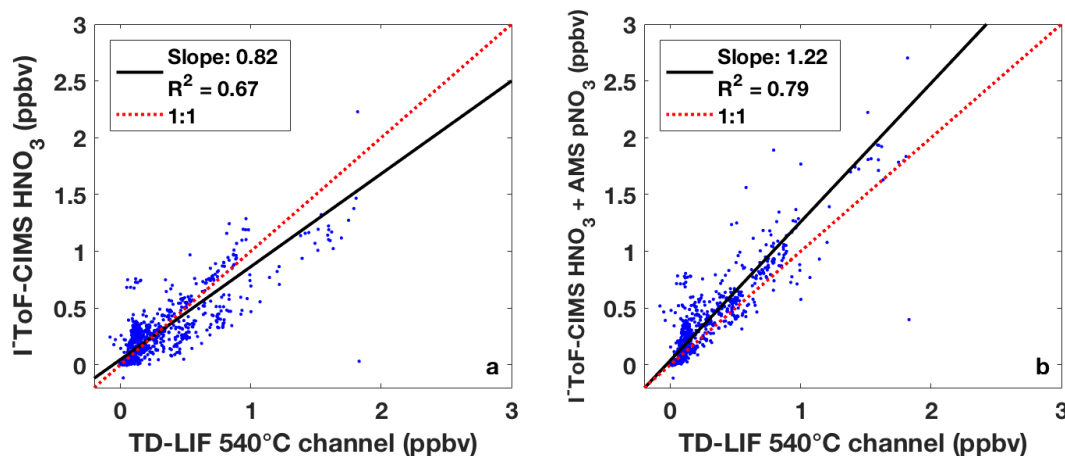


Figure 3.13. Daytime (10:00AM – 4:00PM) comparison of the TD-LIF 540°C channels with I⁻ToF-CIMS HNO₃ (a) without and (b) with AMS particle nitrate, with red lines indicating a 1:1 correlation.

3.4 Conclusion

The comparisons shown above indicate that the nitrogen oxide-measuring instruments used during WINTER provide measurements that are consistent with each other to within 20% or better. Often correlations agree better than the combined instrument uncertainty, indicating that the instrument uncertainties are conservative estimates. Agreement was slightly worse than the combined uncertainty for NO, but not for the NO_y comparison for the same instruments, suggesting that the source of disagreement is unique to NO. Nonlinearity was observed at high concentrations for NO₂ and NO_y. The majority of data is at lower concentrations and is unaffected by this nonlinearity, but in the future, special attention should be given to calibrations when sampling is expected in high nitrogen oxide concentration regions. For most species, agreement was better within a flight than for the comparison including all data, suggesting agreement could be further improved with better consistency between flights. Budget closure of NO₂ is demonstrated. Further characterization of the thermal dissociation behavior of ClNO₂ is required as we found evidence that the ClNO₂ signal was not entirely observed in one measurement channel on the TD-LIF. Evidence from the NO₂, ClNO₂, and HNO₃ comparisons suggest little particle-phase nitrate is observed by the TD-LIF, CL, and CRDS instruments, which may be due to a high portion of nonvolatile nitrate in the aerosol sampled.

References

- Beaver, M. R., St. Clair, J. M., Paulot, F., Spencer, K. M., Crouse, J. D., Lafranchi, B. W., et al. (2012). Importance of biogenic precursors to the budget of organic nitrates: Observations of multifunctional organic nitrates by CIMS and TD-LIF during BEARPEX 2009. *Atmospheric Chemistry and Physics*, *12*, 5773–5785. <https://doi.org/10.5194/acp-12-5773-2012>
- Bollinger, M. J., Sievers, R. E., Fahey, D. W., & Fehsenfeld, F. C. (1983). Conversion of Nitrogen Dioxide, Nitric Acid, and n-Propyl Nitrate to Nitric Oxide by Gold-Catalyzed Reduction with Carbon Monoxide. *Analytical Chemistry*, *55*(12), 1980–1986. <https://doi.org/10.1021/ac00262a034>
- Brown, S. S. (2003). Absorption Spectroscopy in High-Finesse Cavities for Atmospheric Studies. *Chemical Reviews*, *103*(12), 5219–5238. <https://doi.org/10.1021/cr020645c>
- Canagaratna, M. R., Jayne, J. T., Jimenez, J. L., Allan, J. D., Alfarra, M. R., Zhang, Q., et al. (2007). Chemical and Microphysical Characterization of Ambient Aerosols with the Aerodyne Aerosol Mass Spectrometer. *Mass Spectrometry Reviews*, *26*, 185–222.
- Crouse, J. D., McKinney, K. A., Kwan, A. J., & Wennberg, P. O. (2006). Measurement of gas-phase hydroperoxides by chemical ionization mass spectrometry. *Analytical Chemistry*, *78*(19), 6726–6732. <https://doi.org/10.1021/ac0604235>
- Day, D. A., Wooldridge, P. J., Dillon, M. B., Thornton, J. A., & Cohen, R. C. (2002). A thermal dissociation laser-induced fluorescence instrument for in situ detection of NO₂, peroxy nitrates, alkyl nitrates, and HNO₃. *Journal of Geophysical Research*, *107*(D6), 4046. <https://doi.org/10.1029/2001JD000779>
- DeCarlo, P. F., Kimmel, J. R., Trimborn, A., Northway, M. J., Jayne, J. T., Aiken, A. C., et al. (2006). Field-deployable, high-resolution, time-of-flight aerosol mass spectrometer. *Analytical Chemistry*, *78*(24), 8281–8289. <https://doi.org/10.1021/ac061249n>
- Dibb, J. E., Talbot, R. W., Klemm, K. I., Gregory, G. L., Singh, H. B., Bradshaw, J. D., & Sandholm, S. T. (1996). Asian influence over the western North Pacific during the fall season: inferences from lead 210, soluble ionic species and ozone. *Journal of Geophysical Research*, *101*(D1), 1779–1792. <https://doi.org/10.1029/94JD03117>
- Dibb, J. E., Talbot, R. W., & Scheuer, E. M. (2000). Composition and distribution of aerosols over the North Atlantic during the Subsonic Assessment Ozone and Nitrogen Oxide Experiment (SONEX). *Journal of Geophysical Research*, *105*(D3), 3709–3717. <https://doi.org/10.1029/1999JD900424>
- Drummond, J., Mackay, G. I., & Schiff, H. I. (1991). Measurement of peroxyacetyl nitrate, NO₂, and NO_x by using a gas chromatograph with a luminol-based detector. *Proc. SPIE 1433, Measurement of Atmospheric Gases*, 242–252. <https://doi.org/10.1117/12.46168>
- Fahey, D. W., Hubler, G., Parrish, D. D., Williams, E. J., Norton, R. B., Ridley, B. A., et al. (1986). Reactive nitrogen species in the troposphere: Measurements of NO, NO₂, HNO₃, particulate nitrate, peroxyacetyl nitrate (PAN), O₃, and total reactive odd nitrogen (NO_y) at Niwot Ridge, Colorado. *Journal of Geophysical Research*, *91*(D9), 9781–9793. <https://doi.org/10.1029/JD091iD09p09781>
- Fuchs, H., Dubé, W. P., Ciciora, S. J., & Brown, S. S. (2008). Determination of Inlet Transmission and Conversion Efficiencies for in Situ Measurements of the Nocturnal Nitrogen Oxides, NO₃, N₂O₅, and NO₂, via Pulsed Cavity Ring-Down Spectroscopy. *Analytical Chemistry*, *80*,

- 6010–6017. <https://doi.org/10.1021/ac8007253>
- Fuchs, H., Dubé, W. P., Lerner, B. M., Wagner, N. L., Williams, E. J., & Brown, S. S. (2009). A Sensitive and Versatile Detector for Atmospheric NO₂ and NO_x Based on Blue Diode Laser Cavity Ring-Down Spectroscopy. *Environmental Science & Technology*, 43(20), 7831–7836. <https://doi.org/10.1021/es902067h>
- Fuchs, H., Simpson, W. R., Apodaca, R. L., Brauers, T., Cohen, R. C., Crowley, J. N., et al. (2012). Comparison of N₂O₅ mixing ratios during NO₃Comp 2007 in SAPHIR. *Atmospheric Measurement Techniques*, 5, 2763–2777. <https://doi.org/10.5194/amt-5-2763-2012>
- George, L. A., & O'Brien, R. J. (1991). Prototype FAGE determination of NO₂. *Journal of Atmospheric Chemistry*, 12(3), 195–209. <https://doi.org/10.1007/BF00048073>
- Guo, H., Sullivan, A. P., Campuzano-Jost, P., Schroder, J. C., Lopez-Hilfiker, F. D., Dibb, J. E., et al. (2016). Fine particle pH and the partitioning of nitric acid during winter in the northeastern United States. *Journal of Geophysical Research: Atmospheres*, 121, 10355–10376. <https://doi.org/10.1002/2016JD025311>
- Hu, W., Campuzano-Jost, P., Day, D. A., Croteau, P., Canagaratna, M. R., Jayne, J. T., et al. (2017). Evaluation of the new capture vapourizer for aerosol mass spectrometers (AMS) through laboratory studies of inorganic species. *Atmospheric Measurement Techniques*, 10(8), 2897–2921. <https://doi.org/10.5194/amt-10-2897-2017>
- Kercher, J. P., Riedel, T. P., & Thornton, J. A. (2009). Chlorine activation by N₂O₅: simultaneous, in situ detection of ClNO₂ and N₂O₅ by chemical ionization mass spectrometry. *Atmos. Meas. Tech.*, 2(1), 193–204. <https://doi.org/10.5194/amt-2-193-2009>
- Knote, C., Brunner, D., Vogel, H., Allan, J., Asmi, A., Äijälä, M., et al. (2011). Towards an online-coupled chemistry-climate model: evaluation of trace gases and aerosols in COSMO-ART. *Geoscientific Model Development*, 4(4), 1077–1102. <https://doi.org/10.5194/gmd-4-1077-2011>
- Lee, B. H., Lopez-Hilfiker, F. D., Mohr, C., Kurtén, T., Worsnop, D. R., & Thornton, J. A. (2014). An iodide-adduct high-resolution time-of-flight chemical-ionization mass spectrometer: Application to atmospheric inorganic and organic compounds. *Environmental Science and Technology*, 48, 6309–6317. <https://doi.org/10.1021/es500362a>
- Lee, B. H., Lopez-Hilfiker, F. D., Veres, P. R., McDuffie, E. E., Fibiger, D. L., Sparks, T., et al. (2018). Flight deployment of a high-resolution time-of-flight chemical ionization mass spectrometer: observations of reactive halogen and nitrogen oxide species. *Journal of Geophysical Research Atmospheres*, 123. <https://doi.org/10.1029/2017JD028082>
- Lee, L., Wooldridge, P. J., Degouw, J., Brown, S. S., Bates, T. S., Quinn, P. K., & Cohen, R. C. (2015). Particulate organic nitrates observed in an oil and natural gas production region during wintertime. *Atmospheric Chemistry and Physics*, 15(16), 9313–9325. <https://doi.org/10.5194/acp-15-9313-2015>
- Middlebrook, A. M., Bahreini, R., Jimenez, J. L., & Canagaratna, M. R. (2012). Evaluation of composition-dependent collection efficiencies for the Aerodyne aerosol mass spectrometer using field data. *Aerosol Science and Technology*, 46(3), 258–271. <https://doi.org/10.1080/02786826.2011.620041>
- Orsini, D. A., Ma, Y., Sullivan, A., Sierau, B., Baumann, K., & Weber, R. J. (2003). Refinements to the particle-into-liquid sampler (PILS) for ground and airborne measurements of water soluble aerosol composition. *Atmospheric Environment*, 37, 1243–1259.

- [https://doi.org/10.1016/S1352-2310\(02\)01015-4](https://doi.org/10.1016/S1352-2310(02)01015-4)
- Pusede, S. E., Duffey, K. C., Shusterman, A. A., Saleh, A., Laughner, J. L., Wooldridge, P. J., et al. (2016). On the effectiveness of nitrogen oxide reductions as a control over ammonium nitrate aerosol. *Atmospheric Chemistry and Physics*, *16*, 2575–2596. <https://doi.org/doi:10.5194/acp-16-2575-2016>
- Ridley, B. A., & Grahek, F. E. (1990). A Small, Low Flow, High Sensitivity Reaction Vessel for NO Chemiluminescence Detectors. *Journal of Atmospheric and Oceanic Technology*, *7*, 307–311. [https://doi.org/10.1175/1520-0426\(1990\)007<0307:ASLFHS>2.0.CO;2](https://doi.org/10.1175/1520-0426(1990)007<0307:ASLFHS>2.0.CO;2)
- Rollins, A. W., Smith, J. D., Wilson, K. R., & Cohen, R. C. (2010). Real time in situ detection of organic nitrates in atmospheric aerosols. *Environmental Science & Technology*, *44*(14), 5540–5545. <https://doi.org/10.1021/es100926x>
- Rollins, A. W., Pusede, S., Wooldridge, P., Min, K. E., Gentner, D. R., Goldstein, A. H., et al. (2013). Gas/particle partitioning of total alkyl nitrates observed with TD-LIF in Bakersfield. *Journal of Geophysical Research Atmospheres*, *118*, 6651–6662. <https://doi.org/10.1002/jgrd.50522>
- Schroder, J. C., Campuzano-Jost, P., Day, D. A., Shah, V., Larson, K., Sommers, J. M., et al. (2018). Sources and Secondary Production of Organic Aerosols in the Northeastern US during WINTER. *Journal of Geophysical Research: Atmospheres*, *123*. <https://doi.org/10.1029/2018JD028475>
- Stith, J. L., Ramanathan, V., Cooper, W. A., Roberts, G. C., DeMott, P. J., Carmichael, G., et al. (2009). An overview of aircraft observations from the Pacific Dust Experiment campaign. *Journal of Geophysical Research*, *114*, D05207. <https://doi.org/10.1029/2008JD010924>
- Thornton, J. A., Wooldridge, P. J., Cohen, R. C., Martinez, M., Harder, H., Brune, W. H., et al. (2002). Ozone production rates as a function of NO_x abundances and HO_x production rates in the Nashville urban plume. *Journal of Geophysical Research*, *107*(D12), 1–17. <https://doi.org/10.1029/2001JD000932>
- Thornton, J. A., Wooldridge, P. J., Cohen, R. C., Williams, E. J., Hereid, D., Fehsenfeld, F. C., et al. (2003). Comparisons of in situ and long path measurements of NO₂ in urban plumes. *Journal of Geophysical Research*, *108*(D16), 4496. <https://doi.org/10.1029/2003JD003559>
- Wagner, N. L., Dubé, W. P., Washenfelder, R. A., Young, C. J., Pollack, I. B., Ryerson, T. B., & Brown, S. S. (2011). Diode laser-based cavity ring-down instrument for NO₃, N₂O₅, NO, NO₂ and O₃ from aircraft. *Atmospheric Measurement Techniques*, *4*, 1227–1240. <https://doi.org/10.5194/amt-4-1227-2011>
- Walega, J., Dye, J., Grahek, F., & Ridley, B. (1991). A compact measurement system for the simultaneous determination of NO, NO₂, NO_y and O₃ using a small aircraft. *Proc. SPIE 1433, Measurement of Atmospheric Gases*, *1433*, 232–241. <https://doi.org/10.1117/12.46167>
- Wendel, G. J., Stedman, D. H., Cantrell, C. A., & Damrauer, L. (1983). Luminol-Based Nitrogen Dioxide Detector. *Analytical Chemistry*, *55*(6), 937–940. <https://doi.org/10.1021/ac00257a027>
- Wild, R. J., Edwards, P. M., Dubé, W. P., Baumann, K., Edgerton, E. S., Quinn, P. K., et al. (2014). A measurement of total reactive nitrogen, NO_y, together with NO₂, NO, and O₃ via cavity ring-down spectroscopy. *Environmental Science and Technology*, *48*, 9609–9615. <https://doi.org/10.1021/es501896w>
- Womack, C. C., Neuman, J. A., Veres, P. R., Eilerman, S. J., Brock, C. A., Decker, Z. C. J., et al.

- (2017). Evaluation of the accuracy of thermal dissociation CRDS and LIF techniques for atmospheric measurement of reactive nitrogen species. *Atmospheric Measurement Techniques*, 10, 1911–1926. <https://doi.org/10.5194/amt-10-1911-2017>
- Wood, E. C., Wooldridge, P. J., Freese, J. H., Albrecht, T., & Cohen, R. C. (2003). Prototype for in situ detection of atmospheric NO₃ and N₂O₅ via laser-induced fluorescence. *Environmental Science & Technology*, 37(24), 5732–5738. <https://doi.org/10.1021/es034507w>
- Wooldridge, P. J., Perring, A. E., Bertram, T. H., Flocke, F. M., Roberts, J. M., Singh, H. B., et al. (2010). Total Peroxy Nitrates (ΣPNs) in the atmosphere: the Thermal Dissociation-Laser Induced Fluorescence (TD-LIF) technique and comparisons to speciated PAN measurements. *Atmospheric Measurement Techniques*, 3, 593–607. <https://doi.org/10.5194/amt-3-593-2010>

Chapter 4

Comparison of measurements by separate thermal dissociation laser-induced fluorescence instruments in the Northern Front Range Metropolitan Area of Colorado

4.1 Introduction

NO_x ($\text{NO}_x \equiv \text{NO} + \text{NO}_2$) is an important atmospheric oxidant that contributes to the production of ozone, a respiratory irritant, and affects production of aerosol. The lifetime of NO_x and therefore its effect as an oxidant is controlled by the rate of loss to the sinks of NO_x , which include production of peroxy nitrates (RO_2NO_2), alkyl and multifunctional nitrates (RONO_2), and nitric acid (HNO_3). The sum of these species produced by NO_x loss processes is defined as NO_z . In order to study NO_x and its loss products, researchers have been making atmospheric measurements for decades. One technique used is thermal dissociation laser-induced fluorescence (TD-LIF), where NO_2 is measured by laser-induced fluorescence and NO_x loss products are measured by conversion to NO_2 via thermal dissociation (Day et al., 2002).

During the summer of 2014, two aircraft-based field campaigns took place at the same time in Colorado. The final deployment of the Deriving Information on Surface Conditions from COlumn and VERTically Resolved Observations Relevant to Air Quality (Discover-AQ) campaign using the NASA P-3B aircraft was based in Colorado and was joined by the Front Range Air Pollution and Photochemistry Experiment (FRAPPE), which utilized the NSF/NCAR C-130 aircraft. A TD-LIF instrument was on board the aircraft for each campaign, giving an opportunity to compare the performance of two different TD-LIF instruments in the same region. We developed a method to compare instrument performance between the campaigns despite the planes having different flight paths. We find that while the bulk of measurements compare well between flights, the alkyl nitrate measurement on the TD-LIF disagrees. We show evidence this is due to the Discover-AQ-based TD-LIF not performing as expected, and we recommend not using the Discover-AQ alkyl nitrate measurements.

4.2 Observations

4.2.1 Campaign summaries

The FRAPPE and Discover-AQ campaigns took place in the Northern Front Range Metropolitan Area (NFRMA) of Colorado during July – August, 2014. This region is of interest because the EPA has classified the NFRMA as a nonattainment region for ozone, and the region has struggled to get into compliance (CDPHE, 2016).

The Discover-AQ campaign included a payload of instruments aboard NASA's P-3B aircraft measuring a variety of species relevant to air quality. Intended as a satellite verification project,

the P-3B flew a regular flight plan that included vertical spirals over six locations. While the P-3B sampled less of the region this way, the repetition allows for comparing air quality in the same location at different times and on different days. Flights departed fairly consistently around 8:00AM local MDT time and typically landed from 4:00PM – 5:00PM MDT, sometimes with a refueling stop in between.

The FRAPPE campaign took place aboard the NSF/NCAR C-130 aircraft. Unlike with Discover-AQ, flight plans varied day-to-day, covering a large swath extending beyond the NFRMA, albeit with some repeated flight patterns that allow for day-to-day comparison. Despite the wider flight range, we only examine FRAPPE data within the same NFRMA region flown by the P-3B, bounded by latitudes 39.5°N and 40.65°N and longitudes 254.75°E and 255.5°E. This area incorporates the Denver metropolitan area as well as a large amount of agricultural and oil and natural gas activity to the north. Along with more varied flight plans, the C-130 was airborne at different times of day, often taking off and landing later than the P-3B.

For both campaigns, our analysis uses only data taken below 2.5 km above sea level (ASL), or approximately 1 km above ground level (AGL) to only incorporate measurements from inside the planetary boundary layer (PBL).

An intercomparison flight on August 8th over rural Nebraska and Colorado provided an opportunity to compare instrument performance between the planes. However, this comparison was limited by the low concentrations observed in rural areas as well as a slight difference in altitude between the planes that may have led to sampling of different atmospheric layers.

4.2.2 Instrumentation

4.2.2.1 Thermal dissociation laser-induced fluorescence

NO₂, total peroxy nitrates ($\Sigma\text{RO}_2\text{NO}_2$), total alkyl nitrates (ΣRONO_2), and HNO₃ were measured on both planes using TD-LIF, as previously described (Day et al., 2002). NO₂ is measured by laser-induced fluorescence, where NO₂ is excited by a pulsed laser and has a delayed fluorescence of photons > 700nm which are detected between laser pulses by a photomultiplier tube. Higher oxides of nitrogen are measured in separate channels heated to the temperature of thermal dissociation for each class of compounds— ~200°C for $\Sigma\text{RO}_2\text{NO}_2$, ~350°C for ΣRONO_2 , and ~550°C for HNO₃. While ambient NO₂ is measured in an unheated channel, the higher oxides are measured as the difference in detected NO₂ between subsequent channels. Since any species matching the RONO₂ formula will be detected in that channel, the measurement is considered a sum of all RONO₂, or ΣRONO_2 , and likewise with $\Sigma\text{RO}_2\text{NO}_2$. Measurements are calibrated with a series of known concentrations of an NO₂ standard in zero air 1-2 times per hour.

The specifics on instrument design differ slightly between the instruments on each plane. On the P-3B, NO₂ is excited by a 532 nm YAG laser, and the zero reading is the photon counts

detected when zero air is flowed through the instrument. In contrast, on the C-130, a 532 nm YAG laser pumps a 585 nm tunable dye laser which tunes on and off an NO₂ absorption feature for a more precise measurement. The dye laser instrument has less noise but is more finicky to operate due to the dye laser, which can lead to worse data coverage. While each variation of the TD-LIF offers different benefits and drawbacks, they have previously been shown in the laboratory to give comparable results.

For the inlet on the P3-B for Discover-AQ, ambient air passes through a 35 mm internal diameter tube off of which the instrument samples through 10 cm of tubing before splitting into separate lines that either lead directly to the instrument for NO₂ or through a heated region for the higher oxides (Nault et al., 2015). Each line has a dedicated cell so detection for all four groups of compounds is continuous.

On the C-130, the instrument samples directly from ambient air perpendicularly through a 28 cm long 4.75 mm internal diameter tube heated to ~ 45°C before splitting into separate lines. While there is a dedicated line and oven for each group of species, due to size restraints from the dye laser, there are only two detection cells, which alternate between sample lines.

4.2.2.2 Other instrumentation

On both the P-3B and C-130, ozone, NO, and NO₂ were measured using chemiluminescence (Ridley & Grahek, 1990; Walega et al., 1991). Additionally, on the P-3B, the same instrument made a total NO_y measurement.

On the C-130, a trace organic gas analyzer (TOGA) instrument measured a large suite of VOCs by GC/MS at a 2-minute frequency (Apel et al., 2003, 2010). Less frequent measurements of additional VOCs were collected by a whole air sampler (WAS) and analyzed by GC (Colman et al., 2001). In order to form a more complete dataset, for times when VOC data is missing due to the less frequent whole air sampling, concentrations are estimated by scaling a closely correlated, TOGA-measured VOC by the campaign-averaged observed ratio between the two species. The suite of VOCs measured by TOGA and WAS include a variety of specific alkyl nitrates (as opposed to the TD-LIF's total measurement which includes any species with the RONO₂ formula).

Additional FRAPPE measurements used include CO, CH₄, H₂O, ethane, PAN, PPN, total nitrate aerosol, and inorganic aerosol nitrate, the techniques for which are provided in Table 4.1. Observed data is reported as a 10-second average, while calculations incorporating VOC measurements use 2-minute averaged data to align with the TOGA measurement frequency. Additional measurements from Discover-AQ include H₂O, formaldehyde, CO₂, CH₄, and CO, with details in Table 4.2.

Table 4.1. Summary of FRAPPE measurements.

Measurement	Instrument	Source
NO ₂ , ΣRO ₂ NO ₂ , ΣRONO ₂ , HNO ₃	Thermal dissociation laser-induced fluorescence (TD-LIF)	Day et al., 2002
VOCs	Trace organic gas analyzer (TOGA)	Apel et al. 2003, 2010
VOCs	Whole air sampler (WAS)	Colman et al., 2001
CO	Aero-laser vacuum UV resonance fluorescence	Gerbig et al., 1999
CH ₄ , H ₂ O	Picarro cavity ring-down spectroscopy	Picarro Model G2401
Ethane	Compact atmospheric multi-species spectrometer (CAMS)	Richter et al., 2015
O ₃ , NO, NO ₂	Chemiluminescence	Ridley & Grahek, 1990; Walega et al., 1991
PAN, PPN	PAN Chemical ionization mass spectrometer (CIMS)	Zheng et al., 2011
Total pNO ₃	Aerosol mass spectrometer (AMS)	Jayne et al., 2000
Inorganic NO ₃ ⁻	Particle into liquid sampler (PILS)	Orsini et al., 2003

Table 4.2. Summary of Discover-AQ measurements.

Measurement	Instrument	Source
NO ₂ , ΣRO ₂ NO ₂ , ΣRONO ₂ , HNO ₃	Thermal dissociation laser-induced fluorescence (TD-LIF)	Day et al., 2002
CO, CH ₄	Differential absorption CO measurement (DACOM)	Sachse et al., 1987
H ₂ O	Diode laser hygrometer (DLH)	Diskin et al., 2002
Ethane	Tunable infrared laser direct absorption spectrometer (TILDAS)	Yacovitch et al., 2014
CO ₂	Atmospheric vertical observations of CO ₂ in the earth's troposphere (AVOCET)	Vay et al., 2011
O ₃ , NO, NO ₂ , NO _y	Chemiluminescence	Ridley & Grahek, 1990; Walega et al., 1991
CH ₂ O	Difference frequency generation absorption spectrometer (DFGAS)	Weibring et al., 2006, 2007

4.3 Measurement discrepancy between campaigns

We expect that both the TD-LIF instruments would measure the same concentration if they were sampling the same air. However, during FRAPPE, much higher alkyl nitrate concentrations were measured, up to 3.76 ppbv, than during Discover-AQ, which saw concentrations up to 2.07 ppbv. The spread of measurements shown in Figure 4.1 demonstrates this difference. It may be that this difference is real, perhaps because FRAPPE's C-130 did not have a set flight path and sought out more hot spots for emissions, or it may be that the instruments didn't measure the same values for the same air.

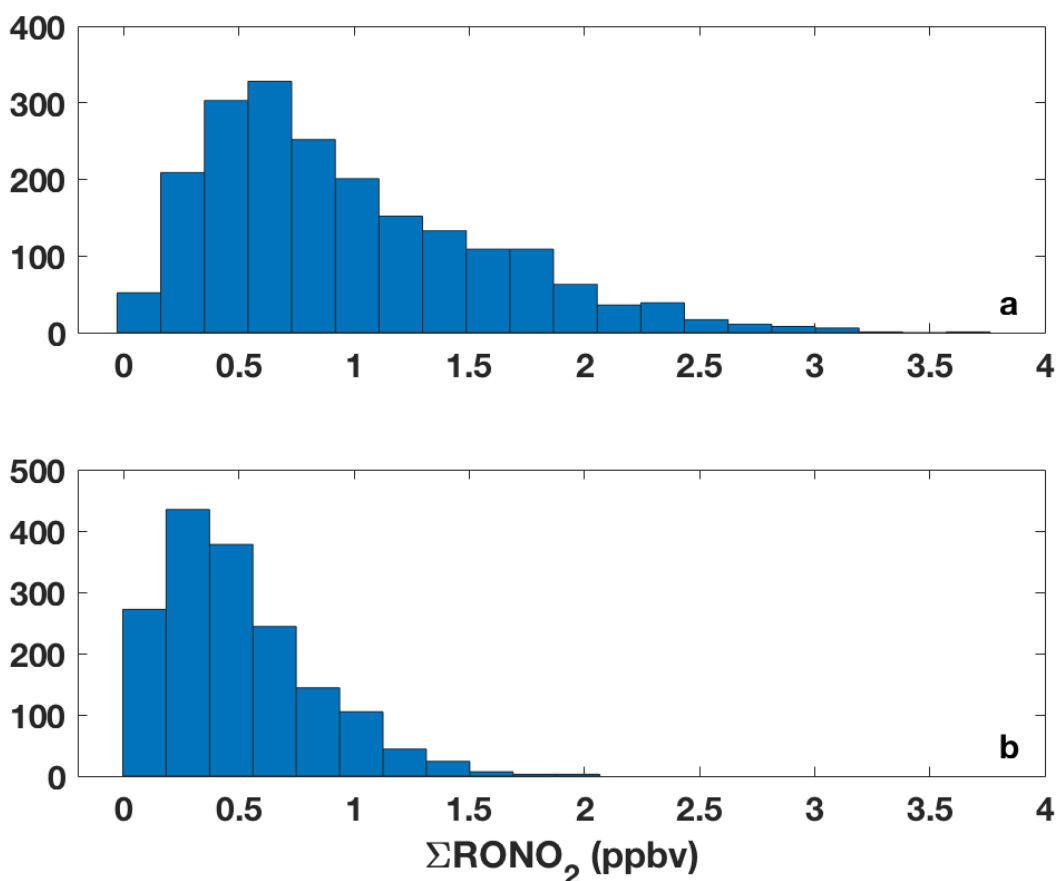


Figure 4.1. Histogram of ΣRONO_2 measurements for (a) FRAPPE and (b) DISCOVER-AQ.

Despite the difference in flight paths, the C-130 covered much of the same territory as the P-3B, as shown in Figure 4.2 which shows flight paths in the same region colored by alkyl nitrate concentration. While the C-130 flights explored more territory than the P-3B, it does not appear that all the highest alkyl nitrate concentrations are in locations solely explored during FRAPPE. In particular, the region between Boulder and Denver was thoroughly explored by both planes, but FRAPPE measured much higher alkyl nitrate concentrations. This suggests that the first hypothesis, that FRAPPE explored more hotspots than Discover-AQ, is unsupported by the data.

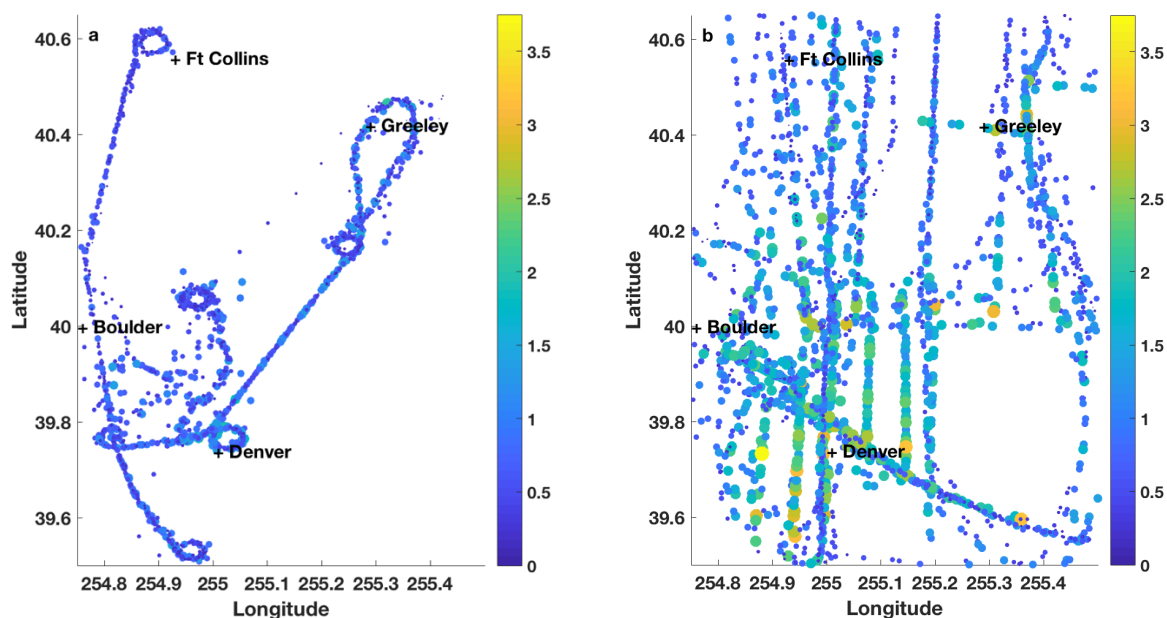


Figure 4.2. Flight paths for (a) Discover-AQ and (b) FRAPPE bounded by the region regularly explored by Discover-AQ flights, colored and sized by alkyl nitrate concentration in ppbv.

This turns us to the second hypothesis, that the FRAPPE TD-LIF systematically measured higher concentrations than that of Discover-AQ, which we can investigate by comparing instrument response while sampling the same air. A direct comparison of the instruments on the ground prior to the campaign was never conducted, as previously laboratory studies showed that they compare well despite using slightly different techniques. The concentrations of the NO_2 standards used for each campaign were verified by comparison to the same standard, so the difference is unlikely to be a matter of calibration. This leaves us with comparing the instrument's in-flight performance. While the planes were in each other's immediate vicinity during a flight intercomparison, this was done in a rural area with low overall concentrations that make it difficult to confidently compare instrument response.

In order to effectively compare measurements, we created a grid of the region and compared concentrations when both planes sampled within the same box within the same hour. Grid boxes were 0.1° latitude by 0.1° longitude between $254.7^\circ - 255.5^\circ$ E and $39.5^\circ - 40.7^\circ$ N, approximately 6.9 mi by 5.3 mi in area. Only data taken below 1 km AGL and between 10:00AM – 6:00PM local MDT time were used, which is the range of times when both planes were regularly flying. There were 51 instances where both planes sampled in the same grid box during the same hour, which corresponds to 33 – 40 comparisons depending on the data availability of the species being compared. Figure 4.3 shows this grid and all points included in this analysis.

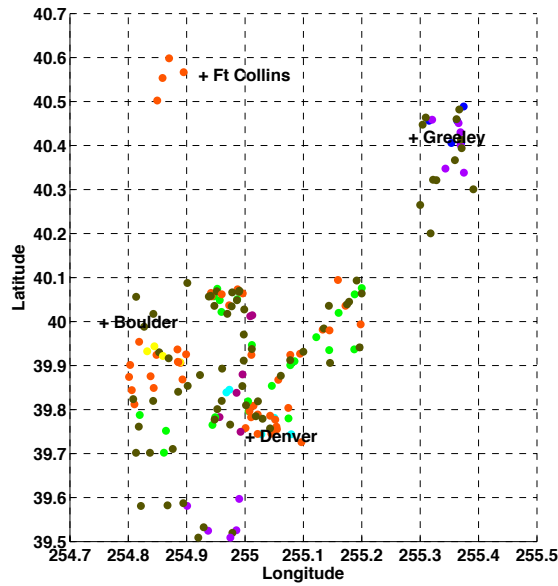


Figure 4.3. Grid for comparison between FRAPPE and Discover-AQ measurements. Points are measurements from either plane that occur in the same hour and grid box as a measurement from the other plane, colored by flight day. Some grid boxes include multiple hours on the same or different days that satisfy this criterion.

The average was taken of all measurements from each plane while in a particular grid box in the same hour and the averages were compared between planes. By plotting the average in a shared grid box of one plane vs. the other for each species, a difference between the campaigns is seen if the data lie off the 1:1, and the factor by which FRAPPE measurements are higher or lower is given by the slope, as in Figure 4.4. For NO_2 and $\Sigma\text{RO}_2\text{NO}_2$, DISCOVER-AQ and FRAPPE agree within 15%, although $\Sigma\text{RO}_2\text{NO}_2$ comparison points lie largely above the 1:1, indicating larger DISCOVER-AQ measurements. For ΣRONO_2 , DISCOVER-AQ is about 50% lower than FRAPPE, which supports the theory that the instruments do not agree for their ΣRONO_2 measurement. Points for HNO_3 lie somewhat on the 1:1 line and somewhat below, so there may be slightly lower measurements for DISCOVER-AQ compared to FRAPPE.

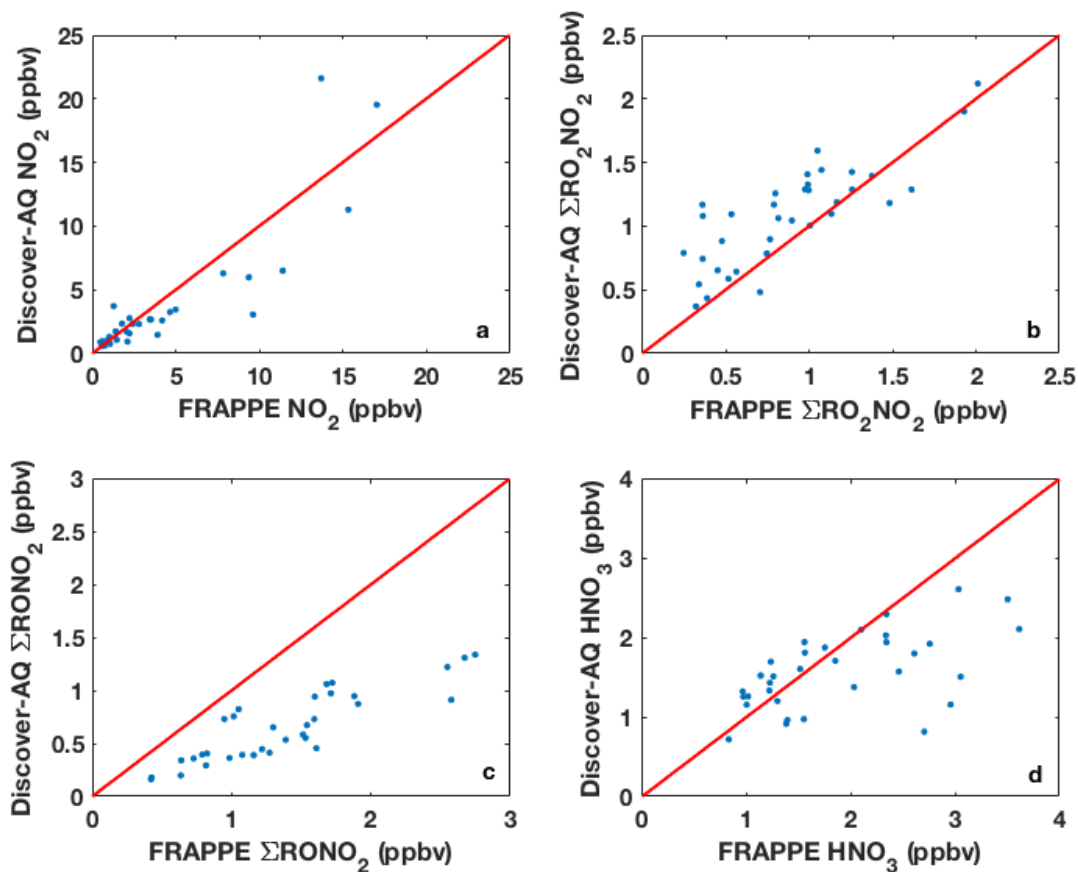


Figure 4.4. Discover-AQ vs. FRAPPE for average of concentrations in the same grid box during the same hour for (a) NO_2 , (b) $\Sigma\text{RO}_2\text{NO}_2$, (c) ΣRONO_2 , and (d) HNO_3 . Red lines indicate 1:1 agreement.

As an additional method for comparison, a difference, Δ , was calculated as the Discover-AQ average subtracted from the FRAPPE average for each instance of co-location. By definition, a good comparison between instruments would yield a Δ close to zero. A positive Δ indicates a higher measurement on the C-130, while a negative Δ indicates a higher measurement on the P-3B. Comparisons of several species from a variety of instruments that were represented on both planes were made in order to determine if this method should yield a good comparison with Δ 's close to zero or if even within these boxes one plane sampled higher concentrations of a variety of correlated pollutants. The median Δ of all available instances of comparison was taken, and then to standardize Δ 's across the wide range of typical concentrations among species examined, median Δ 's were divided by the average concentrations from FRAPPE for each species.

Figure 4.5 shows the standardized Δ 's for each species examined. Among non-TD-LIF measurements, most species have a standardized Δ close to zero with the highest deviation at 0.14 for H_2O . The non-TD-LIF comparisons were made by four different instruments on the C-130 and by six different instruments on the P-3B, with each measurement not necessarily

measured by the same team or with the same technique between planes. That there is such good agreement among several different instruments indicates that this grid analysis is a good strategy for comparing instrument performance.

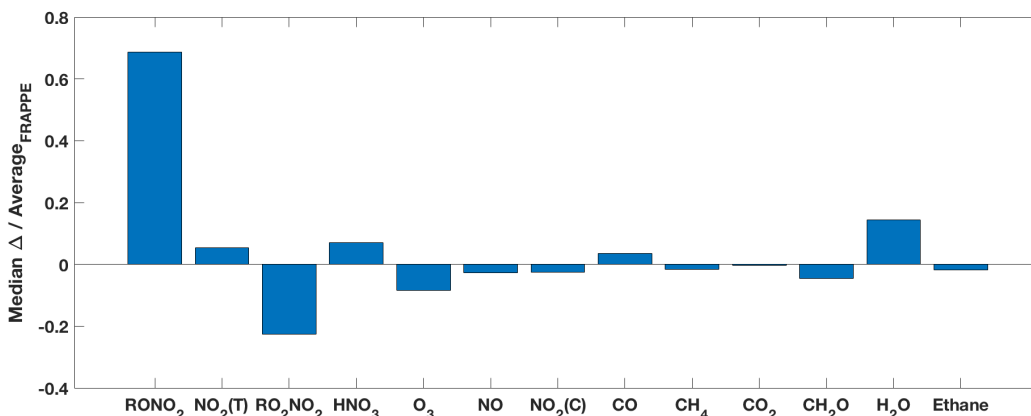


Figure 4.5. Standardized Δ from FRAPPE for a variety of species. Values close to zero show good instrument comparison. The (T) and (C) refer to NO_2 measured by TD-LIF (T) and chemiluminescence (C).

Among TD-LIF measurements, NO_2 and HNO_3 have a standardized Δ near zero similar to the other species. The Δ for $\Sigma\text{RO}_2\text{NO}_2$ is somewhat greater at -0.23. The negative indicates that the DISCOVER-AQ measurements are higher than FRAPPE, consistent with what was observed in Figure 4.4. While these results indicate the possibility of some deviation in the $\Sigma\text{RO}_2\text{NO}_2$ measurements, the scale of the deviation is not large. The Δ is for ΣRONO_2 at 0.69, which shows that indeed the instruments are inconsistent with each other and FRAPPE measurements are much greater than those from DISCOVER-AQ.

This analysis suggests that the FRAPPE TD-LIF systematically measured higher values for ΣRONO_2 . To determine if one or either instrument had poor performance, we attempt to independently verify measurements using other instrumentation on the same plane, focusing first on ΣRONO_2 which had the greatest discrepancy. Given the reliability and good comparisons the TD-LIF has had in other experiments, we think it is unlikely that both instruments had unusually poor performance, but we attempt to verify both (see Chapter 3; Beaver et al., 2012; Day et al., 2002; Thornton et al., 2003).

4.3.1 Validation of FRAPPE measurements

Measurements of select individual alkyl nitrates were made on the C-130, which allows us to compare the reasonableness of the TD-LIF total ΣRONO_2 concentration based on how much we expect the individually measured alkyl nitrates to comprise of the total. Individual alkyl nitrates were measured by TOGA and WAS. Species measured include a variety derived from $\text{C}_1 - \text{C}_5$ alkanes. For $\text{C}_1 - \text{C}_5$ alkyl nitrates that weren't measured, the branching ratio for the precursor was used from the Master Chemical Mechanism (MCM) to determine the expected concentration of unmeasured alkyl nitrates with the same precursor as a measured one.

The total ΣRONO_2 measurement should be higher than the sum of $\text{C}_1 - \text{C}_5$ alkane-derived species. To estimate how much higher, we used calculations of RONO_2 production from measured VOCs (see Chapter 2 for details on the RONO_2 production calculation). We assume that the ratio that $\text{C}_1 - \text{C}_5$ RONO_2 are produced relative to all RONO_2 will be approximately the same ratio that they are present in concentrations. As demonstrated in equation 4.1, by calculating production from $\text{C}_1 - \text{C}_5$ alkanes compared to total production and knowing the measured concentrations of $\text{C}_1 - \text{C}_5$ alkyl nitrates, we can determine an estimated concentration of total alkyl nitrates and compare this to the TD-LIF measured total alkyl nitrates.

$$\frac{\Sigma P(\text{RONO}_2)_{\text{C}_1-\text{C}_5}}{\Sigma P(\text{RONO}_2)_{\text{All}}} \approx \frac{\Sigma[\text{RONO}_2]_{\text{C}_1-\text{C}_5}}{\text{Est. } \Sigma[\text{RONO}_2]_{\text{All}}} \quad (4.1)$$

The comparison of the estimated and measured total alkyl nitrates is in Figure 4.6. Since the production calculations only include measured VOCs, we would expect the estimated total to be slightly below the measured total, which is what is observed. This supports that the FRAPPE TD-LIF total alkyl nitrates measurement is reasonable compared to other instruments on the plane.

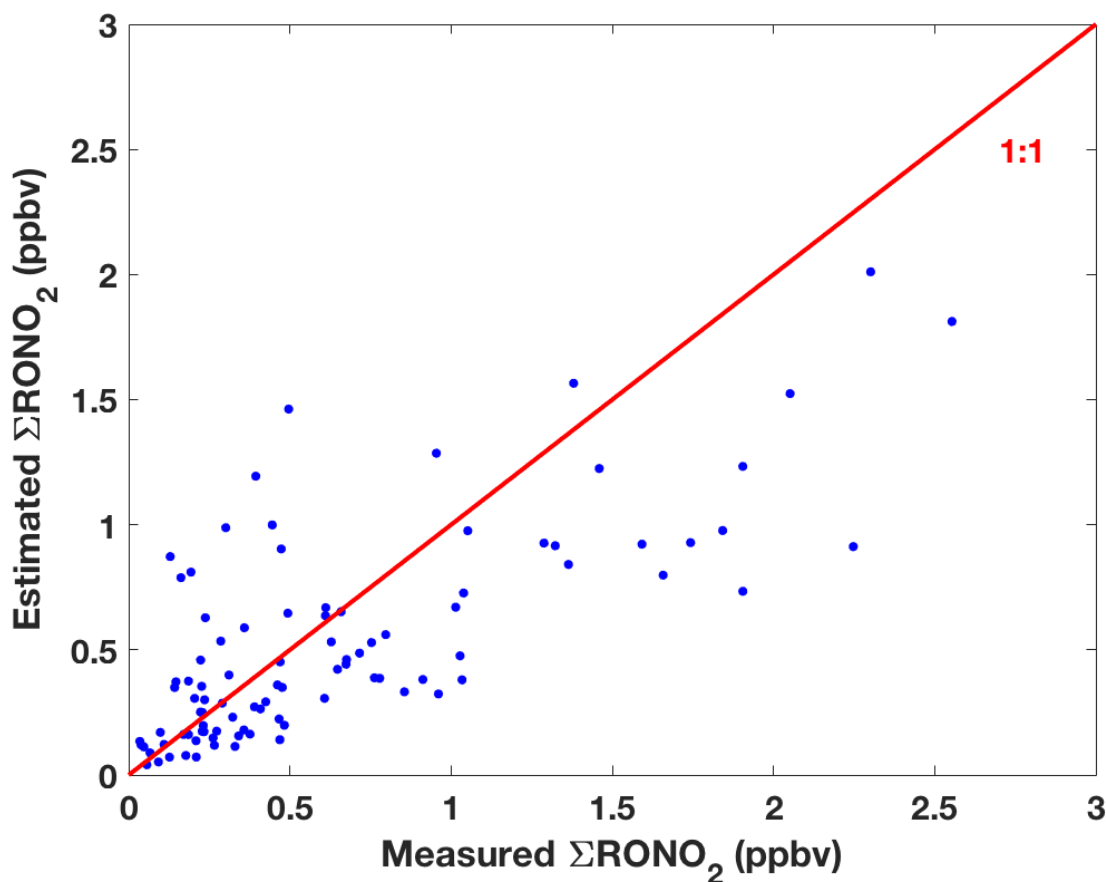


Figure 4.6. Estimated vs measured total alkyl nitrates. The red line is the 1:1 line.

4.3.2 Validation of Discover-AQ measurements

The Discover-AQ total alkyl nitrate measurement is harder to verify since there are no individual alkyl nitrate measurements to compare to or VOC measurements to calculate productions from. One advantage the Discover-AQ dataset has, however, is a total NO_y measurement by chemiluminescence. Since the TD-LIF measurements without NO_2 comprise a measurement of NO_z , this sum should compare well to the total NO_y measurement minus NO and NO_2 if the measurements are reasonable. If the TD-LIF sum is lower than NO_z , this would be consistent with the idea that some factor made the TD-LIF Discover-AQ ΣRONO_2 measurements too low compared with FRAPPE. The NO_z comparison is shown in Figure 4.7.

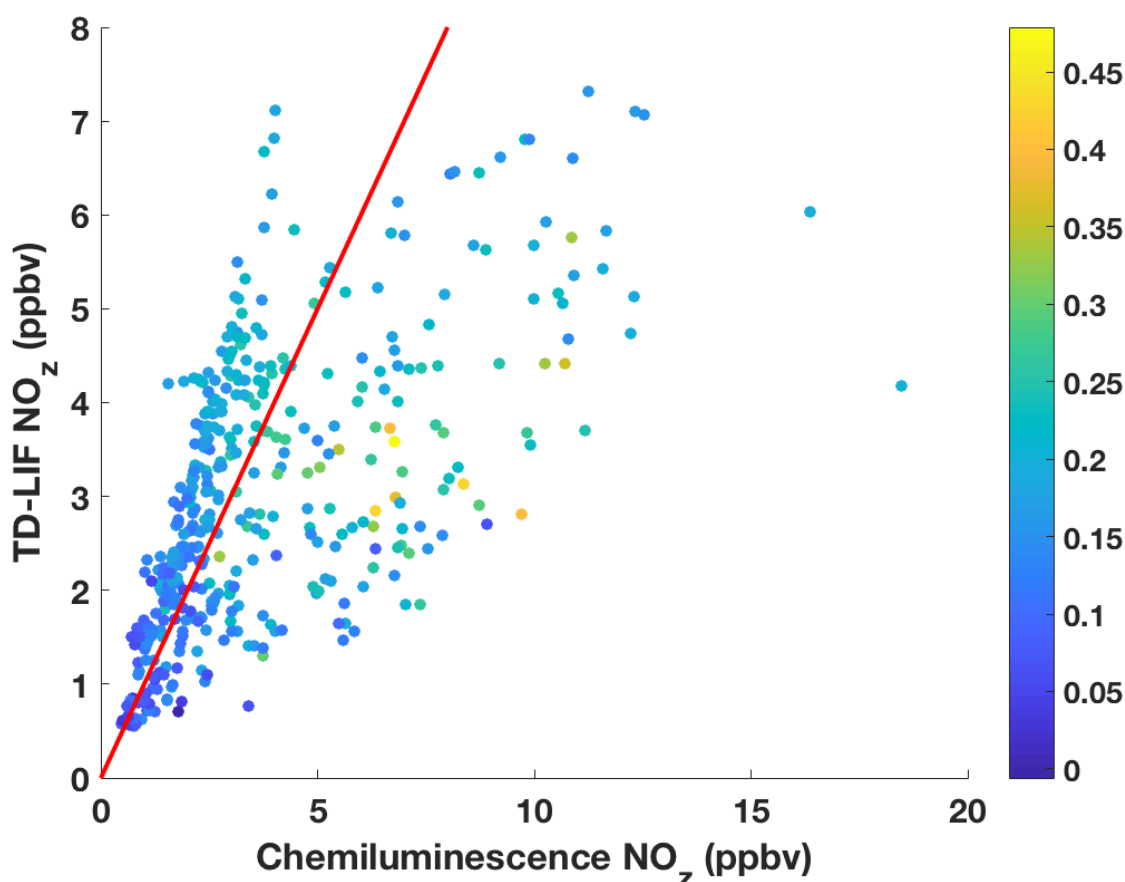


Figure 4.7. Discover-AQ TD-LIF vs Chemiluminescence NO_z colored by ΣRONO_2 as a percentage of TD-LIF NO_z .

While there are some points where the TD-LIF measures higher, perhaps indicative of a calibration offset between the two instruments, a portion of points have much higher chemiluminescence measurements than the TD-LIF. This includes the points where RONO_2 as a percentage of NO_z is at its highest. ΣRONO_2 are most influential on NO_z in the region where the TD-LIF is measuring low, which is consistent with the theory that the Discover-AQ data is low and that for FRAPPE is reasonable.

Additional evidence that it is the Discover-AQ ΣRONO_2 measurements that are off is the corollary of the good agreement of FRAPPE's measured and estimated ΣRONO_2 from Figure 4.6. If the FRAPPE measurements are scaled by 50% to be in agreement with the Discover-AQ measurements, almost all points would lie above the 1:1 line, which would indicate that the TD-LIF is measuring much less, on the order of half, of what is expected.

4.3.3 Possible explanations for discrepancy

It is unclear what would make the Discover-AQ alkyl nitrate measurements falsely low. One possibility is that the oven temperature set points are off, which would lead some of one species to be measured in a different channel. If this was the case, making the DISCOVER-AQ ΣRONO_2 measurement low, we would expect to see the opposite in one of the adjacent channels, where DISCOVER-AQ would be higher due to having excess signal from RONO_2 . The HNO_3 measurement is also slightly lower for DISCOVER-AQ, so there couldn't be excess signal in that channel. The direction of disagreement for $\Sigma\text{RO}_2\text{NO}_2$ is opposite of ΣRONO_2 , so there may be some excess ΣRONO_2 signal in the $\Sigma\text{RO}_2\text{NO}_2$ channel due to a temperature set point being too high. However, the median magnitude of the difference between the campaigns for $\Sigma\text{RO}_2\text{NO}_2$ is 170 pptv compared to 685 pptv for ΣRONO_2 , so a temperature offset cannot account for the entire discrepancy for ΣRONO_2 .

One possibility that could explain why both the ΣRONO_2 and HNO_3 channels are lower for DISCOVER-AQ is that both of these channels see particle phase nitrates, organic nitrate particulate in the ΣRONO_2 channel and inorganic ammonium nitrate in the HNO_3 channel. If the Discover-AQ inlet was somehow not allowing a significant number of particles through that were getting through the FRAPPE TD-LIF and Discover-AQ NO_y inlets, the Discover-AQ TD-LIF measurements would read lower. This phenomenon would not cause a difference in the NO_2 or peroxy nitrate channels, as these should have no influence from particles. Additionally, the scale of the discrepancy is so much greater for ΣRONO_2 than for HNO_3 that organic particles would have to have a much greater concentration than inorganic nitrate particles, or at least as a percentage of the ΣRONO_2 and HNO_3 measurements.

In order to estimate whether aerosol could account for the discrepancy, we compare observed ΣRONO_2 and HNO_3 with measurements of aerosol nitrate. Organic particulate nitrate is calculated as the total nitrate minus the inorganic nitrate measurement. Figure 4.8 shows a timeseries of alkyl nitrates and organic particle nitrate (pNO_3), showing that aerosol is often a substantial portion of the total measurement.

The median organic particle nitrate as a percentage of ΣRONO_2 is 23%, excluding negative particle measurements, and the median inorganic particle nitrate as a percentage of HNO_3 is 13%. The portion of the HNO_3 measurement that is from inorganic pNO_3 is potentially even lower, as the TD-LIF does not measure all types of inorganic pNO_3 , only ammonium nitrate.

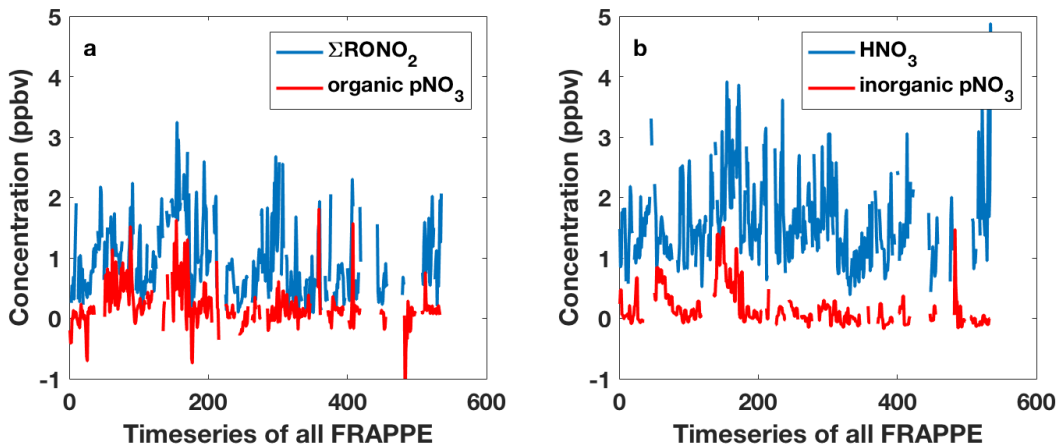


Figure 4.8. Timeseries of (a) ΣRONO_2 and organic pNO_3 and (b) HNO_3 and inorganic pNO_3 for the entire FRAPPE campaign.

Figure 4.9 shows the correlation between Discover-AQ and FRAPPE for ΣRONO_2 if the organic particle nitrate measurement from FRAPPE is added to Discover-AQ, representing the assumption that the Discover-AQ ΣRONO_2 measurement saw no particle nitrate. The comparison is improved, with some points falling along the 1:1 line. The majority of points still fall below the line, however, so while a difference in particle intake between the instruments may be contributing to the ΣRONO_2 discrepancy, it cannot account for all of it.

Neither of the TD-LIF inlets are well characterized for particle intake, but we have had no reason to suspect they would behave very differently. A differing intake of aerosol between planes may be a contributing factor to the discrepancy, but cannot explain the difference in its totality.

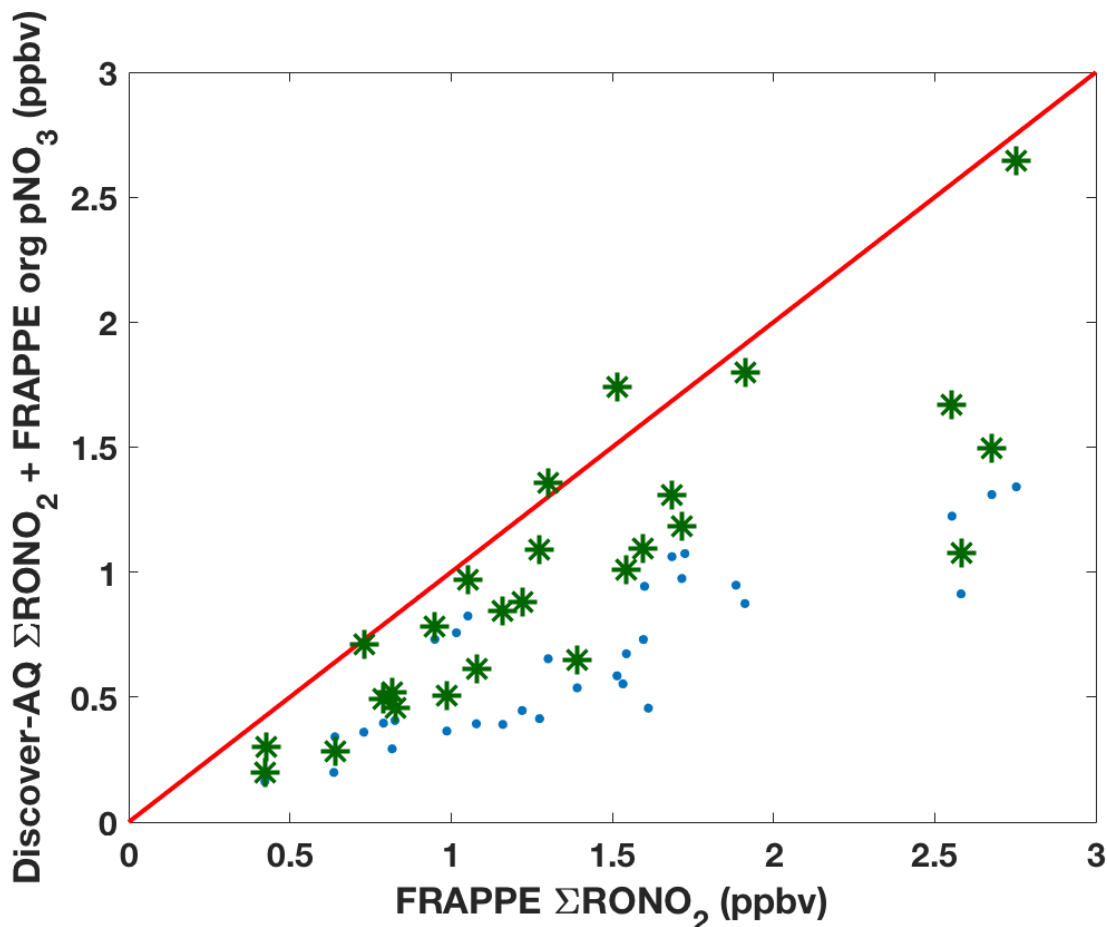


Figure 4.9. Blue points show the same comparison as Figure 4.4c. Green stars show this comparison but with the FRAPPE organic particle nitrate added to the Discover-AQ ΣRONO_2 measurement. The 1:1 line is shown in red.

The Discover-AQ ΣRONO_2 measurements are low compared to the independently validated FRAPPE measurements. We have shown that factors including a low oven temperature set point and a difference in aerosols observed by the instruments may contribute partially to the discrepancy, and there may be other unknown factors, such as a leak in the Discover-AQ instrument.

4.3.4 Comparison of other species for validation

While our validation has so far been focused on alkyl nitrates, as that is the species most of interest for this work, we can additionally validate with other TD-LIF measurements for which there are corresponding measurements from other instruments, which include NO_2 and RO_2NO_2 .

NO_2 was measured using chemiluminescence by the same group on both planes in addition to the TD-LIF measurement, and a comparison within each plane should indicate how reasonable the TD-LIF is. In Figure 4.10a, the FRAPPE NO_2 comparison shows that the chemiluminescence

measurements agree well at lower concentrations, but may have some nonlinearity at concentrations above 20 ppbv. The slope of a linear fit is 0.86, which is likely pulled down by the points at higher concentrations. Excluding points above 20 ppbv, the slope improves to 0.93.

The Discover-AQ NO₂ comparison in Figure 4.10b is similarly good but doesn't appear to have nonlinearity. The linear fit slope is 0.92, which is similar to the slope for the linear portion of the FRAPPE comparison. These results indicate that these two methods agree within 10% and the relative calibration is consistent across the campaigns.

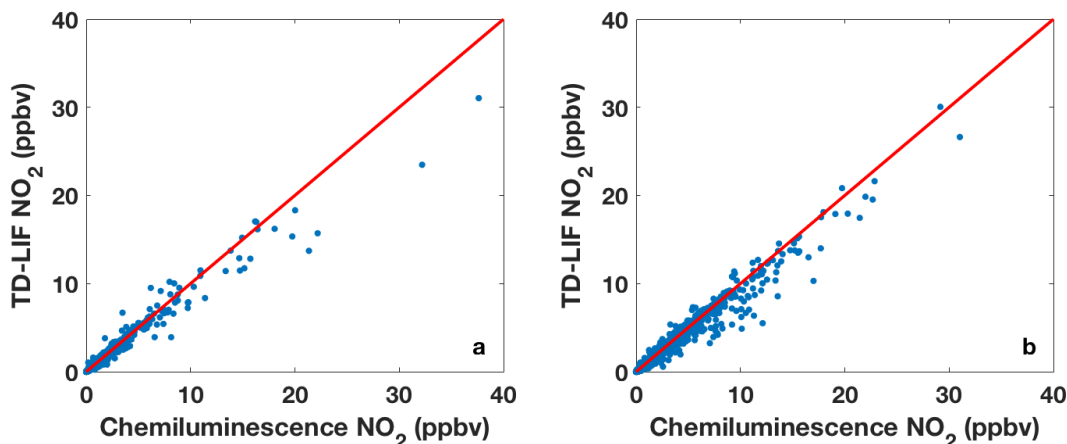


Figure 4.10. NO₂ comparison between TD-LIF and Chemiluminescence for (a) FRAPPE and (b) Discover-AQ.

Similar to how the FRAPPE alkyl nitrates were validated by comparison with other C-130 measurements of individual alkyl nitrates, peroxy nitrates can be validated by comparing with the individually measured peroxyacetyl nitrate (PAN) and peroxypropionyl nitrate (PPN), the most abundant peroxy nitrates. Since few other peroxy nitrates are stable enough to last long in the atmosphere, we would expect the total peroxy nitrates measurement to compare even better with the sum of PAN and PPN than we expected total alkyl nitrates to compare to the measured individual alkyl nitrates. We still expect the sum to be lower than the total measurement, as we have no measurement of methacryloyl peroxy nitrate (MPAN), the next most common peroxy nitrate, and there is evidence that when isoprene is present, peroxy nitrates other than these three can be a substantial portion of the total (Wooldridge et al., 2010).

The sum of measured PAN and PPN is compared to the total peroxy nitrates TD-LIF measurement in Figure 4.11. As expected, the $\Sigma\text{RO}_2\text{NO}_2$ measurement is equal to or higher than the sum of PAN and PPN, suggesting that there are 0 – 1 ppbv of MPAN or other RO₂NO₂ present.

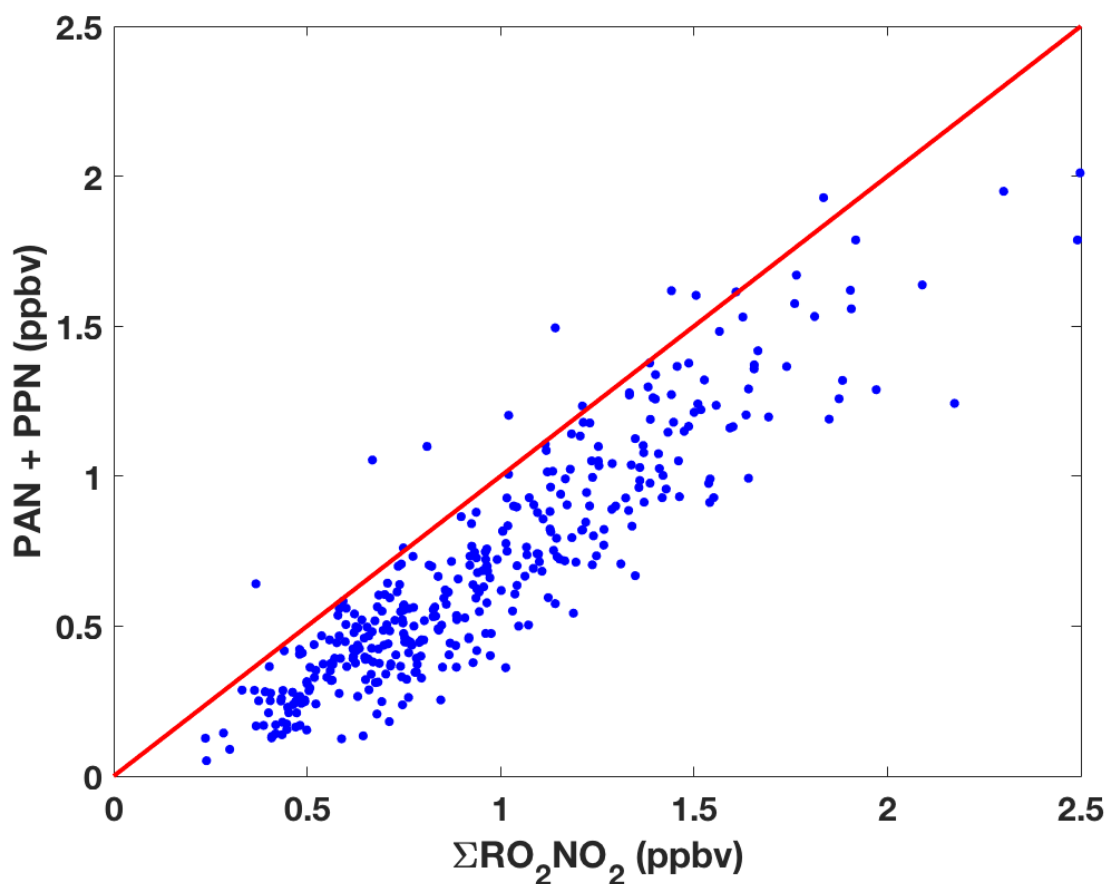


Figure 4.11. PAN + PPN vs $\Sigma\text{RO}_2\text{NO}_2$ comparison for FRAPPE, with a red 1:1 line.

4.4 Conclusion

The alkyl nitrate measurements on the C-130 were verified by independent measurements of individual alkyl nitrates on the same plane, suggesting that the FRAPPE measurements are trustworthy. While the Discover-AQ measurements did not have individual alkyl nitrate measurements to compare to, a comparison of NO_2 was consistent with the Discover-AQ data being biased low. Based on these results, the FRAPPE dataset for ΣRONO_2 is considered most trustworthy and we do not recommend using the Discover-AQ ΣRONO_2 measurements. Possible reasons for the Discover-AQ ΣRONO_2 measurement to be low include the temperature set point being too low, differing uptake of particles between the two instruments, or a leak in the instrument. Since the magnitude of these issues is less than the discrepancy, it is likely a combination of multiple factors. Comparisons of NO_2 and RO_2NO_2 with other instruments generally agreed well except for some nonlinearity at high NO_2 concentrations for FRAPPE.

References

Apel, E. C., Hills, A. J., Lueb, R., Zindel, S., Eisele, S., & Riemer, D. D. (2003). A fast-GC/MS system to measure C_2 to C_4 carbonyls and methanol aboard aircraft. *Journal of Geophysical*

- Research*, 108(D20), 8794. <https://doi.org/10.1029/2002JD003199>
- Apel, E. C., Emmons, L. K., Karl, T., Flocke, F., Hills, a. J., Madronich, S., et al. (2010). Chemical evolution of volatile organic compounds in the outflow of the Mexico City Metropolitan area. *Atmospheric Chemistry and Physics*, 10(5), 2353–2375. <https://doi.org/10.5194/acp-10-2353-2010>
- Beaver, M. R., St. Clair, J. M., Paulot, F., Spencer, K. M., Crouse, J. D., Lafranchi, B. W., et al. (2012). Importance of biogenic precursors to the budget of organic nitrates: Observations of multifunctional organic nitrates by CIMS and TD-LIF during BEARPEX 2009. *Atmospheric Chemistry and Physics*, 12, 5773–5785. <https://doi.org/10.5194/acp-12-5773-2012>
- CDPHE. (2016). *Moderate Area Ozone SIP for the Denver Metro and North Front Range Nonattainment Area*.
- Colman, J. J., Swanson, A. L., Meinardi, S., Sive, B. C., Blake, D. R., & Rowland, F. S. (2001). Description of the analysis of a wide range of volatile organic compounds in whole air samples collected during PEM-Tropics A and B. *Analytical Chemistry*, 73(15), 3723–3731. <https://doi.org/10.1021/ac010027g>
- Day, D. A., Wooldridge, P. J., Dillon, M. B., Thornton, J. A., & Cohen, R. C. (2002). A thermal dissociation laser-induced fluorescence instrument for in situ detection of NO₂, peroxy nitrates, alkyl nitrates, and HNO₃. *Journal of Geophysical Research*, 107(D6), 4046. <https://doi.org/10.1029/2001JD000779>
- Diskin, G. S., Podolske, J. R., Sachse, G. W., & Slate, T. A. (2002). Open-path airborne tunable diode laser hygrometer. *Proc. SPIE 4817, Diode Lasers and Applications in Atmospheric Sensing*, 196–204. <https://doi.org/10.1117/12.453736>
- Gerbig, C., Schmitgen, S., Kley, D., Volz-Thomas, A., Dewey, K., & Haaks, D. (1999). An improved fast-response vacuum-UV resonance fluorescence CO instrument. *Journal of Geophysical Research Atmospheres*, 104(D1), 1699–1704. <https://doi.org/10.1029/1998JD100031>
- Jayne, J. T., Leard, D. C., Zhang, X., Davidovits, P., Smith, K. A., Kolb, C. E., & Worsnop, D. R. (2000). Development of an aerosol mass spectrometer for size and composition analysis of submicron particles. *Aerosol Science and Technology*, 33(1), 49–70. <https://doi.org/10.1080/027868200410840>
- Nault, B. A., Garland, C., Pusede, S. E., Wooldridge, P. J., Ullmann, K., Hall, S. R., & Cohen, R. C. (2015). Measurements of CH₃O₂NO₂ in the upper troposphere. *Atmospheric Measurement Techniques*, 8(2), 987–997. <https://doi.org/10.5194/amt-8-987-2015>
- Orsini, D. A., Ma, Y., Sullivan, A., Sierau, B., Baumann, K., & Weber, R. J. (2003). Refinements to the particle-into-liquid sampler (PILS) for ground and airborne measurements of water soluble aerosol composition. *Atmospheric Environment*, 37, 1243–1259. [https://doi.org/10.1016/S1352-2310\(02\)01015-4](https://doi.org/10.1016/S1352-2310(02)01015-4)
- Richter, D., Weibring, P., Walega, J. G., Fried, A., Spuler, S. M., & Taubman, M. S. (2015). Compact highly sensitive multi-species airborne mid-IR spectrometer. *Applied Physics B: Lasers and Optics*, 119(1), 119–131. <https://doi.org/10.1007/s00340-015-6038-8>
- Ridley, B. A., & Grahek, F. E. (1990). A Small, Low Flow, High Sensitivity Reaction Vessel for NO Chemiluminescence Detectors. *Journal of Atmospheric and Oceanic Technology*, 7, 307–311. [https://doi.org/10.1175/1520-0426\(1990\)007<0307:ASLFHS>2.0.CO;2](https://doi.org/10.1175/1520-0426(1990)007<0307:ASLFHS>2.0.CO;2)
- Sachse, G. W., Hill, G. F., Wade, L. O., & Perry, M. G. (1987). Fast-Response, High-Precision Carbon Monoxide Sensor Using a Tunable Diode Laser Absorption Technique. *Journal of*

- Geophysical Research: Atmospheres*, 92(6), 2071–2081.
<https://doi.org/10.1029/JD092iD02p02071>
- Thornton, J. A., Wooldridge, P. J., Cohen, R. C., Williams, E. J., Hereid, D., Fehsenfeld, F. C., et al. (2003). Comparisons of in situ and long path measurements of NO₂ in urban plumes. *Journal of Geophysical Research*, 108(D16), 4496. <https://doi.org/10.1029/2003JD003559>
- Vay, S. A., Choi, Y., Vadrevu, K. P., Blake, D. R., Tyler, S. C., Wisthaler, A., et al. (2011). Patterns of CO₂ and radiocarbon across high northern latitudes during International Polar Year 2008. *Journal of Geophysical Research*, 116, D14301.
<https://doi.org/10.1029/2011JD015643>
- Walega, J., Dye, J., Grahek, F., & Ridley, B. (1991). A compact measurement system for the simultaneous determination of NO, NO₂, NO_y and O₃ using a small aircraft. *Proc. SPIE 1433, Measurement of Atmospheric Gases*, 1433, 232–241. <https://doi.org/10.1117/12.46167>
- Weibring, P., Richter, D., Fried, A., Walega, J. G., & Dyroff, C. (2006). Ultra-high-precision mid-IR spectrometer II: System description and spectroscopic performance. *Applied Physics B: Lasers and Optics*, 85(2–3), 207–218. <https://doi.org/10.1007/s00340-006-2300-4>
- Weibring, P., Richter, D., Walega, J. G., & Fried, A. (2007). First demonstration of a high performance difference frequency spectrometer on airborne platforms. *Optics Express*, 15(21), 13476–13495. <https://doi.org/10.1007/BF00425997>
- Wooldridge, P. J., Perring, A. E., Bertram, T. H., Flocke, F. M., Roberts, J. M., Singh, H. B., et al. (2010). Total Peroxy Nitrates (ΣPNs) in the atmosphere: the Thermal Dissociation-Laser Induced Fluorescence (TD-LIF) technique and comparisons to speciated PAN measurements. *Atmospheric Measurement Techniques*, 3, 593–607.
<https://doi.org/10.5194/amt-3-593-2010>
- Yacovitch, T. I., Herndon, S. C., Roscioli, J. R., Floerchinger, C., McGovern, R. M., Agnese, M., et al. (2014). Demonstration of an ethane spectrometer for methane source identification. *Environmental Science and Technology*, 48(14), 8028–8034.
<https://doi.org/10.1021/es501475q>
- Zheng, W., Flocke, F. M., Tyndall, G. S., Swanson, A., Orlando, J. J., Roberts, J. M., et al. (2011). Characterization of a thermal decomposition chemical ionization mass spectrometer for the measurement of peroxy acyl nitrates (PANs) in the atmosphere. *Atmospheric Chemistry and Physics*, 11(13), 6529–6547. <https://doi.org/10.5194/acp-11-6529-2011>